



Technische Universität München

Fakultät für Medizin

Lehrstuhl für Stoffwechselerkrankungen

**“Targeting glia-vascular interactions for the
treatment of obesity and its comorbidities”**

Tim Gruber

Vollständiger Abdruck der von der Fakultät für Medizin der Technischen Universität München zur Erlangung des akademischen Grades eines Doktors der Naturwissenschaften genehmigten Dissertation.

Vorsitzender: Prof. Dr. Thomas Misgeld

Prüfer der Dissertation: 1. Prof. Dr. Dr. h.c. Matthias H. Tschöp

2. Prof. Dr. Ilona Grunwald Kadow

Die Dissertation wurde am **02.10.2019** bei der Technischen Universität München eingereicht und durch die Fakultät der Medizin am **12.05.2020** angenommen

I. Table of Contents

<i>I. Table of Contents</i>	2
<i>I. Acknowledgments</i>	7
<i>II. Eidesstattliche Erklärung</i>	10
<i>III. Glossary of terms</i>	11
<i>IV. List of tables</i>	15
<i>V. List of figures</i>	16
<i>VI. Abstract</i>	18
<i>VII. Zusammenfassung</i>	19
1 Introduction	21
1.1 The epidemic of obesity and diabetes mellitus in the modern world	21
1.2 The central regulation of bodyweight and feeding behavior	21
1.3 The discovery of leptin and the concept of a brain-centered ‘lipostatic’ control of body fat	24
1.3.1 Biological functions of leptin.....	25
1.3.2 The leptin receptor (LepR) family	25
1.4 The arcuate nucleus of the hypothalamus: a major mediator of leptin action	26
1.5 Beyond neuronal circuits: the emerging field of glial cells in the control of whole-body energy homeostasis	27
1.5.1 Glial cells.....	27
1.6 Astrocytes: abundant and multifaceted glial cells	28
1.6.1 Astrocytes in physiology and pathology	28
1.6.2 Phylogeny of astrocytes and astrocyte-like cells.....	29
1.6.3 Astrocyte heterogeneity among and within different brain regions.....	30
1.6.4 Astrocytes tune synaptic transmission at the ‘tripartite synapse’	31
1.6.5 Astrocytes are key components of the neuro-glia-vascular unit	32
1.7 The cerebral vasculature: sustainment of brain oxygenation, nutrient supply and homeostatic feedback	32
1.7.1 The blood-brain barrier and its anatomical organization	33
1.8 Brain oxygenation: coupling of brain function to metabolism	34

Table of Contents

1.8.1	Hypoxia: mismatch between vascular perfusion and oxygen demand	36
1.8.2	Angiogenesis as a hallmark of vascular remodeling	43
1.8.3	Vascular-endothelial growth factors (VEGF) – the angiogenic master switch.....	45
1.8.4	Physiological relevance of VEGF	50
1.9	Glia-vascular dysfunction in obesity	52
1.9.1	Hypothalamic astrogliosis in obesity	52
1.9.2	Vascular dysfunction in obesity	54
1.9.3	Microvascular dysfunction in susceptible tissues as a consequence of high-calorie diets.....	55
1.9.4	Systemic macrovascular dysfunction and arterial hypertension in obesity.....	55
1.9.5	Sympathetic hyperactivation of cardiovascular targets in obesity.....	56
2	<i>Aim of the thesis</i>.....	57
3	<i>Material and Methods</i>.....	58
3.1	Animals experiments	58
3.1.1	Genotyping of mouse lines.....	59
3.1.2	Body composition analysis and metabolic phenotyping	59
3.1.3	Measurement of mean arterial pressure in conscious mice by the tail cuff system (<i>collaboration</i>) 60	
3.1.4	Arterial pressure and heart rate recording in anesthetized mice (<i>collaboration</i>)	60
3.1.5	Leptin administration <i>in-vivo</i>	61
3.1.6	Glucose metabolism studies in mice <i>in-vivo</i>	61
3.1.7	Viral targeting of astrocytic VEGF signaling in the mediobasal hypothalamus (MBH).....	61
3.2	Ex-vivo measurements.....	63
3.2.1	<i>Ex-vivo</i> luciferase assay of HIF1/ODD-Luc brain homogenates	63
3.2.2	Vascular reactivity experiments in aorta segments (<i>collaboration</i>).....	63
3.2.3	Determination of VEGF content of brain homogenates and serum in mice	64
3.2.4	Magnetic-activated and fluorescence-assisted cell sorting (MACS/FACS)	64
3.2.5	Bulk transcriptomics data analysis (<i>collaboration</i>)	65
3.2.6	Pathway Enrichment (<i>collaboration</i>)	66
3.3	Histology and Imaging.....	66
3.3.1	Fluorescent angiography	66
3.3.2	Image acquisition and analysis of vascularity in consecutive brain sections.....	67
3.3.3	Brain sectioning and immunohistochemistry	67
3.3.4	3DISCO-assisted optical clearing of whole brains	68
3.3.5	Light-sheet microscopy imaging	69
3.3.6	Analysis of vascularity in 3D whole-brain data sets	69
3.3.7	Protein extraction and Western blot	70
3.3.8	RNA isolation and qPCR analysis	70

Table of Contents

3.4	Cell culture	70
3.4.1	Primary astrocyte cell culture.....	70
3.4.2	Induction of Cre recombinase-mediated recombination <i>in-vitro</i>	71
3.5	Human data	72
3.5.1	Correlating plasma leptin concentration with markers of microvascular function in humans.....	72
3.5.2	Imaging of retinal microvasculature (<i>collaboration</i>)	72
3.6	Statistics	73
4	Results	74
4.1	Hypertension in obesity is driven by angiogenic signaling in hypothalamic astrocytes	74
4.1.1	HFHS feeding induces microangiopathy specifically in the hypothalamus prior to the development of systemic hypertension in mice.....	74
4.1.2	Hypervascular microangiopathy of the hypothalamus is reversible in male, but not in female mice	76
4.1.3	Hypothalamic microangiopathy occurs at the onset of bodyweight gain coinciding with increased circulating leptin levels.....	77
4.1.4	Circulating leptin concentrations predict risk for CNS-microvascular abnormalities in obese humans and mice	79
4.1.5	Leptin signaling in the brain rather than obesity <i>per se</i> acts as a driver in the development of hypothalamic neovascularization.....	82
4.1.6	Astrocytes regulate the production of VEGF within the hypothalamus <i>via</i> leptin receptor	84
4.1.7	Astrocyte-specific loss of HIF-1 α abrogates HFHS-induced VEGF expression and hypervascularization in the hypothalamus.....	88
4.1.8	Astrocyte-derived VEGF is necessary and sufficient for dynamic hypothalamic microvascular remodeling	93
4.1.9	Blocking VEGF expression in MBH astrocytes prevents arterial hypertension and sympathetic hyperactivity in diet-induced obesity.....	95
5	Discussion	98
5.1	Hypertension in obesity is driven by angiogenic signaling in hypothalamic astrocytes	98
5.1.1	Astrocytic VEGF exerts unique effects at the cerebral endothelium as opposed to blood-borne, macrophage-derived VEGF	99
5.1.2	Integration of tonic <i>versus</i> phasic metabolic information: differential roles of hypothalamic astrocytes and tanycytes?.....	99
5.1.3	Diet-induced hyperleptinemia contribute to microvascular dysfunction at body-brain interfaces	100
5.1.4	Leptin and the post-translational regulation of HIF-1 α activity: a role of phosphorylation?.....	101

Table of Contents

5.1.5	Increased serum leptin bridges hypothalamic microangiopathy with the development of obesity-associated arterial hypertension	101
5.1.6	Leptin-mediated remodeling of the hypothalamic microvasculature constitutes a prerequisite for obesity-associated arterial hypertension	102
5.2	Conclusion and Outlook.....	103
6	References	104
VIII.	Appendix.....	121
	N21479	124
	N21480	124
IX.	Curriculum vitae	131

I. Acknowledgments

“There are three basic problems: how a mind can know the world of nature, how it is possible for one mind to know another, and how it is possible to know the contents of our own minds without resort to observation or evidence. It is a mistake, I shall urge, to suppose that these questions can be collapsed into two, or taken into isolation.”

— Donald Davidson

A scientist’s pursuit to learn about the world of nature cannot be separated from learning about (and thus from) other people. When you, Matthias, kindly invited me to attend the *Diabetes Conference* back in 2014, I was immediately gripped by the overarching spirit as well as by the people incorporating it and started to dream about becoming a part of this ever since. With my deepest gratitude I want to thank you for giving me the opportunity to pursue a PhD in your lab, for surrounding me with the greatest people, for being patient with my flaws and keeping me in check, for inspiring me scientifically and how to carry oneself, and lastly for always supporting me in crucial moments. Thank you!

Shift of scenes: A glass of red wine in my hand while watching the sunset over Tuscany after lengthy but incredibly insightful days at the Neuroscience Summer School, which you, Tamas, organized in Sienna in 2017. Not only on this Tuscan terrace, though, but every time we talked, you broadened my way of thinking tremendously in both scientific as well as philosophical terms in your own natural way. Most importantly, however, you gave me hope and courage in the face of my personal situation and motivated me to give my very best in both regards.

My special thanks and appreciation go to my second supervisor, Wolfgang Wurst, for all the support and encouragements *via* emails and in our personal meetings. Thank you!

Acknowledgments

“I liked the talk about hormones and astrocytes by this Spanish lady quite a lot.” One thoughtless answer to Matthias at the IDO winter retreat before taking on my PhD and here I am – in the Astrocyte Biology Unit. I can hardly express how lucky I consider myself to be part of ‘Mama’ Cristina’s team, and how honoured I feel to be her first PhD student. Joining at a time when you, Cristina, just transitioned to become a junior group leader, I look back now and cannot help but being deeply impressed about your path. Your natural and charming way of taking the lead, showing the path and providing a feeling of security for your group members, your self-sacrifice in the background to always back us up, your positive – sometimes ‘chitty chatty’ – but always authentic and motivational attitude makes you an ideal supervisor in my opinion. Certainly, you are my ideal supervisor! Especially since you figured out right away how to perfectly guide me with a balance of freedom and gentle persistence, dealing elegantly with my peculiarities. I am sure these – almost maternal – vibes you conveyed evoked plenty of oxytocin release within my brain for permanent rewiring of the gratitude-circuit.

For me, the IDO is one of the most extraordinary places and I am proud being part of it. I feel blessed to be able to meet such a number of great people with diverse personalities, interests and backgrounds. Over the course of my PhD I enjoyed the collaborative spirit and plenty of great scientific discussions... and plenty of non-scientific discussions as well, because many of the IDO people turned into actual friends. Without now singling out one by one, I am sure you will know how much I appreciate each of you. Thank you all!

I want to particularly thank all my collaborators for sharing expertise and joining efforts in a common endeavour.

Obviously, a big thank you goes to the entire Astrocyte Biology Unit in its past and present constellations, and especially to the technicians. Without your help I could not have made it. Thank you for all the ‘favors’ and your patience, Clarita, Nicole, Heidi and Cassie.

Acknowledgments

Last but not least I want to thank my family. I want to thank Emilia and Valentin, my little ‘world discoverers’, and Katharina for being them a great mother. I want to thank my father and brother and last but not least my mother for their unconditional support and belief in me.

II. Eidesstattliche Erklärung

Ich erkläre an Eides statt, dass ich die bei der Fakultät für Medizin zur Promotionsprüfung vorgelegte Arbeit mit dem Titel:

“Targeting glia-vascular interactions for the treatment of obesity and its comorbidities”

am Institut für Diabetes und Adipositas (Helmholtz Zentrum München) unter der Anleitung und Betreuung durch Prof. Dr. Tschöp ohne sonstige Hilfsmittel erstellt und bei der Abfassung nur die gemäß § 6 Abs. 6 und 7 Satz 2 angegebenen Hilfsmittel benutzt habe.

Ich habe keine Organisation eingeschaltet, die gegen Entgelt Betreuerinnen und Betreuer für die Anfertigung von Dissertationen sucht, oder die mir obliegenden Pflichten hinsichtlich der Prüfungsleistungen für mich ganz oder teilweise erledigt.

Ich habe die Dissertation in dieser oder ähnlicher Form in keinem anderen Prüfungsverfahren als Prüfungsleistung vorgelegt.

Die vollständige Dissertation wurde noch nicht veröffentlicht.

Ich habe den angestrebten Doktorgrad noch nicht erworben und bin nicht in einem früheren Promotionsverfahren für den angestrebten Doktorgrad endgültig gescheitert.

Die öffentlich zugängliche Promotionsordnung der TUM ist mir bekannt, insbesondere habe ich die Bedeutung von § 28 (Nichtigkeit der Promotion) und § 29 (Entzug des Doktorgrades) zur Kenntnis genommen. Ich bin mir der Konsequenzen einer falschen Eidesstattlichen Erklärung bewusst.

Mit der Aufnahme meiner personenbezogenen Daten in die Alumni-Datei bei der TUM bin ich einverstanden.

München, den

Tim Gruber

III. Glossary of terms

ADM	Adrenomedullin
AgRP	Agouti-related peptide
ARC	Arcuate nucleus of the hypothalamus
ARNT	aryl hydrocarbon receptor Ahr nuclear translocator
ATP	Adenosintriphosphate
AVR	Arteriole-to-venule ratio
BBB	Blood-brain-barrier
BMI	Body mass index
BnST	Bed nucleus of the stria terminalis
C-MYC	myelocytomatosis virus oncogene cellular homolog
CA-IX	Carbonic anhydrase 9
Ca ²⁺	Calcium ion
CBP/p300	CREB-binding protein/E1A binding protein 300
CNS	Central nervous system
CNS	Central nervous system
CO ₂	Carbondioxide
COX4-2	Cytochrome c oxidase subunit 4 isoform 2
CXCR-4	C-X-X chemokine receptor type 4
DBB	Diagonal band of Broca
DMH	Dorsomedial nucleus of the hypothalamus
DMX	Dorsal motor nucleus of the vagus nerve
EDTA	Ethylenediaminetetraacetic acid

Glossary of terms

EG-VEGF	Endocrine gland-derived VEGF
ENG	Endoglin
EPO	Erythropoietin
FH	Fumarate hydratase
FIH1	Factor inhibiting HIF-1
FITC	Fluorescein isothiocyanate
FLT-1 (VEGFR-1)	Fms related tyrosine kinase 1
GABA	γ -aminobutyric acid
GFAP	Glial-fibrillary acidic protein
GLAST	Glutamate-aspartate transporter
GLUT-1	Glucose transporter 1
GWAS	Genome Wide Association Study
HIF	Hypoxia-inducible factor
HK1/2	Hexokinase 1/2
HOMA-IR	Homeostatic model assessment for insulin resistance
HRE	Hypoxia response element
i.c.v.	intracerebroventricular
i.p.	intraperitoneal
i.v.	intravenous
IC ₅₀	Half maximal inhibitory concentration
IGF2	Insulin-like growth factor 2
IPR	Isoproterenol
K _m	Michaelis-Menten constant
LDHA	Lactate dehydrogenase A
LEP	Leptin

Glossary of terms

LepR	Leptin receptor
LH	Lateral hypothalamus
LPR1	Low-density lipoprotein receptor related protein 1
MAPK	mitogen-activated protein-kinase
MC4R	Melanocortin receptor 4
MCT-4	Monocarboxylate transporter 4
ME	Median eminence
mmHG	Millimetre of mercury
MMPs	matrix metalloproteinases
NAcc	Nucleus accumbens
NHE-1	Sodium-hydrogen antiporter 1
NOS2	Endothelial nitric oxide synthase
NPY	Neuropeptide Y
NTS	Nucleus of the solitary tract
O ₂	Molecular oxygen
<i>ob</i>	<i>Obese</i> gene encoding leptin
ODD	Oxygen-dependent degradation domain
PBN	Parabrachial nucleus
PDGF	Platelet-derived growth factor
PDGFR β	Platelet-derived growth factor receptor β
PDK1/4	Pyruvate dehydrogenase kindase 1/4
PE	Phenylephrine
PEG	Polyethylene glycol
PFKFB-3	6-phosphofructo-2-kinase/fructose-2,6-biphosphatase 3

Glossary of terms

PHD1-3	prolyl-4-hydroxylase domain enzymes 1-3
PI3K	phosphatidylinositol-3-kinase
POMC	Pro-opiomelanocortin
PVN	Paraventricular nucleus of the hypothalamus
RMn/RPa	Nucleus raphé magnus/pallidus
ROS	Reactive oxygen species
s.c.	subcutaneous
SDF-1	stromal derived growth factor 1
SDH	Succinate dehydrogenase
shRNA	Small-hairpin RNA
SNP	Sodium nitroprusside
SON	Supraoptic nucleus of the hypothalamus
STAT3	signal transducer and activator of transcription 3
TGF- β 3	Transforming growth factor β 3
TNF	Tumor necrosis factor
uPAR	urokinase receptor
VEGF	Vascular-endothelial growth factor
vHL	Von Hippel-Lindau E3 ubiquitin ligase
VMH	Ventromedial nucleus of the hypothalamus

IV. List of tables

Table 1: Overview of various oxygen tensions in human tissues.	35
Table 2: Biologically relevant oxygen tensions	36
Table 3: HIF-responsive target genes.....	42
Table 5: Reagents and chemicals	121
Table 6: Antibodies and fluorescent dyes	123
Table 7: Genotyping PCR for HIF-1 α ^{<i>loxP/loxP</i>} mice	125
Table 8: Genotyping PCR for LepR ^{<i>loxP/loxP</i>} mice	126
Table 9: Genotyping PCR for LepR ^{<i>loxP/loxP</i>} mice	126
Table 10: Genotyping PCR for GLAST.CreER ^{T2} mice	127
Table 11: Genotyping PCR for GLAST.CreER ^{T2} mice	127
Table 12: Genotyping PCR for hGFAP.CreER ^{T2} mice.....	128
Table 13: Genotyping PCR for hGFAP.CreER ^{T2} mice.....	128
Table 14: TaqMan probes	129
Table 15: Viral vectors	129
Table 16: Software	130
Table 17: Instruments.....	130

V. List of figures

Figure 1: Schematic diagram of brain regions involved in the regulation of energy homeostasis and body weight.	23
Figure 2: Schematic diagram of posttranslational regulation of HIF-1 α activity.	41
Figure 3: Schematic overview on the main splice variants of the human VEGF gene.	46
Figure 4: The VEGF/VEGFR superfamily of growth factors.	50
Figure 5: Schematic diagram of astrogliosis in the mediobasal hypothalamus induced by high-fat/high-sucrose feeding.	53
Figure 6: HFHS diet-feeding induces hypervascular microangiopathy specifically in the hypothalamus.	75
Figure 7: Diet-induced vascular changes are reversible by weight loss in male but not in female mice.	77
Figure 8: Impaired glucose metabolism does not induce vascular remodeling in the hypothalamus. ...	78
Figure 9: HFHS-induced hypervascularization of the hypothalamus coincides with significant bodyweight gain, hypothalamic expression of angiogenic genes and increased serum leptin.	79
Figure 10: Circulating leptin levels predict neurovasculopathies in both human and mice.	81
Figure 11: Leptin signaling induces pro-angiogenic signaling in the hypothalamus.	83
Figure 12: Hypothalamic astrocytes are the cellular source of HFHS-induced VEGF.	85
Figure 13: Evaluation of genetic mouse lines to target astroglial HIF-1 α /VEGF signaling.	86
Figure 14: LepR signaling in hypothalamic astrocytes is required for VEGF induction upon leptin administration.	87
Figure 15 : Validation of the successful ablation of HIF-1 α exon 2 locus in astrocytes.	89
Figure 16: Astrocyte-specific loss of HIF-1 α abrogates VEGF upregulation and hypothalamic angiopathy in response to HFHS feeding.	91
Figure 17: Loss of astroglial HIF-1 α signaling prevents vascular impairment and reactive microgliosis under HFHS feeding.	92
Figure 18 : Astroglial VEGF is necessary and sufficient to remodel the hypothalamic angioarchitecture upon HFHS feeding.	95
Figure 19: VEGF blockade in hypothalamic astrocytes protects from the development of HFHS-induced systemic hypertension.	96

VI. Abstract

Vascular complications are both highly prevalent in obese and diabetic patients conferring risk for progressive organ failure, cardiovascular disease and death. Despite them occurring often concomitantly, microvascular and macrovascular damage are largely addressed in separation. Recently, an unrecognized phenomenon has been described in which microvascular beds in the hypothalamus of both mice and humans were shown to undergo pathologic hypervascularization as a consequence of dietary obesity. In the course of this thesis, I studied the vascular comorbidities of obesity and diabetes particularly focusing on the previously described diet-induced hypothalamic angiopathy. Results obtained in this thesis unveil that microvascular remodeling in the hypothalamus occurs at the onset of body weight gain under high-fat/high-sugar (HFHS)-feeding of mice particularly affecting pre-autonomic brain centers implicated in the control of systemic blood pressure. Strikingly, this thesis reveals unprecedented evidence that astroglial HIF-1 α /VEGF (Hypoxia-inducible factor 1 α / Vascular endothelial growth factor) signaling in the hypothalamus is tuned to the hypercaloric state by directly sensing elevated serum leptin levels. This thesis further demonstrates that hyperleptinemia highly correlates with neurovascular damage in both mice and humans. Consistently, microvascular remodeling in the hypothalamus was found to be absent in both leptin receptor-deficient (Lep^{db}) and leptin-deficient (Lep^{ob}) mice, in the latter of which hypothalamic hypervascularization can be induced by substituting exogenous leptin. Importantly, mice lacking leptin receptors exclusively in glial fibrillary acidic protein (GFAP)-expressing astrocytes furthermore failed to leptin-dependently induce astroglial VEGF in the hypothalamus. Remarkably, entire protection from diet-induced hypothalamic angiopathy was achieved by ablating HIF-1 α , the transcriptional activator of VEGF, from both GFAP and GLAST (GLutamate ASpartate Transporter)-expressing astrocytes. Lastly, the local blockade of astroglial VEGF in the hypothalamus by viral shRNA not only abrogated microvascular changes in residing centers of blood pressure control but also protected these mice from developing arterial hypertension and sympathetic hyperactivity as a consequence of HFHS feeding, regardless of excessive body weight. In conclusion, results obtained in the course of this thesis demonstrate that elevated leptin levels in obesity trigger HIF-1 α /VEGF signaling in hypothalamic astrocytes to couple the remodeling of local micro-angioarchitecture with systemic blood pressure dysregulation.

VII. Zusammenfassung

Adipöse und diabetische Patienten weisen ein hohes Risiko für verschiedene Gefäßerkrankungen auf, welche insgesamt die Lebensqualität und -erwartung bedeutend negativ beeinflussen. So führen mikrovaskuläre Gefäßschäden unter anderem zu fortschreitendem Organversagen wie in der Netzhaut, der Niere oder peripheren Nerven, wohingegen makrovaskuläre Komplikationen insbesondere mit Herz-Kreislaufversagen in Verbindung stehen. Obwohl mikrovaskuläre und makrovaskuläre Komplikationen häufig gemeinsam auftreten, werden sie größtenteils separat adressiert und behandelt. Kürzlich wurde ein bisher unbekanntes Phänomen entdeckt und schlussfolgernd beschrieben, dass der chronische Konsum einer hyperkalorischen Ernährung zu einer pathologischen Reorganisation des Gefäßsystems innerhalb des Hypothalamus führt. Im Rahmen dieser Dissertation habe ich die vaskulären Begleiterkrankungen von Adipositas und Diabetes untersucht und mich dabei insbesondere auf die zuvor beschriebene ernährungsinduzierte hypothalamische Angiopathie konzentriert. Die Ergebnisse dieser Dissertation legen dar, dass die mikrovaskuläre Reorganisation innerhalb des Hypothalamus zeitgleich mit signifikanter Körpergewichtszunahme auftritt, und somit erstaunlich frühzeitig im Verlauf einer fett- und zuckerhaltigen Überernährung in Mäusen. Zudem zeigt diese Dissertation, dass insbesondere solche hypothalamischen Gehirnregionen betroffen sind, die an der prä-sympathischen Regulation des systemischen Blutdrucks beteiligt sind. Die hier vorgelegten Ergebnisse zeigen zudem, dass der hyperkalorische Zustand insbesondere Astrozyten des Hypothalamus beeinflusst und in diesem Zelltyp die pro-angiogene Signalkaskade HIF-1 α /VEGF (Hypoxie-induzierbarer Faktor 1 α / Vaskulärer endothelialer Wachstumsfaktor) aktiviert. Es wird weiter gezeigt, dass hypothalamische Astrozyten den kalorischen Überschuss in Form von erhöhten Serum-Leptinspiegeln wahrnehmen. Interessanterweise korreliert Hyperleptinämie mit neurovaskulären Schäden in sowohl Mäusen als auch Menschen korrelieren. In Übereinstimmung mit dieser Beobachtung entwickeln Mäuse mit gestörtem Leptin-Signalweg, entweder bedingt durch genetischem Leptin- (Lep^{ob}) oder Leptin-Rezeptor- (Lep^{db}) Mangel, keine hypothalamische Angiopathie trotz der ausgeprägten Adipositas dieser Mausmodelle. Sobald Leptin-defiziente Lep^{ob} Mäuse allerdings mit exogenem Leptin substituiert werden, ist eine signifikante Hypervaskularisierung des Hypothalamus festgestellt worden. Mäuse, in denen das Gen für den Leptinrezeptor ausschließlich in Astrozyten

Zusammenfassung

deletiert wurde, sind im Gegensatz zu Kontrolltiere nicht in der Lage die VEGF Expression in Folge einer Leptingabe zu erhöhen. Die genetische Ablation von HIF-1 α , dem Transkriptionsfaktor von VEGF, in verschiedenen Subpopulationen von Astrozyten bewirkte die vollständige Protektion vor den typischen Gefäßschädigungen auf einer hyperkalorischen Ernährung. Zu guter Letzt verhinderte die lokale Blockade von astrozytärem VEGF mittels viraler RNA-Interferenz nicht nur mikrovaskuläre Veränderungen in den Zentren der hypothalamischen Blutdruckregulation, sondern schützte diese Mäuse auch vor der Entwicklung von arterieller Hypertonie und sympathischer Hyperaktivität als Folge der kalorienreichen Fütterung. Zusammenfassend legen die Ergebnisse dieser Arbeit dar, dass ein erhöhter Leptinspiegel bei Adipositas die HIF-1 α /VEGF-Signalkaskade in hypothalamischen Astrozyten induziert um damit die Reorganisation der lokalen Gefäßarchitektur mit Auswirkungen auf die systemische Blutdruckregulation zu vermitteln.

1 Introduction

1.1 The epidemic of obesity and diabetes mellitus in the modern world

Modern societies are currently facing one of the biggest health care crises with obesity and obesity-related pathologies expanding at tremendous rates all across the globe (Hales et al., 2017). Epidemic dimensions have meanwhile been reported for the United States with more than 68% of the adult population being classified as either overweight or obese (2011-2012, Center for Disease Control). Characterized by an excessive accumulation of body fat, obesity is a result of mismatched energy intake and expenditure. Importantly, obesity frequently involves debilitating derangements in glucose and lipid metabolism that underlie major obesity-associated comorbidities such as cardiovascular complications, dyslipidemia and diabetes mellitus amongst others (Lavie et al., 2017; Collaborators, 2017; Lancet, 2017). Given the frequency and severity of its sequelae, obesity was recently proclaimed to be among the five leading causes of death (WHO, 2009). Up to date, global mortality rates are more significantly impacted by overweight compared to underweight (WHO Obesity and overweight, October 2017; <http://www.who.int/en/news-room/fact-sheets/detail/obesity-and-overweight>). Importantly, the steep rise in obesity prevalence implicates a great burden not only for affected individuals but also for national healthcare systems. With a field as-yet barren of safe and efficacious anti-obesity strategies it becomes increasingly evident that there is a paramount need to better understand obesity's complex aetiology in order to pave the way for therapeutic avenues able to avert its human, economical and societal impact.

1.2 The central regulation of bodyweight and feeding behavior

A series of historical studies during the mid-20th century demonstrated for the first time that damaging distinct hypothalamic brain areas by electrolytic lesioning could dramatically alter body weight and adiposity in rats. Depending on the targeted region, such ablations were readily able to induce either hyperphagic obesity or severe anorexia (Hetherington and Ranson, 1940). From these seminal experiments an axiomatic structure emerged in which the brain, in particular the hypothalamus, took center stage in the regulation of food intake and body weight (**Figure 1**). Subsequent research efforts throughout the following decades

Introduction

consistently substantiated this viewpoint by applying a wide range of increasingly sophisticated methodologies. Just recently, a large-scale GWAS underscored the eminent role of the hypothalamus for human obesity by mapping most genetic risk variants for increased body mass index to functions within the CNS (Locke et al., 2015). In light of the prevailing evidential base, the scientific community hence began to regard obesity primarily as a 'brain disease' rather than a derangement of peripheral metabolism. Up to present days, however, research activities have been largely gravitating towards one particular cell type - the neuron. By taking advantage of the toolbox of modern system neuroscience, a detailed picture was unravelled sketching out how neuronal subtypes are arranged into intricate neurocircuitries with the aim to defend whole-body homeostasis.

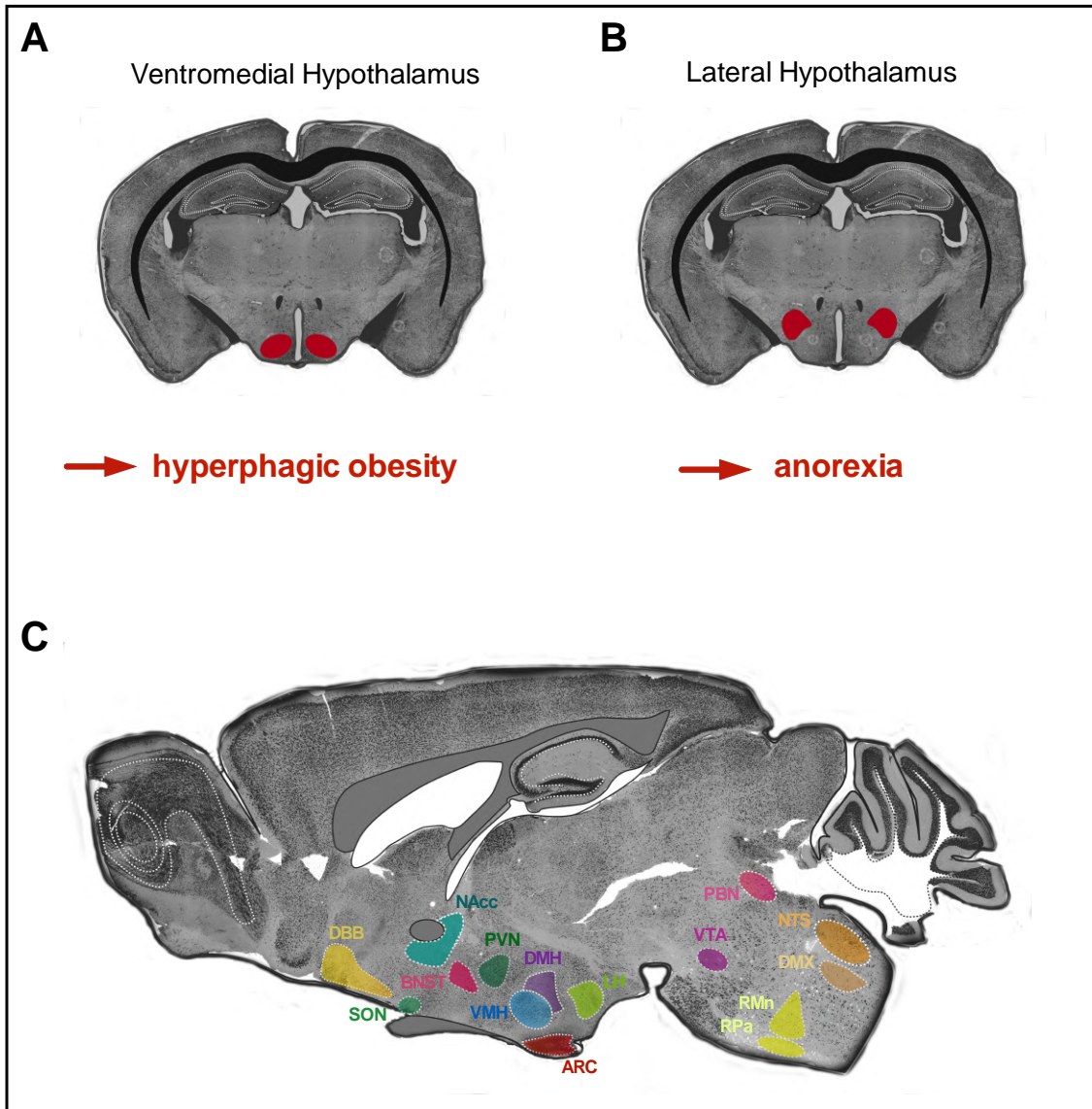


Figure 1: Schematic diagram of brain regions involved in the regulation of energy homeostasis and body weight.

(A) Coronal section of a mouse brain highlighting the ventromedial hypothalamus (VMH; red) whose lesioning triggers voracious feeding and massive obesity in rodents. (B) Electrolytic lesions placed in the lateral hypothalamus (LH; red) oppositely induces anorexia and loss of bodyweight instead. (C) Sagittal section of the mouse brain highlighting various different brain regions that contribute to the regulation of feeding behavior and energy expenditure. Predominantly located in the hypothalamus and brainstem, these nuclei govern whole-body energy homeostasis by integrating and processing feedback signals emanating from the periphery such as hormones and nutrients. DBB: diagonal band of Broca; NAcc: nucleus accumbens; BnST: bed nucleus of the stria terminalis; SON: supraoptic nucleus; PVN: paraventricular nucleus of the hypothalamus; VMH: ventromedial hypothalamus; DMH: dorsomedial hypothalamus; ARC: arcuate nucleus of the hypothalamus; LH: lateral hypothalamus; VTA: ventral tegmental area; PBN: parabrachial nucleus; NTS: nucleus of the solitary tract; DMX: dorsal motor nucleus of the vagus nerve; RMn/RPa: nucleus raphé magnus/pallidus.

1.3 The discovery of leptin and the concept of a brain-centered ‘lipostatic’ control of body fat

The ground-breaking results obtained in these early hypothalamic lesion studies prompted researchers to further explore which signal(s) might be involved in informing the hypothalamus about the animal’s feeding status. In 1959, a parabiosis experiment suggested for the first time that circulating factors would suppress feeding under physiological conditions, an effect that is lost upon hypothalamic lesioning (Hervey, 1959). Around the same time, a spontaneous mutation occurred in a single mouse within the husbandry of the *Jackson Laboratory* that displayed massive hyperphagia and obesity (Ingalls et al., 1950). From thereon, the descendent mutant mouse strain was termed the *ob/ob* mouse according to the obese phenotype due to loss-of-function mutations in the *obese (ob)* gene. Intriguingly, this obese phenotype was readily reduced by exposing *ob/ob* mice to the circulation of lean mice in parabiosis experiments suggesting that they lack a putative ‘satiety factor’ in their circulation and its absence is making them eat voraciously (Coleman, 1973). In conjunction, Coleman’s and Hervey’s experiments together lead to the conclusion that a humoral factor is circulating in normal mice that acts on the hypothalamus in order to regulate feeding and adiposity. However, it took several decades until this circulating factor, the gene product of the *ob* gene, got finally characterized. Jeffrey Friedman and colleagues at Rockefeller University succeeded in the positional cloning of the *ob* gene (Zhang et al., 1994), which was found to be mainly expressed in white adipose tissue giving rise to a 16 kDa hormone that was soon given the name ‘leptin’ (greek: λεπτός or leptos for ‘thin’). In an endeavour that turned out as one of the most impactful discoveries in neuroendocrinology, Friedman and colleagues went on specifying the role of leptin. Over the next two decades, multiple research groups participated in unfolding the underlying principles of such an adipose-brain crosstalk and started to implement increasingly innovative technologies. Ultimately, the discovery of leptin catapulted the previously rather archaic study of eating physiology into a new era – that of modern molecular genetics and system neuroscience.

1.3.1 Biological functions of leptin

Leptin is produced in and secreted by white adipocytes and circulates in proportion to adipose tissue mass (Considine et al., 1996). Serum leptin concentrations thus reliably reflect long-term energy storage and convey information to the brain that adequate energy is available to sustain physiological processes such as fertility, thermoregulation, immune function, bone health and cognition. Conversely, reduced leptin concentrations, *e.g.* during starvation, were found to impact these physiological functions directly as well as indirectly by impairing various neuroendocrine axes including thyroid, adrenal and gonadal regulation (Wolfe et al., 2004). Intriguingly, substitution of exogenous leptin was demonstrated to partly correct certain aspects of respective neuroendocrine adaptations. Besides acting as a tonic signal, leptin concentrations have additionally been shown to also change abruptly in the face of acute changes in energy availability.

1.3.2 The leptin receptor (LepR) family

The major biological effects of leptin are mediated *via* its cognate receptor (LepR), which was discovered shortly after leptin itself. Importantly, six isoforms have been identified (LepRa-f), which all belong to the class I cytokine receptor superfamily and share the N-terminal domains. Importantly, however, the isoforms LepRa, c, d, and f possess truncated intracellular domains of 30-40 amino acids, are hence termed ‘short isoforms’ and induce only a restricted signaling cascade. In contrast, the only long form leptin receptor, LepRb, possesses the full intracellular domain and is responsible for mediating the full range of effects. While the short isoforms are widely expressed, the expression of LepRb is more restricted and mainly found in several nuclei of the hypothalamus including the ARC, the DMH, the VMH and the LH. Leptin binding to LepRb activates several different intracellular signaling cascades, including phosphorylation of signal transducer and activator of transcription 3 (pSTAT3), phosphatidylinositol-3-kinase (PI3K) and mitogen-activated protein-kinase (MAPK) (Myers et al., 2008). Historically, LepRb expression was believed to only be restricted to neuronal cell-types. More recently however, it got increasingly suggested that leptin acts on various non-neuronal cells as well (Fujita and Yamashita, 2019).

1.4 The arcuate nucleus of the hypothalamus: a major mediator of leptin action

Unarguably, though, the highest levels of LepR expression are found within neuronal cells that are located in distinct hypothalamic nuclei. Therefore, tremendous research effort has been placed on mapping out the neurocircuitries that integrate leptin-mediated information in order to control energy balance and body weight. Across all hypothalamic nuclei, leptin action is particularly evident in one distinct nucleus – the arcuate nucleus (ARC), which is located at the very base of the brain. By being placed directly adjacent to the median eminence, a circumventricular organ, ARC cells are privileged for the direct assessment of circulating feedback signals entering through local fenestrated blood vessel. Within the ARC, leptin profoundly influences two major population of neurons. Importantly, these two populations can be characterized by their distinct molecular signature with one population expressing AgRP/NPY, while the other subset can be identified by the expression of the POMC precursor neuropeptide instead. AgRP/NPY neurons and POMC neurons, respectively, exert opposing effects on feeding behavior and energy expenditure and are tangled up in an antagonistic relationship with each other. For instance, AgRP/NPY neurons get activated by food deprivation and proved necessary and sufficient to trigger feeding by increasing the consummatory drive. Upon a meal or exogenous leptin administration, however, AgRP/NPY neuronal activity is greatly reduced promoting the cessation of food intake. While AgRP/NPY neurons get inhibited by signaling cues of energy surplus, POMC neurons on the other hand increase their activity and promote satiety as well as an increase in energy expenditure. Intriguingly, both AgRP/NPY and POMC neurons exhibit enormously widespread projection patterns and innervate distant brain regions. Intriguingly, their respective innervation fields are overlapping to a great extent further underscoring their direct antagonistic relationship. Unarguably, the circuit of AgRP/NPY and POMC, also referred to as the central melanocortin system, plays an integral role in controlling energy homeostasis by integrating peripheral signals. More recently, however, it has been increasingly suggested that this neurocircuit is heavily reliant on various other, surrounding cell-types to execute all these important homeostatic functions.

1.5 Beyond neuronal circuits: the emerging field of glial cells in the control of whole-body energy homeostasis

Despite an increasing wealth of insights into the architecture of these circuits (Horvath et al., 2004; Zeltser et al., 2012; Andermann and Lowell, 2017) it soon became evident that confining to the cartography of an exclusively ‘neuronal blueprint’ would fail to translate into promising therapeutic strategies against the obesity pandemic. Hence, the field recently started to evolve from such a rather restrictive ‘neurocentric’ view towards a more holistic and integrated perspective taking various other cell types into account. This paradigm shift got significantly fuelled by the growing interest in one particular group of cells, the so-called glial cells.

1.5.1 Glial cells

Historically, the glia were considered as pure ‘brain glue’ or ‘gum’ (greek: γλία) fulfilling merely passive support functions such as the provision of structural stability. However, this early perspective has undergone tremendous transformation and the contemporarily held view on glial cells is that of highly abundant and heterogenous entities, which actively carry out complex tasks that are of utmost importance for proper brain function (Verkhatsky and Nedergaard, 2018). Over the years, four main types of glia have been identified each of which has been ascribed pivotal roles in brain physiology. Within these four subtypes, a major distinction is made between the smaller-sized microglia and the macroglia. The macroglia are further subdivided into astrocytes, oligodendrocytes and ependymal cells, which – despite their substantial distinctions – share an ectodermal, neuroepithelial origin.

Microglia, on the other hand, are derived from blood-borne macrophages and infiltrate the brain already during development and populating it from thereon. Microglial cells exist in various subtypes and constitute the immune effector cells of the CNS with important phagocytic as well as antigen-presenting properties.

Oligodendrocytes provide trophic support for neurons and form the very important myelin sheath at axons, which is a prerequisite for saltatory propagation of action potentials. Intriguingly, the precursor cells of oligodendrocytes, which are characterized by their expression of NG2 (chondroitin sulfate proteoglycane), turned out to not only constitute a progenitor pool but to also possess several unique functions themselves. Hence, NG2-positive

glia are increasingly considered a relevant subclass of glial cells with unique functional characteristics.

Ependymal cells line the ventricular system of the brain. They possess cellular specializations such as motile microvilli by which they are believed to circulate cerebrospinal fluid. Therefore, ependymal cells are speculated to participate in the distribution of signaling cues present in the cerebrospinal fluid throughout the brain *via* the ventricular route (volume transmission).

1.6 Astrocytes: abundant and multifaceted glial cells

1.6.1 Astrocytes in physiology and pathology

Astrocytes are highly abundant, star-shaped cells (latin: *astrum* for star), and generally considered as ‘housekeeper’ cells guaranteeing normal brain physiology by acting almost inconspicuously in the background. However, these glial cells are far from mere support cells but represent the cellular basis of additional information processing layered on top of neuronal circuits, tuning their activity state and thus impacting various brain functions including alertness (Papouin et al., 2017), autonomic function (Bouyakdan et al., 2019), decision making (Wang et al., 2017), depression-like symptoms (Cui et al., 2018) as well as learning and memory (Adamsky et al., 2018). While sophisticated methodology is required to unveil these delicate biological functions of astrocytes, the significance of this cell type becomes readily evident by any kind of brain injury as observed already by Rudolf Virchow during his first attempts to describe the *neuroglia* or ‘*Nervenkitz*’ (Virchow, 1856). Strikingly, the terminology used to document his *post-mortem* examinations of diseased nervous tissue was astonishingly specific and largely resembling what modern neuroscientists nowadays would refer to as ‘reactive astrogliosis’ or ‘glial scarring’. For instance, the histological assessment of an injured spinal cord revealed to him the presence of “*vielfach verfilzte, äußerst feine, aber derbe Fibrillen*” (multiple felted, extremely thin, however coarse, fibrils): a description, in which modern pathologists would immediately find analogy to the injury-induced changes in astrocytes. Compared to Virchow’s early chromic counter-staining, however, modern visualization methods of neuropathologists got more refined focusing now instead directly on changes in astrocytes as the most responsive cell type. The cytoskeletal protein glial fibrillary acidic protein (GFAP), an intermediate filament, is the most common marker used to visualise astrocytes and their primary cellular shape (Eng et al., 1971).

Early on, various kinds of injuries have been reported to increase its production by local astrocytes in and around the lesion site giving them a peculiar hypertrophic, bushy appearance typical for reactive astrocytes. Ever since its discovery up to present days, GFAP thus serves as the *bona fide* marker of astrocyte reactivity in response to injuries. Strikingly, however, the insults reported to induce GFAP reactivity are not limited to brain trauma, but occur also in neurodegeneration, sepsis and stroke amongst other neuro-pathologies (for review see Liddelow and Barres, 2017).

1.6.2 Phylogeny of astrocytes and astrocyte-like cells

Astrocyte-like cells were found in as distant species as flies further corroborating the essentiality of such cell-types. Notably, these cells perform seemingly analogous functions within the insect nervous system as compared to their mammalian counterparts (Freeman, 2015). Despite those analogies, phylogenetic comparative approaches suggest that astrocytes underwent dramatic increases in number and complexity along the evolutionary timescale. Thus, the nervous systems of more complex organisms tend to exhibit a higher astrocyte-to-neuron ratio correlating with more developed cognitive abilities. Accordingly, primates show a particularly high ratio with astrocytes additionally presenting a much more complex structure and morphology compared to *e.g.*, rodent astrocytes (Oberheim et al., 2006; Oberheim et al., 2009; Vasile et al., 2017). Human astrocytes in particular tend to be circa 3-fold larger and 10 times more ramified than rodent astrocytes. This in turn results in a way more sophisticated organization of human astrocytes and their integration into neurocircuitries. The unmet complexity of the human astroglial ‘interactome’ can be illustrated by the fact that a single human astrocyte can readily interact with 20-times as many synapses as a mouse astrocyte (mouse: 100,000 synapses *versus* human: 2,000,000 synapses) (Oberheim et al., 2009). One of the most striking examples supporting a superior contribution of hominid astrocytes to overall brain function stems from a pioneering study in which human astroglial progenitor cells got engrafted into neonatal immunodeficient mice. This engraftment protocol did not only result in the successful integration of donor cells into the host glial network, including the formation of intact gap junctions, but also in functional improvements (Han et al., 2013). Furthermore, recent gene expression profiling of both rodent and human astrocytes revealed intriguing transcriptional differences (Zhang et al.,

2016). Overall these findings suggest that higher cognitive abilities might result from the complexification within the hominid astrocyte niche rather than within the neuronal compartment.

1.6.3 Astrocyte heterogeneity among and within different brain regions

Astrocytes have traditionally been considered to be a homogenous, glue-like mass of cells. Yet, they constitute a highly diverse class of cells displaying substantial inter- and intra-regional heterogeneity in their morphology, transcriptional profiles and function (Haim and Rowitch, 2016), what seems to depend on the brain region and neurocircuits they are embedded in (Farmer et al., 2016). Astrocytes constitute territorial cells parcelling out the entire CNS. Despite their highly ramified and bushy appearance, individual astrocytes cover strictly separated domains defined by finger-like processes with as little as 5% overlap at their boundaries under physiological conditions (Bushong et al., 2002). Importantly, these interdigitations can remain constant even when astrocytes adopt a reactive, morphologically more complex state such as upon brain injury (Wilhelmsson et al., 2006). Besides this non-overlapping anatomical organisation, astrocytic subtypes have recently been demonstrated to segregate also functionally within the same brain region. In the course of an elegant study, Martín *et al.*, disentangled two separate genetically-defined neuroglia networks located in the basal ganglia, an anatomically well-cartographed forebrain structure. In the course of this work, it was found that one set of local astrocytes mediates between homotypic synapse of the direct nigrostriatal pathway, while another astrocytic subtype coordinates homosynaptic activity within the indirect striatopallidal pathway (Martín et al., 2015). Notably, astrocytes across different brain regions display even greater distinctions in their morphological, molecular and functional properties. Indeed, hippocampal astrocytes, which are primarily embedded in glutamatergic neurocircuits, were found to exhibit significantly different properties when compared to striatal astrocytes that are predominantly engaged in GABA-ergic neurocircuits (Chai et al., 2017). In conclusion, astrocytes show pronounced intra-and interregional specializations.

1.6.4 Astrocytes tune synaptic transmission at the ‘tripartite synapse’

Astrocytes constitute highly arborized cells and protrude their fine, stellar-like processes into the neuropil. Up to 95% of an astrocyte’s cell volume can be comprised of processes what further signifies the morphological complexity of this cell type (Shigetomi et al., 2013). However, it was not until the advent of electron microscopy in the 1950ies that it became possible to visualize and trace how these intricate processes infiltrate the grey matter (Gray, 1959). Strikingly, the subsequent analyses of brain ultrastructure revealed that astrocytic processes physically engulf synaptic contacts, an observation that immediately triggered speculations on the functional significance of such astrocyte-synapse spatial interactions. Given their intimate arrangements, astrocytes later got described to form a ‘glial cradle’ shielding the synaptic cleft by tight structural ensheathment. Not surprisingly, the initial standpoint of astroglia being only passive bystanders soon came into question and it got increasingly suggested that astrocytes readily sense synaptic activity taking place within their ‘glial cradle’. From 1990 onwards, a series of exciting *in-vitro* studies indeed began to provide supporting evidence for such a postulate. The addition of neurotransmitters to cultured astrocytes, for instance, was found to prominently evoke intracellular Ca^{2+} transients resulting in an oscillating signal that propagates to neighbouring cells in the form of waves (Cornell-Bell et al., 1990). Few years later, it was observed that astrocytes by themselves are capable of modulating the activity of surrounding neurons what promoted the appreciation of a bidirectional communication between astroglia and neurons – at least in cell culture systems (Nedergaard, 1994; Papura et al., 1994). In the course of the following two decades, the putative impact of astrocytes on neuronal excitability and synaptic activity was convincingly validated by hallmark electrophysiological studies conducted in both mice and human tissue preparations (Angulo et al., 2004; Pirttimaki and Parri, 2012; Navarrete et al., 2013). On the basis of these collective observations a new concept emerged by the end of the 20th century in which the traditionally held view on how the synaptic complex is organized was complemented by the involvement of astrocytes that form perisynaptic processes to actively participate in brain functions. Thus, the prevailing ‘neurocentric doctrine’ got ultimately dissolved and substituted by a more holistic concept coined the ‘*tripartite synapse*’ (Araque et al., 1999), which now allocates information processing and storage to neuron-glia networks utilizing both binary and analogue decoding.

Importantly, astrocyte-neuron spatial interactions turned out to be a highly dynamic process with environmental changes constantly tuning their formation and elimination. Thus, glial

processes have been found to rapidly engage with or retract from synapses in response to *e.g.*, parturition, long-term starvation and overnutrition or - even more acutely - in response to hunger and satiety (Stern and Armstrong, 1998; Langle et al., 2003; Di et al., 2013; Horvath and Diano, 2004). Evidently, these highly intriguing observations warrant for more detailed analysis of the involved mechanisms and their biological significance. Recent efforts successfully started to extend the molecular toolbox holding promise to resolve these nanoscaled interactions even at light-microscopic levels (Octeau et al., 2018).

1.6.5 Astrocytes are key components of the neuro-glia-vascular unit

The early neuroanatomists Camillo Golgi and Ramón y Cajal in the late 1800s have already claimed that astrocytes seem privileged for taking on important roles due to their unique anatomical positioning within the brain (Golgi, 1903, 1894; y Cajal, 1955). Astrocytes are situated at the interface between neurons and blood vessels and by that connect neuronal and vascular function. Strikingly, astrocytes cover most of vasculature of the brain with morphological specializations, the so-called perivascular endfeet (Matthijsen et al., 2010) . Indeed, most of protoplasmic astrocytes form direct contacts with the given blood vessels within its domain, a feature described in both rodent models as well as humans (Oberheim et al., 2009). Astrocytes also detect the release of neurotransmitters at the synapse to in turn guide blood flow towards brain regions with increased neural activity ('neurovascular coupling' or 'functional hyperemia') (Petzold and Murthy, 2011), which is crucially important in order to provide sufficient metabolic energy to fuel neuronal function.

1.7 The cerebral vasculature: sustainment of brain oxygenation, nutrient supply and homeostatic feedback

Despite constituting only 2% of human's mass, the brain occupies up to 25% of the body's entire glucose utilization. In order to burn this glucose effectively, nervous tissue requires the constant presence of sufficient amounts of oxygen. Thus, the brain is particularly reliant of constant and sufficient oxygen supply and hence exhibits a sophisticated, highly branched and dense angioarchitecture. Blood supply to the brain is guaranteed by two bilateral sets of sources: the internal carotid arteries (branching into anterior, middle and posterior cerebral arteries) and the two vertebral arteries, which merge at the pons to form the

basilar artery (giving rise to the pontine, cerebellar and posterior cerebral arteries). Intriguingly, the internal carotids join with the basilar artery to form an arterial ring-like structure at the base of the brain, which is referred to as ‘circle of Willis’; in case of the occlusion of any major supply artery, this safety organization serves as backup circulation in order to sustain at least minimal perfusion of the brain. For the quantitative study of brain function and disease, accurate and detailed information is urgently required on how blood supply of the brain is organized – even down to the capillary level. Indeed, a brief interruption of blood supply to the brain in the range of seconds to minutes may imply fatal consequences such as loss of consciousness, brain damage or even death. Driven by several technical advances, *e.g.* in three-dimensional imaging and deep learning algorithms, a more and more detailed atlas has emerged providing a valuable resource on the organization of the mouse brain vasculature (Blinder et al., 2013; Xiong et al., 2017; Todorov et al., 2019).

1.7.1 The blood-brain barrier and its anatomical organization

Besides its intricate and complex distribution, the cerebrovasculature exhibits certain additional peculiarities, which are summarized under the concept of the blood-brain-barrier (BBB). Specifically, cerebral blood vessels possess a selective barrier function and prevent neurotoxic plasma components and pathogens from entering the brain. Two important cellular components are involved in sealing the brain endothelium: tight junctions (*e.g.*, claudins, occludins and zonulins) and adherens junctions (*e.g.* cadherins) (Tietz and Engelhard, 2015). These proteins are expressed by brain endothelial cells and tightly interconnect them such that unlimited paracellular transport across the BBB is prevented. In addition to these endothelium-intrinsic specializations, other cell types crucially contribute to the development and maintenance of the BBB as well, such as pericytes.

Pericytes are specialized mural cells that adhere to the abluminal side of the endothelium. In fact, pericytes are embedded right within the basement membrane of the vasculature. By that, pericytes form peg-socket focal contacts with endothelial cells and are ideally situated to exchange metabolites, ions and second messengers. Overall, pericytes act as microvascular stabilizers and are considered indispensable for vascular integrity. Interestingly, pericyte detachment and degeneration represent features of several neurological disorders such as Alzheimer’s disease (Nortley et al., 2019), amyotrophic lateral sclerosis (Winkler et al.,

2013) and stroke (Hall et al., 2014). Moreover, pericyte loss can be induced in mouse models by disrupting PDGF/PDGFR β signaling and typically result in severe phenotypes further underscoring the significance of this cell type for the maintenance of proper vascular function (Lindhahl et al., 1997; Ogura et al., 2017).

As mentioned above, **astrocytes** constitute another cell type crucially involved in regulating vessel properties within the brain. Astroglial endfeet cover most of the cerebrovasculature in order to provide structural support. In addition, astrocytes release trophic and vasomodulatory factors in the immediate vicinity of the endothelium. For instance, astrocytes turned out being crucially important for the correct deposition of the extracellular matrix protein laminin and a defect in astrocyte-secreted laminin results in severe breakdown of the BBB (Yao et al., 2014).

1.8 Brain oxygenation: coupling of brain function to metabolism

Life on earth could not have had emerged in such complexity and diversity without the presence of molecular oxygen. Around 3 billion years ago, the appearance of the first photosynthetic systems in oceanic cyanobacteria lead to a dramatic shift in the atmospheric composition with widespread consequences. The rising production of molecular oxygen during this period ('Great Oxygenation Event') is largely considered the driving force of complex life on earth. From thereon, the story of evolution had especially been shaped by the triumphant advent of heterotrophic organisms. Ranging from yeast to man, heterotrophs generally rely on the uptake and oxidation of organic molecules in order to meet their energetic needs; however, the efficiency of their respective energy metabolism varies tremendously. The highest yield of cellular energy is obtained by the entire combustion of organic compounds what requires the presence of a final electron acceptor such as molecular oxygen ('aerobic oxidation'). The unsurpassed thermodynamic efficiency of aerobic oxidation provides an abundance of cellular energy so it can be utilized to fuel increasingly complex processes and organismal organizations such as multi-cellularity. Multi-cellularity in particular, however, additionally implicates that oxygen needs to adequately reach all the oxygen-thriving cells of a metazoan organism. In order to suffice this need, various specialized systems evolved.

Introduction

In mammals the optimization of oxygen transport culminated in the development of the so-called cardio-pulmonary–vascular system. Here, distribution of oxygen is carried out by the blood, a body fluid with high oxygen-binding capacity due to specialized cells (erythrocytes) which make up 40-45% of the blood. After being laden with oxygen in the lungs, erythrocytes get circulated throughout the body *via* pressure waves generated by the pumping heart in order to release oxygen at distal sites (oxygen tensions in human tissue: see **Table 1 and 2**). Though, adequate oxygen supply has to be guaranteed under the most varying circumstances ranging from deep sleep to extreme physical activities like an ascent to 4,000 meters altitude. As a consequence, there need to be a tight coordination of all involved components. The high dynamic range of this system as a whole becomes immediately apparent for everybody who is running stairs and consequently increasing heart rate and respiratory frequency.

Table 1: Overview of various oxygen tensions in human tissues.

<i>Organ</i>	<i>physiological pO_2 (mmHg)</i>	<i>% O_2</i>
<i>Trachea</i>	<i>150</i>	<i>19.7</i>
<i>Alveoli</i>	<i>110</i>	<i>14.5</i>
<i>Arterial blood</i>	<i>100</i>	<i>13.2</i>
<i>Pulmonary arterial blood</i>	<i>40</i>	<i>5.3</i>
<i>Brain</i>	<i>35</i>	<i>4.4</i>
<i>Kidney</i>	<i>72</i>	<i>9.5</i>
<i>Liver</i>	<i>41</i>	<i>4.5</i>
<i>Muscle</i>	<i>29</i>	<i>3.8</i>

(adapted from (Koh and Powis, 2012))

1.8.1 Hypoxia: mismatch between vascular perfusion and oxygen demand

Vascularization of large, complex organisms such as mammals serves to distribute metabolic fuel as well as oxygen towards distal tissues. In a seminal study carried out in 1919, August Krogh provided the first experimental evidence suggesting that the metabolic need of the given target tissue itself might signal adaptive changes to regulate its own vascularity. This initial observation of a tight coordination between vessel density and oxygen demand (Krogh, 1919a, 1919b) spurred the search for a putative oxygen-sensing mechanism within the common cell. However, the temporal lag between a hypoxic period and increased vessel formation of at least two to three weeks hampered the identification of direct and immediate signaling cascades.

Table 2: Biologically relevant oxygen tensions

<i>Condition</i>	<i>pO₂ (mmHg)</i>	<i>% O₂</i>
<i>Normoxia (ambient)</i>	<i>159</i>	<i>21</i>
<i>Physiological Hypoxia (Physoxia)</i>	<i>15-68</i>	<i>2-8</i>
<i>Mild Hypoxia</i>	<i>8-28</i>	<i>1-5</i>
<i>Hypoxia</i>	<i><8</i>	<i>< 1</i>
<i>Anoxia</i>	<i><0.08</i>	<i>< 0.1</i>

Given this chasm, researchers shifted focus and started to investigate another adaptive mechanism instead that evolved in mammals in order to counteract hypoxia – namely the remarkably rapid increased production of red blood cells (erythropoiesis). Following hypoxic stimulation, massive amounts of the hormone erythropoietin (EPO) are secreted by interstitial fibroblasts within the renal cortex. In turn, EPO signals to the red bone marrow as the major hematopoietic organ, where it induces the proliferation and differentiation of red blood cell precursors (Jelkmann, 2007). With a 100-fold increase in circulating EPO at 7.5% oxygen, this response represents one of the most striking adaptive processes ever observed across endocrine systems. In light of such magnitude and immediacy, researchers suspected experimentally traceable elements that could help to identify the molecular link between hypoxia detection and the body's counterregulation.

Introduction

A research duo at the John Hopkins University School of Medicine, personified by Gregg Semenza and Guang Wang, were indeed successful in their search for a direct sensing mechanism of oxygen. Between 1992 and 1993, they described the purification of a nuclear transcription factor, which is induced by hypoxia through *de-novo* protein synthesis and physically engages with a short nucleotide sequence within the 3'-flanking region of the human EPO gene to enhance gene transcription (Semenza and Wang, 1992; Wang and Semenza, 1993). The newly-identified protein was consequently termed hypoxia-inducible factor 1 (HIF-1). However, our early conception of this factor transformed almost immediately as HIF-1 soon turned out not being restricted to the kidney only but to play pivotal roles in almost every mammalian cell.

In retrospect, the initial discovery of HIF-1 in renal fibroblast is now rather regarded as the ignition cap of one of the most flourishing research fields. It soon became obvious that HIF-1 constitutes a key regulator of a broad range of adaptive responses to reduced oxygen availability in the entire body. Those responses turned out to range from the adjustment of bioenergetics on the cellular level up to systemic changes such as hormone secretion, erythropoiesis and - as will be emphasized more in the following - the growth of new blood vessels (angiogenesis).

Molecular Structure of HIF-1. Investigations of its crystal structure revealed HIF to be composed of two independent subunits, each presenting features of generic helix-loop-helix proteins of the bHLH-PAS family (PER, AHR, ARNT and SIM family; Wang et al., 1995; Wu et al., 2015). The constitutively expressed subunit HIF-1 β /ARNT (aryl hydrocarbon receptor Ahr nuclear translocator) is a non-oxygen-responsive protein which is constantly present in the cell's nucleus. Interestingly, it displays several transcriptional roles on its own other than those dedicated to hypoxia adaptation (*e.g.*, xenobiotic response and neuroendocrine development; Swanson et al., 1995). The actual oxygen-dependent regulation occurs at the remaining cognate α -subunit. Despite getting translated constitutively as well, the α -subunit is subjected to constant degradation at normoxic conditions. However, as soon as cells get exposed to oxygen concentrations less than 6% (40 mmHg at sea level) the α -subunit escapes its degradation what leads to its exponential build-up and eventual translocation into the nucleus. Such post-translational regulation appears wasteful; in fact, however, it is absolutely essential for cell adaptations to life-threatening conditions that have to be executed immediately and require bypassing of lengthy processes such as gene transcription and translation. Thus far, three separately encoded isoforms of the α -subunit

have been discovered: HIF-1 α constitutes the archetypal, principal isoform and exhibits ubiquitous and very pronounced effects on animal physiology. In addition, HIF-2 α (also known as endothelial (E)PAS) exist as an isoform sharing 48% amino acid sequence identity and is expressed in a more restricted manner such as in the endothelium, type II pneumocytes in the lung, liver parenchymal cells, renal interstitial cells and in the cartilage (reviewed in Bertout et al., 2008). Likewise, it turned out that HIF-1 α associates with substantially more HRE-binding sites than HIF-2 α (546 for HIF-1 α versus 143 for HIF-2 α). Despite similar binding affinities to the HRE motif, a reduced contribution of HIF-2 α to the transcriptional responses to acute hypoxia was observed – at least in *in-vitro* models (Mole et al., 2009; Xia and Kung, 2009). However, in certain tissues with predominant HIF-2 α expression such as the lung, cartilage or the kidney, HRE occupancy might likely be dominated by HIF-2 α instead. Intriguingly, it has been suggested that HIF-1 α and HIF-2 α expression might shift in pathological conditions such as tumorigenesis in certain cancers (*e.g.*, non-small-cell lung cancer, head and neck squamous cell carcinoma and neuroblastoma; reviewed in Bertout et al., 2008). In these malignancies, HIF-2 α expression has been identified as being a negative prognostic factor probably conferring increased oncogenic activity (reviewed in Kaelin and Ratcliffe, 2008). In conclusion, these lines of evidence suggest that despite a similar HRE-binding, HIF-1 α and HIF-2 α appear to produce a largely non-overlapping, non-redundant transcriptional output. The third isoform is named HIF-3 α (IPAS) and appears to have inhibitory function by preventing HIF-1 α to bind its obligate heterodimeric partner HIF-1 β .

Post-translational regulation of HIF- α stability and transactivation function. Under normal oxygen levels (normoxia; see **Table 2**) the constitutively expressed HIF- α subunit is immediately subjected to enzymatic modifications destining it for its subsequent destruction. The N-terminal transactivation domain of the HIF- α protein contains two highly conserved proline residues (Pro402 and Pro564 in HIF-1 α , and Pro405 and Pro531 in HIF-2 α , respectively), which are all targeted by so called prolyl-4-hydroxylase domain (PHDs) enzymes. Importantly, PHD enzymes are part of a superfamily of oxygenases, whose activity is not only dependent on the presence of ferrous iron (Fe(II)) and α -ketoglutarate, but especially on the availability of intracellular oxygen. Three isoforms have been described so far (PHD1-3), from which PHD2 is displaying the most pronounced impact on HIF signaling (Appelhoff et al., 2004). Under normoxia, PHD enzymes will enzymatically split molecular oxygen to subsequently hydroxylate HIF- α at one (or both) of its conserved proline residues.

Introduction

The actual incorporation of oxygen atoms into HIF- α to form oxidized amino acids has been confirmed by isotopic tracing using ^{18}O (Hewitson et al., 2002). This hydroxylation is key for the binding of the von Hippel-Lindau (vHL) E3 ubiquitin ligase complex, what results in the polyubiquitination of the HIF- α protein targeting it to the proteosomal degradation pathway (reviewed in Kaelin, 2018). Hence, the part within the N-terminus of the HIF- α subunit containing these conserved proline residues is generally referred to as O_2 -dependent degradation domain (ODD). Nowadays, it is well-established that the ODD is targeted by PHD1-3 enzymes. Studies on the enzymatic kinetics of PHD1-3 revealed K_M values for oxygen concentrations to be around 100 μM and therefore way above the intracellular $p\text{O}_2$ (typically 10-30 μM). This implies that under physiological conditions, PHD1-3 are typically exposed to oxygen concentrations well within its most sensitive range of actions rendering it an ideal ‘oxygen sensor’ across the physiological range. As soon as oxygen availability is reduced, such as during hypoxic stress, less O_2 molecules are available for HIF- α hydroxylation so it more frequently escapes its degradation to onset adaptive transcriptional responses (**Figure 2**). Importantly, however, considering HIF signaling merely as an ‘on-off’ switch is likely not reflecting reality but rather should it be considered as a ‘rheostat’ tuning cell physiology in incremental fashion. Aside from oxygen concentrations, PHD1-3 enzymes are profoundly regulated by the availability of Fe(II). As for many dioxygenases, correct enzyme metalation and incorporation of Fe(II) into the catalytic center is essential for its hydroxylase activity (reviewed in Kaelin and Ratcliffe, 2008). Thus, PHD1-3 additionally act as a cellular iron sensor and increases HIF signaling in response to iron shortage. Notably, however, HIF signaling on the one hand and iron status of the cell influence each other in a mutual and reciprocal manner. Activated HIF signaling significantly increases cellular iron by directly upregulating the expression of several proteins involved in iron transport and storage. Such a tight coordination of oxygen and iron homeostasis appears intuitive from a physiological perspective given the substantial requirement of iron *e.g.*, for the process of erythropoiesis, the production of oxygen-carrying red blood cells. In addition, various other ferro-proteins are known to play important roles in oxygen transport and homeostasis in individual organ systems, exemplified by myoglobin in muscle (Gros et al., 2010) or neuroglobin in nervous tissue (Fago et al., 2004). The pharmacological inhibition of PHD1-3 using iron chelators or transition metals like cobalt works by displacing Fe(II) and can be employed for inducing HIF signaling. A substantial therapeutic interest exists in harnessing this iron-sensitive molecular pathway for clinical applications such as the treatment of ischemic disease. The most advanced pharmaceuticals constitute two oral PHD

Introduction

inhibitors FG-2216 and FG-4592 (*Roxadustat*), which have been evaluated for their use in renal anemia in clinical trials (van de Groenendaal et al., 2016). However, several additional molecular targets emerged permitting beneficial HIF activation under circumstances such as wound healing in diabetic mice (Botusan et al., 2008) or ischemic/hemorrhagic stroke (Karuppagounder and Ratan, 2012). In addition to iron, several cellular metabolites have been identified to profoundly influence PHD1-3 activity. Within the catalytic center, PHD1-3 contain a two-histidin-one-carboxylate triade to coordinate Fe(II) while exposing two additional positions for the binding of α -ketoglutarate, also known as 2-oxoglutarate, an important intermediate metabolite of the Krebs cycle. In order to guarantee functional catalysis of the hydroxylation reaction, presence of α -ketoglutarate is absolutely mandatory as it serves as an acceptor molecule for the remaining oxygen atom. As a consequence, α -ketoglutarate undergoes oxidative decarboxylation to form succinate and CO₂. Biochemical investigations then shed light on a range of intermediate metabolites in the Krebs cycle, which interfere with the facilitative action of α -ketoglutarate on PHD1-3 activity. Among them, succinate and fumarate turned out to be particularly powerful in outcompeting α -ketoglutarate with similar IC₅₀s, by that suppressing PHD1-3 and activating HIF signaling as a consequence (Koivunen et al., 2007). Consistently, mutations in the genes encoding for fumarate hydratase (FH) (Isaacs et al., 2005) and succinate hydrogenase (SDH) (Selak et al., 2005; Pollard et al., 2005) both confer high oncogenicity by accumulating respective metabolites and activating excessive HIF signaling. Given that these metabolites typically cannot diffuse across cell membranes, cell-permeable derivatives have been developed with the aim to either suppress or increase HIF signaling by using cell-permeable versions of α -ketoglutarate (MacKenzie et al., 2007) or succinate/fumarate, respectively (Ehinger et al., 2016). Last but not least, PHD1-3 activity is additionally regulated by reactive oxygen species (ROS), which are typically increased under hypoxic stress with O₂ lacking as final electron acceptor. Oxidative stress, particularly free radicals escaping at the mitochondrial complex III (cytochrome c reductase), potently inhibit PHD1-3 activity and are thus suggested to signal oxygen shortage from the mitochondria to cytosolic PHD1-3/HIF- α proteins (Guzy et al., 2005; Klimova and Chandel, 2008). A second important mechanism exist in which an asparagine residue (Asn803 in HIF-1 α and Asn851 in HIF-2 α) located in the C-terminus of the protein gets hydroxylated by another oxygenase enzymes named factor inhibiting HIF-1 (FIH1) (Mahon et al., 2001; Lando et al., 2002). The resultant steric change in conformation prevents the recruitment of the essential co-activator CBP/p300 (CREB-binding protein/E1A binding protein 300). Intriguingly, FIH1 is operating at lower oxygen

levels as compared to PHD1-3 and is hence suggested to suppress remaining HIF signaling under normoxia (Dayan et al., 2006). In addition, differences exist in terms of the susceptibility of the two different isoforms with HIF-2 α being relatively more resistant to asparagyl hydroxylation (Bracken et al., 2006). Thus, FIH1-mediated silencing of HIF-2 α might occur delayed and depend on deeper hypoxia relative to HIF-1 α . In conclusion, various different mechanisms exist efficiently suppressing HIF signaling under well-oxygenated conditions while allowing for a rapid accumulation of HIF- α as soon as oxygen becomes scarce (**Figure 2**).

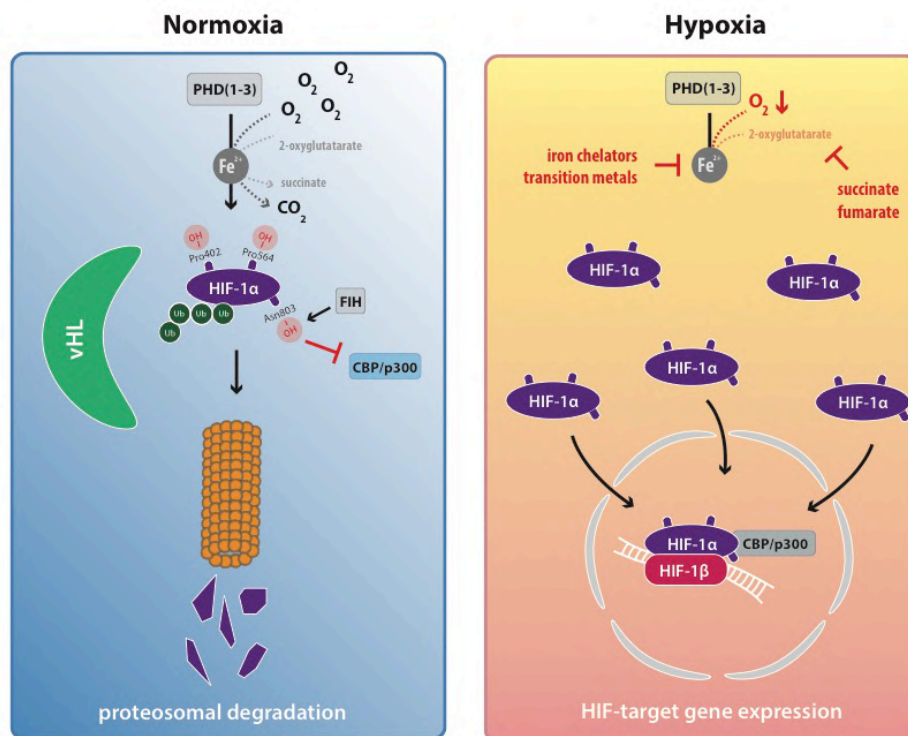


Figure 2: Schematic diagram of posttranslational regulation of HIF-1 α activity.

Under normoxic condition, HIF-1 α is subjected to constant hydroxylation of two proline and one asparagine residue triggering its proteasomal degradation and silencing of transcriptional activity, respectively. Under reduced oxygen concentrations, shortage of ferrous iron and/or excessive levels of succinate and fumarate, HIF-1 α bypasses its degradation, starts to accumulate and ultimately translocates into the nucleus where it forms a functional dimer in order to initiate the transcription of its target genes. HIF-1 α : hypoxia-inducible factor 1 α ; PHD(1-3): prolyl-4-hydroxylase domain enzymes 1-3; O₂: oxygen; CO₂: carbondioxide; OH: hydroxyl groups; vHL: von Hippel-Lindau E3 ubiquitin ligase; ub: ubiquitin; FIH: factor inhibiting HIF; CBP/p300: CREB-binding protein/E1A binding protein 300.

Introduction

Under extended conditions of hypoxia, the HIF- α subunit gets induced, accumulates and translocates into the nucleus. As soon as the α - and β -subunits assemble into a functional dimer, the complex binds DNA at a core pentanucleotide sequence (RCGTG) with high specificity. This core motif was shown to be enriched in so-called ‘hypoxia response elements’ (HRE), which has initially been demonstrated in 50 gene loci identified *a priori* to contain hypoxia-inducible target genes (Wenger et al., 2005).

HIF-responsive target genes. Later on, a series of genome-wide transcript analyses using microarrays indicated an even larger number of HIF-induced target genes and way more frequent HIF-DNA interactions as previously assumed (Greijer et al., 2005; Mole et al., 2009). In support of these collective observations, a tiled promoter assay using chromatin immunoprecipitation (ChIP) identified more than 800 binding sites for HIF to be present across the human genome (Schödel et al., 2011). It needs to be noted, though, that these experiments have been conducted *in-vitro* using MCF7 breast cancer cells. Thus, caution should be taken for any generalization or extrapolation to other cell types in *in-vivo* contexts. Cell culture conditions including uniform oxygen concentrations, cell line immortalization *et cetera* could result in aberrant cellular behavior and chromatin accessibility misestimating HIF-DNA interaction sites. Regardless of their total number, a subset of several dozens of core target genes emerged across numerous studies, providing us with a characteristic signature of HIF-dependent gene expression (see **Table 3**).

Table 3: HIF-responsive target genes.

<i>Function</i>	<i>Target gene</i>
<i>Angiogenesis</i>	<i>VEGF, FLT-1, ENG, LEP, LRP1, ADM, TGF-β3, EG-VEGF</i>
<i>Erythropoiesis</i>	<i>EPO</i>
<i>Glucose metabolism</i>	<i>LDHA, GLUT1, PDK-1, PFKFB-3, HK-1/2, COX4-2, MCT-4</i>
<i>pH buffering</i>	<i>CA-IX, NHE-1</i>
<i>Vasodilation</i>	<i>NOS2</i>
<i>Proliferation and chemotaxis</i>	<i>IGF2, C-MYC, CXCR-4, SDF-1</i>
<i>Extracellular matrix remodeling</i>	<i>MMPs, uPAR</i>

Introduction

Abbreviations: VEGF: vascular-endothelial growth factor; FLT-1: fms related tyrosine kinase 1 (aka VEGFR-1); ENG: endoglin; LEP: leptin; LPR1: low-density lipoprotein receptor-related protein 1; ADM: adrenomedullin; TGF- β 3: transforming growth factor β 3; EG-VEGF: endocrine gland-derived VEGF; EPO: erythropoietin; LDHA: lactate dehydrogenase A; GLUT1: glucose transporter 1; PDK1: pyruvate dehydrogenase kinase 1; PFKFB-3: 6-phosphofructo-2-kinase/fructose-2,6-biphosphatase 3; HK-1/2: hexokinase 1 and 2; COX4-2: cytochrome c oxidase subunit 4 isoform 2; MCT-4: monocarboxylate transporter 4; CA-IX: carbonic anhydrase 9; NHE-1: sodium-hydrogen antiporter 1; NOS2: endothelial nitric oxide synthase; IGF2: insulin growth factor 2; C-MYC: myelocytomatosis virus oncogene cellular homolog; CXCR-4: C-X-X chemokine receptor type 4; SDF-1: stromal derived growth factor 1; MMPs: matrix metalloproteinases; uPAR: urokinase receptor.

1.8.2 Angiogenesis as a hallmark of vascular remodeling

The vessel architecture is exquisitely designed for coupling metabolic insufficiencies on the one hand, as well as toxic hyperoxygenation on the other. In the embryo, the vasculature gets formed strikingly early (21 days *post-conceptionem* in humans) by a process called ‘vasculogenesis’. During this event, mesoderm-derived endothelial precursor cells (free angioblasts) aggregate and assemble themselves into primitive tubular structures by electrostatic repulsions between opposing apical cell surfaces. This early vascular tube, or endothelial cord, then undergoes elongation, flattening and a widening of its lumen. Following its initial formation, however, the vascular system is far from being static but retains the capacity for extensive remodeling throughout the entire life span of an organism. Despite its apparent significance for whole-body physiology, the underlying mechanisms governing adult neovascularization remained elusive for a long time.

August Krogh, a Danish physiologist, was among the first to promote the idea that the oxygen demand of a given target tissue elicits signals to regulate its own vascularization. While studying striated muscles from various animals, he observed an astonishing correlation between capillary density and the metabolic rate of the given muscle demand (Krogh, 1919a, 1919b). Such tight coupling between the angioarchitecture and tissue metabolism was repeatedly corroborated by subsequent research (Kayar et al., 1988). Elegant interventional approaches additionally proved that muscle capillary density is subject to profound adjustment being readily reducible by immobilization on the one hand (Józsa et al., 1980) while constant neural stimulation on the other hand results in a vast increase in vascularity (Hudlicka et al., 1982). With the advent of molecular biology it became possible to identify the underlying mechanisms that coordinate the postnatal formation of blood vessels, which turned out to be distinct from those observed during *de-novo* vasculogenesis.

Introduction

Importantly, the postnatal adaptive process that optimises oxygen transport requires pre-existing vasculature and involves the sprouting of new vessel branches by endothelial proliferation – a process later coined ‘angiogenesis’ (Adams and Alitalo, 2007). Upon stimulation, endothelial cells have been observed to possess the capacity for exiting quiescence, entering proliferation and develop cellular specifications such as highly motile and invasive filopodia protrusions. Attracted by guidance cues, a sub-fraction of endothelial cells adopts a ‘tip cell’ phenotype in order to form a spearhead that protrudes into surrounding tissue. The following ‘stalk cells’ receive suppressive, paracrine signaling from the leading tip cells, rendering them less invasive with fewer filopodia, however, with a high proliferative capacity instead for supporting branch elongation. As soon as tip cells from neighbouring sprouts approach each other, vessel loops are generated by a process called anastomose, a continuous lumen is generated and perfusion of the new sprout gets established. Vessel maturation is ultimately completed by the built up of a basement membrane and the recruitment of mural cells like pericytes or vascular smooth muscle cells (arteriogenesis) (Jain, 2003). Despite a long research history, however, the exact molecular signature that orchestrates physiological angiogenesis remains incompletely understood. This is largely due to the vast array of chemically diverse signals that are participating in this process. The orchestration of signals is thought to follow (i) highly balanced spatial patterns (ii) along nuanced concentration gradients while (iii) being subjected to precise temporal sequences. The specific interplays between multiple signals in various spatiotemporal dimensions inevitably culminates in a phenomenon hard to grasp. Hence, our basic understanding of what constitutes physiological angiogenesis is still in its beginnings - let alone the screening for strategies to therapeutically harness such an angiogenic program in a safe way *e.g.*, for re-vascularizing ischemic tissues. While the control of physiological angiogenesis is far from being understood, the processes leading to pathological vessel formation (*e.g.*, in tumors and wounds) are laid out more conclusively in the scientific literature (Thomlinson and Gray, 1955; Knighton et al., 1981). First and foremost, this is due to the rather basic and crude angiogenic program driving it. Only a small subset of excessively secreted cytokines has been shown to be sufficient what rendered pathologic angiogenesis a way simpler constellation and hence opened up much better modelling possibilities. In turn, these insights began to fuel high hopes for its therapeutic applicability for instance in the realms of blocking abnormal vessel formation. From a morphological standpoint, irregular vasculature is known to branch non-uniformly, to be hyperpermeable towards plasma proteins and to form abnormal structures including hemangioma, microaneurisms, torturous vessels and arteriovenous shunts.

Overall, locally defective vasculature seriously exacerbates diseased tissue function, often rendering it non-responsive for therapeutic intervention due to hampered drug distribution.

1.8.3 Vascular-endothelial growth factors (VEGF) – the angiogenic master switch

The early observation that the transplantation of tumor cells results in a massive neovascularization of the surrounding tissue suggested the involvement of secreted factors with pro-angiogenic activity (Ide et al., 1939). Subsequent research identified several of those soluble molecules including the fibroblast growth factor family (acid and basic FGF), transforming growth factor β (TGF β), angiopoietins, angiogenin and platelet-derived growth factor β (PDGF β), to just name a few. Among them, however, one factor stood out and emerged as a crucial master switch of vessel formation in both health and disease, the so called vascular-growth factor A (VEGF-A; from now on only referred to as VEGF).

The significance of VEGF for the field of angiogenesis and vascular biology becomes immediately evident when noticing that a PubMed search for the term ‘angiogenesis’ *per se* yields circa 107,000 hits whereas searching ‘vascular-endothelial growth factor’ already identifies almost 90,000 publications and thus only marginally less (retrieved 06.06.2019). This fact not only provides a first glance at the magnitude of these two research fields but already hints at their intimate interconnections and mutual influence. Importantly, VEGF (VEGF-A) constitute the founding, first to-be-identified member of an entire family of related factors. Initially, however, the archetypal VEGF was termed ‘vascular permeabilizing factor’ (VPF) instead given its extremely pronounced permeabilizing activity at microvessels (40,000-times greater than histamine on a molar basis; Senger et al., 1983/1993). Though, the subsequent discovery of a broad range of effects exerted by VEGF resulted in a shift in emphasis with most attention unarguably drawn towards VEGF-induced angiogenesis. Native VEGF constitutes a homodimeric glycoprotein (MW:45kDa) with a high binding affinity towards heparin. The human *VEGFA* gene is composed of eight exons interrupted by seven introns. Alternative splicing gives rise to four major isoforms namely VEGF₁₂₁, VEGF₁₆₅, VEGF₁₈₉, and VEGF₂₀₆ (**Figure 3**; Harper and Bates, 2008). Otherwise identical, murine VEGF isoforms are consistently one residue shorter in length than their human equivalents. VEGF₁₆₅ (and VEGF₁₆₄ in mice) constitute the predominant isoform which is not only the most frequently expressed but also the one exerting the most physiologically relevant effects

Introduction

(reviewed in Ferrara et al., 2003 and Olsson et al., 2006). In terms of molecular characteristics, VEGF₁₆₅ is situated between the highly diffusible VEGF₁₂₁ and the rather large and immobile VEGF₁₈₉, which is largely retained within the adjacent extracellular matrix due to its high binding affinity to heparin. Differences in heparin-binding among the different isoforms can be explained genomically since the heparin-binding domains are encoded by exon 6 and 7, which are present in VEGF₁₈₉ and absent in VEGF₁₂₁, respectively. The intermediate VEGF₁₆₅ contains only exon 7 and is thus more ambiguous and versatile in its molecular behavior.

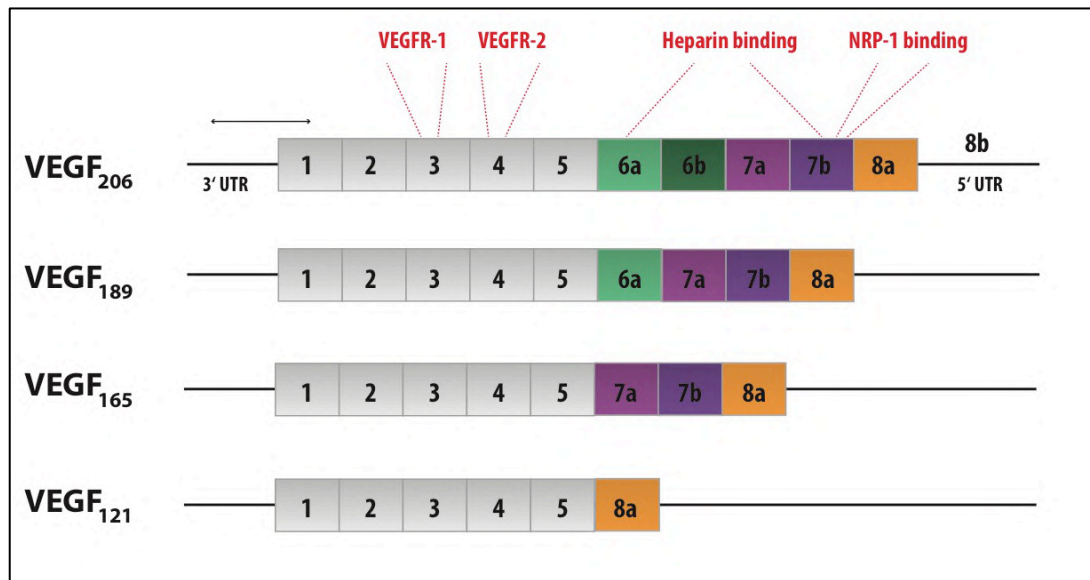


Figure 3: Schematic overview on the main splice variants of the human VEGF gene.

The VEGF gene is composed of eight exons, the first five of which are necessary for its biological function. Exon six to eight, however, allow for substantial alternative splicing with each splice variant giving rise to isoforms of distinct molecular behaviors. The longest isoform (VEGF₂₀₆) for instance is highly affine to heparin, hence poorly diffusible and mainly retained within the extracellular matrix. On the other hand, Exon 7b encodes for binding sites of NRP-1 (neuropilin-1 co-receptor) and is consistently absent in the less angiogenic, but highly diffusible, isoform VEGF₁₂₁. Importantly, VEGF₁₆₅ constitutes the predominant isoform with intermediate properties in terms of diffusibility and angiogenicity. Adapted from (Harper and Bates, 2008).

While VEGF is considered a highly potent master switch with vast downstream effects, the action of the remaining family members within the VPF/VEGF family appear more specific and nuanced. Namely, those are comprised by VEGF-B, -C, and -D as well as the placental growth factor (PlGF) all constituting dimeric glycoproteins of approximately 40 kDa.

Specifically, VEGF-B has been demonstrated to be crucial for the vascularization of the heart and particularly for development of coronary arteries (Joukov et al., 1997). In contrast, VEGF-C and -D primarily promote lymphangiogenesis but have the potential to exhibit mild angiogenic and permeabilizing properties in specific contexts (Tammela and Alitalo, 2010). Originally being confined to the placenta, more recent evidence suggests that PlGF is also expressed in tumors where it seems to play a significant role in pathological angiogenesis (Carmeliet et al., 2001). This intriguing observation immediately stimulated the investigation of anti-PlGF therapy as an alternative treatment options in oncology (Fischer et al., 2007). Finally, the VEGF family is complemented by structurally-related, homologous molecules that have been discovered in parapoxvirus (VEGF-E) and snake venom (class of VEGF-Fs) (Suto et al., 2005).

The family of VEGF receptors. VEGF/VEGF family members interact with a cognate receptor system consisting of three high-affinity receptor tyrosine kinases: VEGFR-1 (Flt-1), VEGFR-2 (KDR/Flk-1) and VEGFR-3 (FLT-4). Normal vascular endothelium displays abundant expression of both VEGFR-1 and VEGFR-2. Even though, the latter exhibits a ten-fold lower affinity for VEGF this is compensated by a generally much higher expression level. In addition to the level of receptors to be expressed, their exact cellular localization within the vascular endothelium is of high significance as well. Endothelial cells are highly polarized and thus exhibit specialized receptor distributions. For instances, blood-neural interfaces of the retina and the brain, however not in the lung, display a clear segregation of the two receptors within the endothelial cell with VEGFR-1 being localized to luminal side while VEGFR-2 rather faces the abluminal-parenchymal side. Such apicobasal polarization allows for a precise adjustment of vascular physiology by initiating distinct signaling pattern depending on whether VEGF is blood-borne or emanating from the parenchyma (Hudson et al., 2014). Structurally, both VEGFR1 (Flt-1) and VEGFR-2 (KDR/Flk-1) share seven immunoglobulin-like extracellular domains of circa 750 amino acids, one transmembrane domain as well as a tyrosine kinase motif with a kinase-insert domain interspersed (Shibuya, 2013). Their activity status is determined first and foremost by the availability of its primary ligand VEGF, whose binding is required for receptor dimerization and precise juxta-positioning of the monomeric receptor subunits (Ruch et al., 2007). As with most growth factor receptors (including platelet-derived or epidermal growth factor receptor), their intracellular domains can undergo substantial structural transformations so that they reveal additional docking sites for the diversification of downstream signal transduction.

Introduction

Besides more generalized processes (cell survival, proliferation and migration), VEGF receptor signaling promotes several unique effects such as the formation of three-dimensional vascular tubes, endothelial fenestration as well the regulation of vascular permeability that may lead to oedema and swelling.

Historically, VEGFR-1 (Flt-1) was the first VEGF receptor to be discovered and was found to generally exhibit weak autophosphorylation in response to VEGF binding. Specifically, ligand interaction has been mapped to occur first and foremost at the second immunoglobulin domain (Davis-Smyth et al., 1996; Wiesmann et al., 1997). Notably, VEGFR-1 was later postulated to rather not represent the primary receptor transmitting the angiogenic signal but to constitute a negative regulator of VEGF action instead. By sequestering bioactive VEGF, it has been suspected that VEGFR-1 acts as some sort of 'decoy' receptor (Park et al., 1994). Repression of signal transduction could well be a consequence of a peculiar folding that has been reported for the intracellular domain, which appears to prevent the accessibility of certain docking sites. Consistently, the classic tyrosine residue Tyr416 in the Src kinase domain that is indicative for positive regulation remains unphosphorylated in activated VEGFR-1 (Ito et al., 1998). Moreover, an alternative splice form of VEGFR-1 exists, which is shed of the membrane (soluble Flt-1) in order to act as an endogenous, systemic VEGF inhibitor (Kendall and Thomas, 1993). It is important to note, though, that the effects exerted by VEGFR-1 may well be subject to intense regulation varying across tissues and developmental stages. In contrast, VEGFR-2 (Kdr/Flk-1) unarguably constitutes an active and crucial factor regarding all aspects in physiological and pathological vessel biology. Its key role for developmental angiogenesis/vasculogenesis and hematopoiesis was underscored by the lethality of *Flk1*-null mice (*Vegfr2* *-/-*) observed between embryonic day 8.5 and 9.5 *in-utero* (Sakurai et al., 2005). Much in contrast to VEGFR-1, stimulation with already low-level VEGF leads to the rapid and robust autophosphorylation of VEGFR-2 (K_d ca. 75-125 pM) (Terman et al., 1992). Structural and functional analysis of its crystal structure mapped VEGF binding to the immunoglobulin domain 3 (Fuh et al., 1998), what results in the engagement of characteristic tyrosine residues such as Tyr1054 and Tyr1059 (Dougher and Terman, 1999). This in turn initiates major downstream signaling cascades *inter alia* comprising the phosphoinositol₃ kinase-proteinkinase B (PI₃K-PKB/Akt) cascade, the mitogen-activated protein kinase-extracellular signal regulated kinase 1/2 (MAPK-ERK1/2) pathway or the phospholipase C γ -proteinkinase C (PLC γ -PKC) cascade. It is now well-established that VEGFR-2 is the major effector of VEGF action in terms of its angiogenic and hematopoietic effects. Lastly, VEGFR-3 on the other hand does not bind VEGF but only

VEGF-C and -D. Its primary implications are in the formation of the lymphatic system and is thus substantially distinct from the rather endothelial action of the other two receptors.

Co-receptors of VEGF. The presence of additional (co-)receptors has been suspected given that the binding sites for VEGF have been observed within the endothelium that intriguingly appear distinct in size and ligand affinity from the already described VEGFR. Subsequent investigations identified two cell surface glycoproteins named neuropilin-1 and -2 (NRP1, NRP2), which readily bind VEGF and VEGF-C, respectively (Soker et al., 1998), but lack intrinsic catalytic activity upon ligand binding. Instead, neuropilins modulate signal transduction at the classical VEGF receptors in *trans* (NRP1 at VEGFR-2 and NRP2 at VEGFR-3, respectively). By allowing for a more effective and durable interaction of the ligands with the VEGFR signaling complex, neuropilins potently tune the respective downstream effect. In the case of NRP1, an intriguing isoform-specificity has been observed with the co-receptor binding only VEGF₁₆₅ but not the shorter splice variant VEGF₁₂₁, which lacks the residues encoded by exon 6 and 7 (reviewed in Olsson et al., 2006). Those residues appear crucial for the binding to NRP1, though, and putatively underlie the higher angiogenic potency of VEGF₁₆₅ relative to VEGF₁₂₁. The essentiality of these non-kinase co-receptors for VEGF signaling is further corroborated by the dramatic phenotype observed in genetic loss-of-function mouse models. Here, it has been demonstrated that lacking either of the neuropilins is incompatible with life as evidenced by the embryonic lethality of *Nrp1*-null and *Nrp2*-null mice as a consequence of defective vascular development (Kawasaki et al., 1999; Takashima et al., 2002; Jones et al., 2008) taking place between E8.5 and E13.5 depending on the genetic background (Kitsukawa et al., 1997). Despite their obvious significance for vascular and lymphatic biology, neuropilins have first been found to also be expressed in neural cell types. In neural cells, neuropilins appear to mediate equally important developmental processes such as axonal guidance upon binding an alternative ligand, semaphorin B (He and Tessier-Lavigne, 1997). Given that there is a tight spatiotemporal coupling between neural and vascular development this observation fuelled the idea that VEGF and the VEGFR-neuropilin system may act at the neuro-vascular intersect, where it plays a crucial coordinating role.

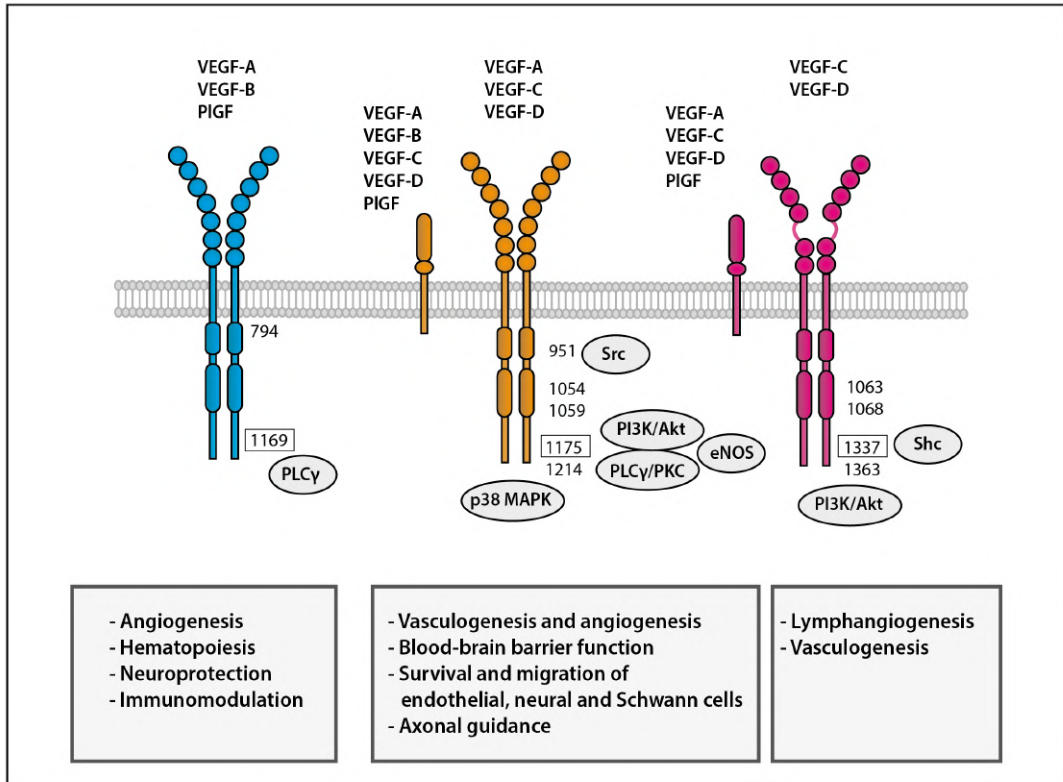


Figure 4: The VEGF/VEGFR superfamily of growth factors.

Schematic illustration of the three main receptor tyrosine kinases VEGFR-1 (blue), VEGFR-2 (yellow) and VEGFR-3 (purple), the latter of which associate with their corresponding co-receptors NRP-1 (yellow) and NRP-2 (purple), respectively. Receptor affinities towards the known VEGF isoforms (VEGF-A, VEGF-B, VEGF-C and VEGF-D) as well as PlGF are depicted. Major cellular effects induced by ligand-receptor interactions on the vasculature and CNS are illustrated. VEGF: vascular-endothelial growth factor; PlGF: placental growth factor; NRP1/2: neuropilin 1/2; PLC γ : phospholipase ; Src: proto-oncogene tyrosine-protein kinase Src; PI3K/Akt: phosphoinositol 3 kinase/Akt; PKC: protein kinase C; eNOS: endothelial nitric oxide synthase; p38 MAPK: p38 mitogen activated protein kinase. Adapted from (Lange et al., 2016).

1.8.4 Physiological relevance of VEGF

VEGF and its homologues were found to constitute extremely ancient, evolutionary conserved molecules even dating back to Cnidarians (*Hydra*). Given the lack of any vascular system in these organisms, this surprising finding immediately caused a re-thinking about the physiological role of VEGF signaling.

VEGF – a coordinator of neural and vascular function alike. In lower organisms, VEGF signaling is crucially involved in the development of their peculiar ‘nerve net’. This intriguing observation prompted the suggestion that VEGF might have evolved rather as a neural factor in its early emergences while being seized and co-opted as a vascular signal only later on. In mammals, VEGF signaling retained various actions on neural cells that are distinct from its vascular effects. Those actions include the promotion of neuronal migration and axon pathfinding. In the mouse, cerebellar granule cells were shown to require functional VEGFR-2 signaling to be guided along an extracellular VEGF gradient for proper migration (Ruiz de Almodovar et al., 2011). Likewise, motoneurons of the facio-branchial nerve in the hindbrain were shown to navigate *via* VEGF/Nrp-1 signaling (Schwarz et al., 2004). From an ontogenic perspective, the development of the nervous system and that of the CNS vasculature are precisely coordinated in which VEGF plays a crucial concatenating role. Being secreted from neural tube cells, VEGF ultimately triggers the *de novo* formation of the perineural vascular plexus and the invagination of vessel sprouts into the neural tube. VEGF is considered a key molecule for mediating the appropriate vascularisation of the expanding CNS during development thus being crucial for brain growth *per se* (reviewed in Ruhrberg and Bautsch, 2013). In the adult mammalian brain, VEGF remains being expressed in a region-specific manner. Various important processes have been assigned to its action such as regulation of microvascular density and permeability. Intriguingly, VEGF is particularly prominent in radial glia in neurogenic niches, where VEGF stimulates proliferation of neural stem cell and boosts neuronal differentiation, axonal extension and synapse formation (Cao et al., 2004; Kirby et al., 2015). Other brain regions with high VEGF abundance are found in and around circumventricular organs, which represent designated brain-body interfaces for extensive exchange of soluble signals. Circumventricular organs comprise *inter alia* the choroid plexus and the hypothalamic arcuate nucleus-medium eminence (ARC-ME) complex, in the latter of which VEGF was shown to govern the delicate regulation of endothelial fenestration in order to promote access of hormones to the brain (Langlet et al., 2013).

VEGF within the adult brain: a double-edged sword. VEGF constitutes an absolutely crucial neurovascular regulator from development onwards all throughout adulthood. By maintaining cerebrovascular function, VEGF guarantees proper perfusion of the brain supplying it with nutrients and oxygen. Besides maintenance, however, VEGF expression in the brain has additionally been observed to be highly responsive to neural injury and was

found to be elevated upon traumatic brain injury (Sun et al., 2003; Dore-Duffy et al., 2007), an experimental stroke model of middle-cerebral artery occlusion (Hayashi et al., 1997) and entorhinal deafferentation (Wang et al., 2005). Under such pathological circumstances, balanced VEGF action was shown to take on reparative and restorative roles by acting on vessels (pro-angiogenic) or on neural cells directly (neuroprotective and neurotrophic). On the other hand, though, the overproduction of VEGF in the diseased nervous system can significantly aggravate neurological disorders. Excessive concentrations of VEGF can promote the disruption of the BBB by its permeabilizing activity at microvessels ultimately posing a serious threat to CNS homeostasis. In addition, excessive VEGF frequently leads to an uncontrolled neovascularization and endothelial proliferation, which can result in progressive organ failure as described *e.g.* in the diabetic neuroretina (Aiello et al., 1994; Wong et al., 2016). In conclusion, VEGF has complex biological functions in the brain seemingly dependant on concentrations, timing and context of action.

1.9 Glia-vascular dysfunction in obesity

1.9.1 Hypothalamic astrogliosis in obesity

The formation of glial scars in the course brain injury is a process that is historically well appreciated. Thus, it came to an even greater surprise when it got recently revealed that the occurrence of reactive astrogliosis is not only limited to severe insults such as physical trauma, stroke or sepsis but that even the mere consumption of a high-calorie diet is sufficient to induce a marked upregulation of GFAP in hypothalamic astrocytes (Horvath et al., 2010; Thaler et al., 2012; Buckman et al., 2013). On the basis of these observations it got suggested that the chronic consumption of a high-calorie diets could pose a similar threat to the microenvironment of brain as the insults mentioned above. Notably, these diet-induced reactive changes turned out highly regionalized and were particularly found in astrocytes positioned in the mediobasal hypothalamus (MBH), a major neuroanatomical hub in the regulation of energy homeostasis, which receives and integrates metabolic feedback signals from the periphery (**Figure 5**). It has been suggested previously that astrocytes in close proximity to ARC microvessels are particularly prone to turn reactive (Horvath et al., 2010). Strikingly, these morphological changes in astrocytes developed at remarkable rapidity within the course of only several days and were accompanied by the increased production of pro-inflammatory cytokines in the hypothalamus. By this, hypothalamic

Introduction

astrogliosis does not only precede any significant change in bodyweight but occurs even prior to any inflammatory-like changes in the periphery such as in adipose tissue or the liver (Thaler et al., 2012). This temporal succession inevitably sparked the hypothesis that diet-induced astrogliosis within the hypothalamus could be an active contributor in the development of dietary obesity. Until today, however, it remains elusive if structural and secretory changes in hypothalamic astrocytes during short-term overfeeding could indeed onset long-lasting homeostatic derailment and if targeting this phenomenon could constitute a potential strategy to avert the obesity pandemic.

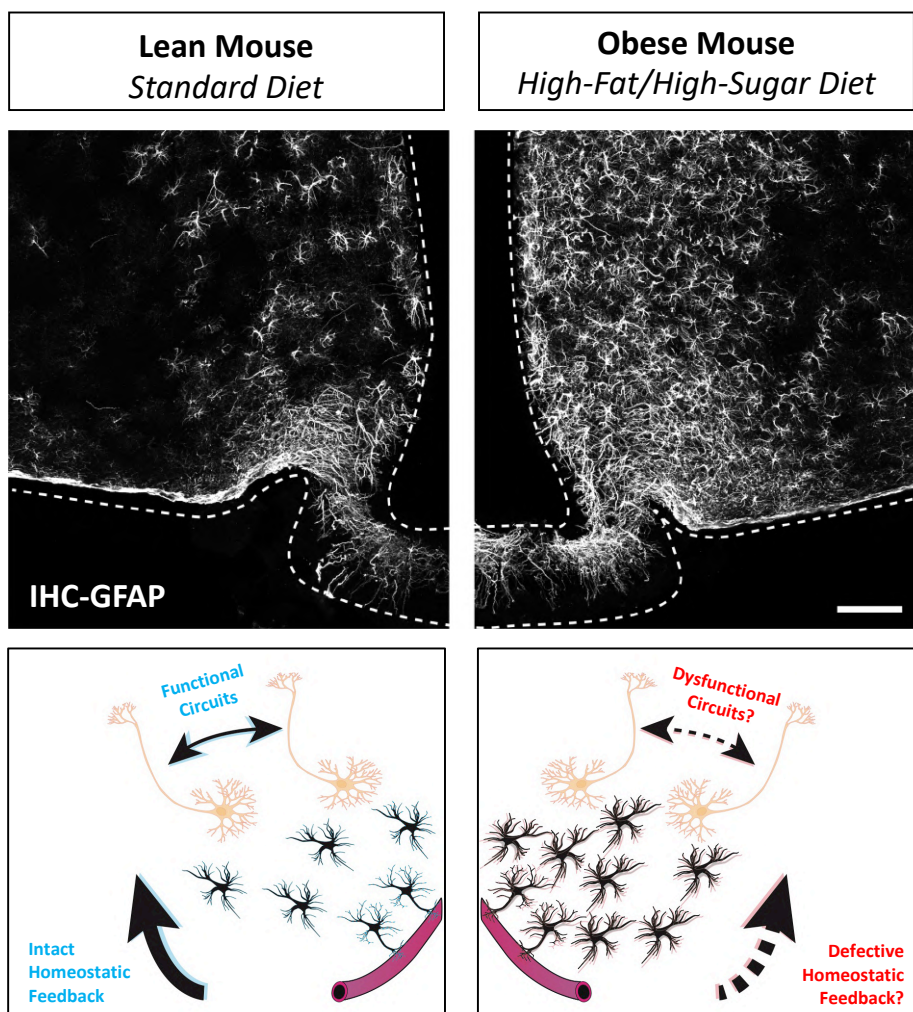


Figure 5: Schematic diagram of astrogliosis in the mediobasal hypothalamus induced by high-fat/high-sucrose feeding.

Feeding high-fat/high-sucrose diet to mice induces a rapid and profound upregulation of GFAP (glial-fibrillary acidic protein) immunoreactivity, an event even preceding substantial bodyweight gain. Increased expression of GFAP shifts the astroglial morphotype towards a more reactive, hypertrophic and bushy appearance. Diet-induced reactive astrocytes in the mediobasal hypothalamus are currently hypothesized to perturb homeostatic feedback from the periphery and to disrupt local neuronal circuits ultimately paving the way to derailed whole-body energy homeostasis. Scale bar: 100 μm .

1.9.2 Vascular dysfunction in obesity

Macrovascular as well as microvascular complications are comorbid with obesity and a well-known consequence of the chronic consumption of a high-calorie Western-style diet. Constituting one of its most serious disease manifestations, vascular dysfunction is considered a primary factor associating obesity with increased mortality and disability (Poirier et al., 2006; Lavie et al., 2009). On the one hand, obesity confers increased risk onto the macrovascular compartment by promoting systolic hypertension, atherosclerosis, left ventricular remodeling, atrial fibrillation and coronary heart disease. On the other hand, obesity negatively impacts the microvasculature within susceptible tissues where it triggers neovascularization and vessel instability posing the threat of progressive organ failure *e.g.* in the retina, the kidney and peripheral nerves (Rask-Madsen and King, 2013). Importantly, arterial hypertension is widely regarded to not only precede but also to functionally contribute to the development of microvascular remodeling by imposing increased capillary pressure (Folkow et al., 1958). Even though micro- and macrovascular complications are often occurring concomitantly with intertwined mechanisms, their individual pathogenesis is mostly addressed separately. Notably, it is widely accepted that macrovascular damage is not only temporally prior (Rydén et al., 2013) but even causative for the development of microvasculature complications. In support of this postulate, a seminal study in nephrology revealed that the development of arterial hypertension imposes a pathological increase of renal capillary pressure what in turn leads to structural remodeling in the kidney (Folkow et al., 1958). This axiomatic assumption, at least in such proclaimed universality, is increasingly coming into question.

1.9.3 Microvascular dysfunction in susceptible tissues as a consequence of high-calorie diets

Microvascular complications are the most debilitating comorbidities of obesity and diabetes and attributable for a significant impact on public health. A large proportion of obese and diabetic patients will acquire microvascular damage in susceptible tissues over the course of disease. Tissues of particular vulnerabilities include the retina, kidney and peripheral nerves, which are all prone to develop neovascularization, pathological microvessel remodeling and vascular instability. The high incidence, severity and typically late diagnosis of these complications renders them as major health threats. In the working-age population of the US, diabetic retinopathy constitutes the leading-cause of blindness while diabetic nephropathy is the leading-cause of end-stage renal failure; diabetic neuropathy, on the other hand, is attributable for a substantial number of extremity amputations as a consequence of nerve die-off. While the pathogenesis of microvascular damage is well understood within the confines of these tissues, the impact of obesity and diabetes on microvessels in other tissues remained elusive. Indeed, it has been recently reported that microvascular remodeling is not solely restricted to those three tissues but instead occurs within the brain as well where the consumption of a high-calorie diet induces a peculiar remodeling of the microvasculature observable in both mice and humans (Yi et al., 2012). Consistently, a series of epidemiological as well as clinical studies demonstrated that high-calorie diets, obesity and diabetes all exert deleterious effects on cerebrovascular function and cognition in humans (Folsom et al., 2018; van den Berg et al., 2009). This cerebrovascular damage is suspected to result from a combination of microvascular instability as well as systemic hypertension implicating higher stroke incident and risk for vascular dementia.

1.9.4 Systemic macrovascular dysfunction and arterial hypertension in obesity

Despite its tight association with obesity, the development of hypertension and its mechanistic underpinnings remain incompletely understood. Putatively contributing factors include fibrotic renal damage, a hyperactive renin-angiotensin system and the physical compression of the kidneys due to expanding adipose tissue. However, intriguing evidence increasingly suggests that the brain significantly contributes to the derailment of systemic blood pressure in obesity by dysregulated outflow of the sympathetic nervous system (SNS).

Brain control of sympathetic tone.

The CNS mediates sympathetic output by a complex array of interconnected nuclei interspersed throughout the hypothalamus and brainstem including the paraventricular nucleus of the hypothalamus (PVN), the raphé pallidus (RPa), the locus coeruleus (LC), the ventrolateral A5 areal in the pons and the rostral ventrolateral medulla (RVLM). These regions form projections that descend down to the thoracolumbar segment (T1 to L3) of the spinal cord where they synapse onto pre-ganglionic neurons in the so-called intermediolateral cell column (IML). Their axons then run through the anterior rootlets to innervate the paravertebral ganglia of the sympathetic trunk as well as a number of larger ventral ganglia (celiac-, stellate-, cervical-, and mesenteric ganglia), whose neurons project extensively throughout the entire body to provide (nor)adrenergic stimulation of target organs. However, some preganglionic nerves even extend to reach the medulla of the adrenal gland, where sympathetic innervation potentially triggers the systemic release of adrenalin into the circulation.

1.9.5 Sympathetic hyperactivation of cardiovascular targets in obesity

Together with the parasympathetic nervous system, the SNS constitutes one of the two branches of the autonomic nervous system, which provides extensive innervation of peripheral organs. The SNS is critically involved in the control of body homeostasis by mediating the so-called ‘fight-or-flight response’. In given emergency situations, sympathetic output promotes the rapid liberation, distribution and utilization of metabolic energy to support states of high physical and mental performance. The systemic effects of increased sympathetic nerve activity (SNA) comprises *inter alia* an increase in heart rate, stimulation of breathing and last but not least vasoconstriction. However, it is important to note that autonomic tone is typically balanced between the two branches and their concerted action is typically far from generic but often highly stimulus- and target organ-specific. This is partly due to the fact that the two arms innervate individual tissues at varying densities. In addition, autonomic outflow towards a given organ is finely coordinated between the two arm. This balance is further defined by the nature of a given stimulus, *e.g.*, a hormone, and can well be tuned in such a way that SNA in the kidney is highly elevated while SNA to the heart is left unaltered.

2 Aim of the thesis

In the course of this thesis, I aimed to interrogate how metabolic diseases such as obesity and diabetes impact the cerebral vasculature. Particular focus was placed on the involvement of astrocytes given their privileged anatomical location at the body-brain interface. By acting as crucial intermediaries within the neuro-glia-vascular arrangement, astrocytes were here hypothesized (a) to survey the metabolic status of the organism and (b) to remodel local vascular beds in both health and in disease. In light of the emerging controversy around separately addressing macrovascular versus microvascular dysfunction, a more holistic approach was implemented probing for their mechanistic interrelations and respective contributions to the acquisition of cerebrovascular damage in obesity and diabetes. Specifically, the thesis comprises the aim to unravel the cellular and molecular mechanisms driving cerebrovascular dysfunction in metabolic diseases and to identify potential pharmacological targets in order to avert the associated health consequences.

3 Material and Methods

3.1 *Animals experiments*

All animal studies were approved by the Animal Ethics Committee of the government of Upper Bavaria, Germany, and all experiments were performed according to the guidelines of the Institutional Animal Care and Use Committee of the Helmholtz Center Munich, Bavaria, Germany and the Yale University, School of Medicine. Wildtype mice (C57Bl6/J, Janvier, Le Genest-Saint-Isle, France) or genetically modified mice aged 12 weeks were provided *ad libitum* access to either a pelleted standard chow (SC) diet (5.6% fat; LM-485, Harlan Teklad) or a high-fat, high-sucrose (HFHS) diet (D12331; 58% of calories from lipids; Research Diets, New Brunswick, NJ). Animals had continuous free access to water and were maintained at 23°C with constant humidity on a 12-h light–dark cycle. Lep^{ob/ob} mice, Lep^{db/db} mice and MC4R^{-/-} mice were originally provided from Jackson Laboratory (strain name: B6.Cg-Lepob/J; BKS.Cg-Dock7m +/+ Leprdb/J; B6.129S4-Mc4rtm1Lowl/J; Maine, USA). LepR^{loxP/loxP} mice (McMinn et al., 2005), HIF-1 α ^{loxP/loxP} mice (Ryan et al., 2015) as well as HIF1/ODD-Luciferase mice (Safran et al., 2006) were generated and described previously and provided from Jackson Laboratory (strain name: B6.129-Hif1at^{m3Rsj0}/J, B6.129P2-Lep^{tm1Rck}/J and FVB.129S6-Gt(ROSA)26Sor^{tm2(HIF1A/luc)Keal}/J, respectively). In order to generally excise sequences flanked by *loxP* sites, mice were crossed with either of the astrocyte-specific Cre-driver lines: (1) the transgenic hGFAP-CreER^{T2} mouse line, which was generated on a C57Bl6/J background and provided by F.M. Vaccarino (Yale University, School of Medicine) or (2) the GLAST.CreER^{T2} mouse line in which Cre recombinase is knocked into the locus of the glutamate-aspartate transporter (GLAST) gene (Mori et al., 2006). All experiments using the GLAST-specific driver mice were performed with the GLAST.CreER^{T2} allele in heterozygosity. In both inducible models, nuclear translocation and hence activation of CreER^{T2} was induced postnatally in 6-week-old mice by repeated injections of Tamoxifen (10 mg/kg bodyweight, *i.p.*) for 5 consecutive days. Tamoxifen (Sigma) was dissolved in sunflower oil at a final concentration of 10 mg/ml at 37°C and filter sterilized. Whenever indicated, mice were further backcrossed to the Cre-dependent reporter mouse line ROSA26^{mT/mG} provided from Jackson Laboratory (strain name: mT/mG) in order to identify recombined cells by means of membrane-localized EGFP expression. As described previously, GFAP-CreER^{T2} driver mice displayed extensive recombination in

thalamic and hypothalamic regions with poor cortical recombination, while GLAST.CreER^{T2} mice showed extensive recombination in all brain regions except for thalamic nuclei.

STZ-induced diabetes. Insulin-dependent diabetes mellitus was experimentally induced by administering the β -cell toxin Streptozotocin (STZ) to 8-week-old, male wild-type mice (C57Bl6/J) according to the multiple low-dose injection protocol of the Diabetic Complications Consortium (50 mg/kg BW; i.p for 5 days versus vehicle (Na-Citrate Buffer)). One group received daily injections of polyethyleneglycosylated (PEGylated)-insulin (25 nmol/kg/day in 5 μ l/g) to achieve normoglycemia in these mice. PEGylated insulin was synthesized by N-terminal amine reductive amination with 20K methoxy PEG propionaldehyde. In brief, human insulin was dissolved in 50 mM sodium acetate buffer (pH 5.0) and 50% acetonitrile. A 30-fold excess of sodium cyanoborohydride and a 1.5-fold excess of methoxy PEG propionaldehyde (M-ALD-20K, JenKem Technology USA Inc., Plano, TX) was added to the insulin-containing buffer for 3 h at room temperature with stirring. Purification by reverse phase chromatography on a C-8 column in 0.1%TFA acetonitrile solvents yielded PEGylated insulin at greater than 95% purity.

3.1.1 Genotyping of mouse lines

Eartags were obtained from mice at the age of 3 weeks and DNA was isolated by boiling the eartags for 30 min in 200 μ l 50 mM NaOH at 95 °C (ThermoMixer C, Eppendorf). Afterwards, 20 μ l 1 M Tris was added to normalize the pH. 2 μ l of isolated genomic DNA was used for the genotyping PCR (Promega) using respective protocols (see **Appendix**).

3.1.2 Body composition analysis and metabolic phenotyping

Body composition (fat and lean mass) was assessed by using a magnetic resonance whole-body composition analyzer (Echo-MRI, Houston, TX). Energy metabolism of individual mice was assessed by using an indirect calorimetry system (TSE PhenoMaster, TSE Systems, Band Homburg, Germany). Upon an acclimatization period of 24 h, O₂ consumption was registered in 10 min intervals.

3.1.3 Measurement of mean arterial pressure in conscious mice by the tail cuff system (*collaboration*)

Mean arterial blood pressure (MBP) measurements were performed in each mouse every other day for two weeks before sacrifice by tail-cuff plethysmography using a Niprem 645 blood pressure system (Cibertec, Madrid, Spain). For that purpose, mice were placed in a quiet area ($22\pm 2^{\circ}\text{C}$) and habituated to the experimental conditions for at least 3 days. Before measurements, mice were prewarmed to 34°C for 10–15 min. Then, the occlusion cuff was placed at the base of the tail and the sensor cuff was placed next to the occlusion cuff. Next, the occlusion cuff was inflated to 250 mm Hg and deflated over 20 s. Five to six measurements were recorded in each mouse and the mean of all measurements was calculated each day per animal.

3.1.4 Arterial pressure and heart rate recording in anesthetized mice (*collaboration*)

Mice were anesthetized with a mixture of ketamine (70 mg/kg) and xylazine (5 mg/kg). Afterwards, the throat was incised from below the mandible to the thoracic inlet. Under a dissecting microscope, the left carotid artery was exposed and carefully separated from other neighboring structures including the vagus nerve. After left carotid isolation, a silk suture (6-0) was placed distally for the complete ligation of the vessel. Then the left carotid artery was proximally occluded with a clamp to produce temporary obstruction of blood flow. Afterwards a small incision was performed in order to insert a polyethylene tube filled with saline containing 100 units heparin/ml. The polyethylene tube had two branches; one for the injection of drugs and the other one with a lateral connection in the perfusion cannula connected to a pressure transducer (Statham Instruments, Los Angeles, CA, EE.UU). Mean arterial blood pressure was recorded using the PowerLab/8e data acquisition system (ADInstruments, Colorado Springs, CO, EE.UU) and the heart rate was obtained from the arterial pressure recording.

The baroreflex control of the heart rate was assessed by administering a bolus of sodium nitroprusside (SNP; 500 $\mu\text{g}/\text{kg}$). The α -adrenergic sensitivity was assessed by measuring the response of the MBP to phenylephrine (PE; 50 $\mu\text{g}/\text{kg}$) and the β -adrenergic sensitivity was assessed by measuring the responses of the MBP and heart rate to isoproterenol administration (IPR; 50 $\mu\text{g}/\text{kg}$).

3.1.5 Leptin administration *in-vivo*

5 mg of recombinant mouse leptin (498-OB, R&D systems, Minneapolis, USA) was dissolved in 1 mL ice-cold Tris-HCl buffer (20mM, pH 8). This stock solution (5 mg/mL) was further diluted with ice-cold PBS (pH 7.4) to get a 1 mg/mL working solution. For vehicle control injections, the equivalent volume of plain 20 mM Tris-HCl was diluted in ice-cold PBS (pH 7.4). Whenever indicated, mice received repetitive leptin administration 3 mg/kg BW *i.p.* twice daily over two days plus another terminal injection in the morning. Mice were sacrificed by transcardial perfusion 45 min following the injection to allow for immunohistochemical detection of both VEGF and pSTAT3. In acute studies, mice received 5 mg/kg BW leptin *i.p.* 90 min before sacrifice to determine HIF-1 α induction by means of Western blot and HIF-1/ODD luciferase activity.

3.1.6 Glucose metabolism studies in mice *in-vivo*

Before glucose tolerance tests, mice were fasted for 4h and then given an intraperitoneal injection of glucose dissolved in 1xPBS (pH 7.4) at 2 g/kg BW. Glycemia was measured by sampling blood from the tail vein before (0 min) and at 15, 30, 60, and 120 minutes post injection *via* a handheld glucometer (Abbott, Wiesbaden, Germany). In order to assess insulin sensitivity, additional blood was collected at 0 min using EDTA-coated microvette tubes (Sarstedt, Nürnberg, Germany) to obtain plasma (5,000 x g for 10 min at 4°C). Insulin concentration was determined using a commercial insulin ELISA following the manufacturer's instructions (Ultra-sensitive Mouse Insulin ELISA Kit, #90080 Crystalchem, Netherlands). HOMA-IR was calculated using the formula: $\text{HOMA-IR} = [\text{fasting insulin (mU/l)} * \text{fasting glucose (mg/dl)} / 405]$ (Matthews et al., 1985).

3.1.7 Viral targeting of astrocytic VEGF signaling in the mediobasal hypothalamus (MBH)

In order to manipulate *Vegf* expression levels in the MBH, recombinant adeno-associated viruses of serotype 2/5 (rAAV_{2/5}) were commercially generated (VectorBioLabs, Malvern, USA) and configured such that viral transgene expression was driven in each case from a synthetic 2.2kb promoter element (Gfa2) faithfully restrictive to astrocytes as described previously (Brenner et al., 1994). Respective rAAVs were injected bilaterally (0.5 μ l per

Material and Methods

hemisphere; 1.0×10^{12} viral genomes ml^{-1}) using a stereotaxic system (KOPF...) combined with a binocular 3.5x-90x stereomicroscope (AMScope, USA) and a 2 μ l syringe (2 μ l with 30G needle; Hamilton, USA). Injection speed was set at 250nl/min and undesired diffusion of viral particles was further prevented by slow retraction of the canula after 5min post injection. The following stereotaxic coordinates were obtained from The Mouse Brain in Stereotaxic Coordinates (Franklin and Paxinos, 2019) and used to target the mediobasal hypothalamus (MBH) of the mouse brain: -1.4 mm posterior and ± 0.2 mm lateral to the bregma and -5.8 mm ventral from the *dura mater*. Anesthesia was performed by a mixture of ketamine and xylazine (100 mg/kg body weight and 7 mg/kg bodyweight, respectively) while acute Metamizol (200 mg/kg, subcutaneous) followed by Meloxicam (1 mg/kg, on three consecutive days, subcutaneous) was administered for postoperative analgesia.

Knock-down of *Vegf* mRNA in astrocytes was achieved by using a rAAV variant (rAAV.shRNA(VEGF)^{v Δ GFAP/+}) driving GFP expression together with a validated shRNA targeted against *Vegf* separated by a 2A linker peptide within the GFP 3'UTR. Control rAAV was identical except for carrying a scrambled RNA sequence (rAAV.scrmbIRNA^{v Δ GFAP/+}). Respective rAAV's were injected into male C57BL6/J mice that were either put on HFHS diet 10 days *post* injection or with already established diet-induced obesity.

Restoration of *Vegf* expression in hypothalamic astrocytes devoid of HIF-1 α was achieved by using a combination of the following rAAV variants to be injected into the MBH of HIF-1 α *loxP/loxP* mice: (1) rAAV.Cre^{v Δ GFAP/+} expressing Cre recombinase combined with (2) rAAV.VEGF^{v.GFAP/+} driving the expression of *Vegf*₁₆₄ together with GFP separated by a 2A linker peptide. As control groups, mice were either injected with rAAV.Cre^{v Δ GFAP/+} (HIF-1 α knock-out group) or injected with rAAV.eGFP^{v Δ GFAP/+} (control). Mice were switched to HFHS diet 10 days *post* injection.

3.2 *Ex-vivo* measurements

3.2.1 *Ex-vivo* luciferase assay of HIF1/ODD-Luc brain homogenates

Luciferase activity in mouse hypothalamus was assessed as previously described (Hoppe et al., 2016). Briefly, HIF1/ODD-Luc mice were decapitated, their hypothalami were rapidly dissected and homogenized in Glo Lysis Buffer (Promega) using a glass homogenizer (Duran Wheaton Kimble, USA) on ice. Cell debris was spun down at 10,000 x g, 4°C for 10 min. Protein concentration of supernatant was determined using BCA protein assay (ThermoFisher Scientific Inc., Rockford, IL USA) and adjusted to 250 µg in a final volume of 100 µl of Glo Lysis Buffer (Promega). Samples were placed in a white opaque 96-well plate, brought to room temperature and mixed with an equal volume (100 µL) of ready-to-use luciferase substrate Bright-Glo Luciferase Assay System (Promega), and luminescence was measured immediately by a luminometer (PheraStar F; BMG LABTECH GmbH, Ortenberg, Germany).

3.2.2 Vascular reactivity experiments in aorta segments (*collaboration*)

For the vascular reactivity experiments, the aorta was carefully dissected, cut in 2 mm segments and kept in cold isotonic saline solution. Each aorta segment was set in a 4 ml organ bath containing modified Krebs–Henseleit solution (mM) (NaCl, 115; KCl, 4.6; KH₂PO₄, 1.2; MgSO₄, 1.2; CaCl₂, 2.5; NaHCO₃, 25; glucose, 11) at 37 °C. The solution was equilibrated with 95% oxygen and 5% carbon dioxide to a pH of 7.3–7.4. For the setting process two fine steel wires (100 µm of diameter) were passed through the lumen of the vascular segment. One wire was attached to the organ bath wall and the other wire was connected to a strain gauge for isometric tension recording (Universal Transducing Cell UC3 and Statham Microscale Accessory UL5, Statham Instruments, Inc.). This arrangement permits to apply passive tension in a perpendicular plane to the long axis of the vascular cylinder. The changes in isometric force were recorded using a PowerLab data acquisition system (ADInstruments, Colorado Springs, CO, USA). After applying an optimal passive tension of 1 g, vascular segments were allowed to equilibrate for 60–90 min. Afterwards, segments were stimulated with potassium chloride (KCl 100 mM) to determine the contractility of smooth muscle. Segments which failed to contract at least 50 mg to KCl were discarded. After equilibration, the segments were pre-contracted with the analogue of thromboxane A₂ U46619 (10⁻⁸ M) (Sigma-Aldrich, St. Louis, MO, USA). Then, in order to

Material and Methods

assess the endothelium-dependent and endothelium-independent relaxation, cumulative dose-response curves in response to acetylcholine (ACh) (10^{-9} - 10^{-4} M) and sodium nitroprusside (10^{-9} - 10^{-4} M) (Sigma-Aldrich, St. Louis, MO, USA) were performed. The relaxation in response to ACh was determined based on the percentage of the active tone achieved by the NO donor sodium nitroprusside (10^{-5} M) (Sigma-Aldrich, St. Louis, MO, USA).

For each dose–response curve, the maximum effect (E_{max}) and the logarithm of the concentration producing 50% of the maximal response (ED_{50}) was calculated by geometric interpolation.

3.2.3 Determination of VEGF content of brain homogenates and serum in mice

Mice received repetitive vehicle or leptin administration 3 mg/kg BW *i.p.* twice daily over two days plus another terminal injection in the morning of the experimental day. Food was removed for 4h before animals were sacrificed and brains rapidly removed. Hypothalami and cortices were dissected and immediately snap frozen on dry ice. Whole blood was collected and centrifuged to obtain serum at 5,000 x g for 10 min at 4°C. All samples were stored at -80°C until being processed. Each piece of tissue was lysed in 50 µl of a homogenization buffer (5 M guanidine-HCl diluted in 50 mM Tris, pH 8) using a glass homogenizer (Duran Wheaton Kimble, USA). Homogenates were mixed on an orbital shaker at room temperature for 4 hours before being diluted ten-fold with ice-cold PBS (pH 7.4) supplemented with 1x protease and phosphatase inhibitor (Halt™ protease and phosphatase inhibitors, ThermoFisher Scientific, USA) to obtain a final volume of 500 µl. VEGF content of tissue lysates and supernatant was determined using a commercial VEGF ELISA following manufacturer's instructions (VEGF-A-Cell Lysate Mouse ELISA Kit, #EMVEGFCL, ThermoFisher Scientific Inc., Rockford, IL USA). Individual protein concentrations were determined *post-hoc* by standard BCA protein assay (ThermoFisher Scientific Inc., Rockford, IL USA) and VEGF tissue content was displayed as pg/mg.

3.2.4 Magnetic-activated and fluorescence-assisted cell sorting (MACS/FACS)

In order to validate the efficient deletion of exon 2 in HIF-1 α ^{fl^{ox}/fl^{ox}} mice, we generated dual fluorescent reporter mice (HIF-1 α ^{loxP/loxP::hGFAP.CreER^{T2}::ROSA26^{mT/mG}}) allowing us to

Material and Methods

differentiate non-recombined (tdTomato⁺EGFP⁻) from recombined (tdTomato⁺EGFP⁺) astrocytes for separate downstream analyses. Cre-mediated recombination was induced by tamoxifen injection at the age of 6 weeks as described before (10mg/5days). At 12 weeks of age, mice were sacrificed, their brains were rapidly removed and one hemisphere, respectively, subjected to magnetic-bead assisted cell sorting (MACS) enrichment using the astrocyte-specific surface marker ACSA-2 (Kantzer et al., 2017)(Batiuk et al., 2017). ACSA-2⁺ astrocytes were enriched according to a commercially available standard protocol (Isolation and Cultivation of Astrocytes from Adult Mouse Brain; Miltenyi Biotec) using LS columns and an elution volume of 1 mL PBS. Right thereafter, cells were subjected to fluorescence-activated cell sorting (FACS) in order to further separate recombined from non-recombined ACSA-2⁺ tdTomato⁺ astrocytes based on EGFP expression. To accurately gate the aforementioned subpopulations, a non-tamoxifen injected littermate reporter mouse (tdTomato⁺ EGFP⁻ ACSA-2⁺) and a non-fluorescent C57BL6J wildtype mouse (tdTomato⁻ EGFP⁻ ACSA-2⁺) were initially analyzed by FACS. Sorting was performed using a FACS-Aria III (BD Biosciences, Heidelberg, Germany) with a 85 µm nozzle. For optimal visualization of all ACSA-2⁺ astrocytes, logarithmic scales and low acquisition voltages (75 and 190) were implemented for forward scatter (FSC) and side scatter (SSC) plots, respectively,

Sorted cells were collected in cold PBS, pelleted by centrifugation for 5 min at 600 x g and 4°C, resuspended in 350 µl RLT buffer supplemented with 0.4 mM DTT and stored at -80°C until RNA extraction (RNeasy MicroKit; Quiagen) and cDNA synthesis (SMARTer® PCR cDNA synthesis kit; TaKaRa) following manufacturer's indications.

3.2.5 Bulk transcriptomics data analysis (*collaboration*)

C57Bl6/J mice either fed SC diet or HFHS diet for 3 months were sacrificed, their brains were rapidly removed and subjected to magnetic-bead assisted cell sorting (MACS) enrichment using the astrocyte-specific surface marker ACSA-2. Astrocytes pre-processing and down-stream analysis of transcriptomics data was performed employing DESeq2 v.1.24 (Love et al., 2014) (Bioconductor R package) in R v.3.5.2 ([R Development Core Team 2008](#)) statistical software. The feature counts matrix was filtered by removing low count genes which contains less than 50 counts over the all samples. Missing values were treated as zeroes. The resulting data set was then normalized using the variance stabilizing

transformation. We modeled the effects of interest on gene expression using a generalized linear model with a negative binomial distribution as implemented in DESeq2, while the testing was performed using Wald test. To identify potentially important differentially expressed genes Benjamini-Hochberg (BH) multiplicity correction was imposed (p-value < 0.05).

3.2.6 Pathway Enrichment (*collaboration*)

Significant differentially expressed genes determined with DESeq2 are used to identify enriched KEGG (Kyoto Encyclopedia of Genes and Genomes; Kanehisa and Goto, 2000) and GO (Gene Ontology; Ashburner et al., 2000) pathways. Differentially expressed genes obtained comparing chow and high-fat diet in each tissue are used for pathway enrichment applying a threshold of FDR<0.05 and the false detection rate is corrected using BH procedure. Hypergeometric distribution test was employed to determine enriched pathways of interest using R software. Among significant enriched KEGG and GO pathways, relevant pathways were selected manually.

3.3 *Histology and Imaging*

3.3.1 Fluorescent angiography

To obtain detailed information of the mouse brain vascular profile, animals were sacrificed with CO₂ and transcardially perfused with 20 mL phosphate buffered saline (PBS) (Gibco™, pH 7.4) supplemented with Lectin-FITC conjugate (25 µg/ml; Tritium vulgaris; L4895; Merck, Germany) by using a peristaltic pump at 120 mmHG (Instech, High Flow P720 equipped with 21G canula). Cohorts of animals already expressing green-fluorescent reporter proteins were perfused with an alternative vessel dye (wheat heat-germ agglutinin (WGA) conjugated to fluorochromophores Alexa Fluor™ 647; W21404; ThermoFisher, Germany). Perfusions were finalized with 20 mL of 4% paraformaldehyde (PFA) in PBS, pH 7.4, brains were removed and post-fixed in 4% PFA at 4°C. In order to rule out potential confounding by applying a uniform pressure source in perfusion-based angiography, we subjected one cohort of mice to intravenous administration of FITC-albumin (10 mg/mL in 0.9% NaCl; MW 69 kDa, Merck, Germany), which was infused slowly into the tail vein over

5 min. After 8 more min in which the dye was allowed to get distributed solely by means of cardiovascular function, mice were decapitated and brains rapidly immersion-fixed in 4% PFA in 0.1M PBS (pH 7.4) for 72h at 4°C.

In either case, brains were then equilibrated with 30% sucrose in Tris-buffered saline (TBS, pH 7.2) for 48h before being sectioned into 40 µm coronal slices using a cryostat (CM3050S; Leica, Germany). Per mouse, three to four brain sections were selected containing the middle portion of the mediobasal hypothalamus (MBH) and either directly mounted on gelatine-coated glass slides, dried and cover-slipped by a polyvinyl alcohol (mowiol®, Merck, Germany) mounting medium supplemented with DABCO (Merck, Germany) or further subjected to additional immunohistochemistry.

3.3.2 Image acquisition and analysis of vascularity in consecutive brain sections

Images were acquired as z-stacks using a confocal microscope (Leica TCS SP5, Germany) with an air-immersed 20x objective and 2µm step size in the z-direction. ImageJ/FIJI was used to trace and manually quantify the length of fluorescently labelled vessels in the MBH. The mean length of vessels was calculated for each experimental group.

3.3.3 Brain sectioning and immunohistochemistry

Brains were post-fixed overnight in 4% PFA at 4°C, followed by equilibration with 30% sucrose in Tris-buffered saline (TBS, pH 7.2) for 48h before being sectioned into 40 µm coronal slices using a cryostat (CM3050S; Leica, Germany). Per mouse, three to four brain sections were selected containing the middle portion of the mediobasal hypothalamus (MBH) and subjected to immunohistochemical protocol.

Brains were first washed with TBS and incubated overnight at 4°C with primary antibodies in a solution containing 0.25% porcine gelatine and 0.5% Triton X-100 in TBS, pH 7.2. The next morning, sections were serially rinsed in TBS, pH 7.2 and incubated with respective secondary antibodies diluted in TBS, pH 7.2 containing 0.25% porcine gelatine and 0.5% Triton X-100 for 2h. Sections were serially washed in TBS with the last washing additionally containing DAPI (2 µg/ml in TBS, pH 7.2) in order to facilitate the demarcation of brain region for downstream image analyses. Where indicated, sections were additionally treated

with fluorescent Nissl stain (1:100 NeuroTrace™ 435/455 or 500/525; ThermoFisher, Germany) in order to identify neuronal cells.

pSTAT3. Slight adjustments of this basic protocol were implemented for the immunohistochemical visualization of pSTAT3 such that brain sections were pre-incubated in 100% methanol at -20°C for 15 min.

Laminin and Collagen-IV. Given that in the adult, formalin-fixed mouse brain most basement membrane proteins tend to be inaccessible for immunohistochemical labelling we hence applied a specific antigen retrieval protocol in order to unmask vasculature-associated laminin and collagen IV as described (Franciosi et al., 2007). In brief, pepsin digestion was carried out on free-floating sections with pre-incubation in distilled water for 5 min at 37°C before being transferred to 1mg/mL pepsin (Dako, Carpinteria, CA) in 0.2N HCl for 10 min at 37°C.

3.3.4 3DISCO-assisted optical clearing of whole brains

To obtain three-dimensional information of the global mouse brain vasculature, animals were transcardially perfused with a vessel tracer conjugated to a fluorochromophor with emission peaks in the far-red range (WGA-Alexa Fluor™ 633; ThermoFisher, Germany) in order to overcome tissue autofluorescence, to facilitate light penetration and to improve signal-to-background ratio. Following the perfusion with 4% PFA and the overnight post-fixation in 4% PFA, brains were washed three times in PBS, pH 7.4 before being subjected to an organic solvent-based, optical clearing protocol (3DISCO) described previously (Ertürk et al., 2012). In brief, brains were serially incubated in 50%, 70%, 80% and 100% (v/v) of tetrahydrofuran (THF) at room temperature on a shaker for 1h followed by incubation in 100% v/v THF overnight. The next morning, THF was refreshed and brains were incubated for another hour. De-lipidation of brains was achieved by incubation in dichloromethane (DCM) for 1 hour at room temperature. Finally, brains got optically cleared by immersion in BABB (benzyl alcohol:benzyl benzoate; 1:2) and stored within until image acquisition.

3.3.5 Light-sheet microscopy imaging

Mouse brains were placed into the imaging chamber having its reservoir filled with the final clearing solution (BABB) in order to match the refractive indices. Importantly, brains were oriented upright and single plane illuminated (light-sheet) image stacks were acquired along the rostrocaudal axis for maximal coronal resolution. Image acquisition was carried out at an Ultramicroscope II (LaVision BioTec), featuring an axial resolution of 4 μm with following filter sets: ex 640/40 nm, em 690/50 nm. For high magnification-whole-brain imaging of the global mouse brain vasculature, a 4x Olympus objective was used (Olympus XLFLUOR 4x corrected/0.28 NA [WD = 10 mm]) combined with an Olympus revolving zoom body unit (U-TVCAAC). Keeping the zoom factor as 1x and setting 2x3 tile scans with 20% overlap, we imaged a field of view of 6.14 x 8.82 mm, covering the entire width and depth of the mouse brain from rostral surface to cerebellum region up to 7.2 mm using a z-step of 8 μm . Exposure time was 70 ms, laser power was adjusted depending on the intensity of the fluorescent signal (in order to never reach the saturation) and the light-sheet width was kept at maximum.

3.3.6 Analysis of vascularity in 3D whole-brain data sets

Whole-brain coronal stacks were loaded in ImageJ/FIJI and divided into sub-stacks in which pre-defined masks were used to crop out selected brain regions from each hemisphere (LS : lateral septum, CPu : caudate putamen, NAcc : nucleus accumbens, S1BF : somatosensory cortex barrel field, HIPPO : hippocampus, PVN : paraventricular nucleus, DMH : dorsomedial hypothalamus, LH : lateral hypothalamus, VMH : ventromedial hypothalamus, ARC : arcuate nucleus). Given slight differences in clearing efficiency across brain regions, individual thresholds were applied for each sub-stack. Next, sub-stacks were subjected to a filter function of 2 pixel at median intensity before being binarized and skeletonized. In the following, each coronal single plane was analyzed by using the histogram function of ImageJ/FIJI in order to relatively quantify vascular *versus* non-vascular pixels. Means of all individual planes derived from a respective brain region were calculated per hemisphere.

3.3.7 Protein extraction and Western blot

Protein content of hypothalamic tissue was extracted using RIPA buffer supplemented with 200 μM CoCl_2 (Sigma-Aldrich Chemie GmbH, Taufkirchen, Germany) and protease and phosphatase inhibitors (1% v/v; ThermoFisher Scientific Inc., Rockford, IL USA) in a final volume of 80 μl using a glass homogenizer (Duran Wheaton Kimble, USA). Cellular debris was centrifuged at 10,000 x g at 4°C for 10 min and protein concentration of the supernatant was determined using BCA protein assay (ThermoFisher Scientific Inc., Rockford, IL USA). Protein was adjusted to 30 μg per sample, complemented with Laemmli loading buffer plus 10% β -mercaptoethanol, denatured by heating at 95°C for 10 min and separated by molecular weight using SDS-PAGE. Protein was blotted on 0.45 μm PVDF membranes and blocked in 5% skimmed milk in TBS with 0.1% Tween-20 (TBS-T) for one hour at room temperature. Membranes were incubated with primary antibodies over night at 4°C, serially washed in TBS-T and incubated with the respective HRP-coupled secondary antibodies for one hour at room temperature. Membrane development was carried out with chemiluminescent HRP substrate (Immobilion Western, Millipore) using films (Hyperfilm ECL, GE Life Sciences; CL-XPosure Film, ThermoFisher Scientific).

3.3.8 RNA isolation and qPCR analysis

RNA was isolated from tissues or primary mouse astrocytes using a commercially available kit (MircoRNeasy Kit, Qiagen, Hilden, Germany). Identical amounts of RNA were reverse-transcribed to cDNA using Superscript III (Invitrogen, Darmstadt, Germany) and gene expression was analyzed using TaqMan probes (ThermoFisher Scientific Inc., Rockford, IL USA) at a ViiATM7 Real Time PCR System or QuantStudio 6 FLEX Real Time PCR System (ThermoFisher Scientific Inc., Rockford, IL USA). Expression changes were calculated using the $2^{-\Delta\Delta\text{Ct}}$ method normalized by *Hprt* or *Rpl32* as housekeeping genes.

3.4 Cell culture

3.4.1 Primary astrocyte cell culture

Mouse pups (postnatal day 1-3) were sacrificed by decapitation and heads were sterilized in ice-cold 70% ethanol before undergoing serial washes in ice-cold HBSS. The cranium was

cut from the neck to the nose and removed to allow access the brain. Then, each hypothalamus and cortex of mouse pups were carefully dissected under a stereomicroscope; in case genetic mouse models of yet-to-determined genotype were used, a remaining piece of brain tissue was collected for further genomic DNA isolation and standard genotyping. Isolated brain tissue was collected in 2 mL of low-glucose MEM (5.5 mM glucose; 2mM L-Glutamine) (11095 MEM; ThermoFisher Scientific Inc., Rockford, IL USA) and gently dissociated by repetitive pipetting. Following tissue dissociation, cell suspension was transferred onto a pre-wetted 70 μ m nylon cell strainer (Falcon®/Corning, USA) to remove undissociated tissue pieces and brought to a volume of 10 mL using low-glucose MEM supplemented with 10% fetal bovine serum (FBS heat-inactivated, Gibco®/ThermoFisher Scientific, USA) and 1% antibiotics-antimycotics (Anti-Anti 100x, Gibco®/ThermoFisher Scientific, USA). Cell suspension was then transferred into cell culture flasks and brought to a final volume of 10 mL or 25mL, respectively. Cells were maintained in an incubator (37°C / 5% CO₂) and cell culture medium was changed every 2-3 days using low-glucose MEM (10% FBS and 1% antibiotics and antibiotics). Under these conditions, primary cells typically became confluent 2-3 weeks after seeding and were then passaged into experimental plates using trypsinization (0.05% trypsin/0.02% EDTA solution, Biochrom GmbH, Germany) in conjunction with gentle shaking. Before each experiment, contaminating microglia was depleted by incubating cells with clodronate liposomes (200 μ g/ml in normal culture medium for 24h), a lysosomotropic compound specifically phagocytosed by microglia (Clodrosome®, Encapsulated Nano Sciences, USA).

3.4.2 Induction of Cre recombinase-mediated recombination *in-vitro*

In the case that primary astrocytes were derived from genetically modified animals (HIF-1 α -KO: HIF1 α ^{*loxP/loxP*}::GLAST.CreER^{T2}::ROSA26^{mT/mG} ; WT: HIF1 α ^{*loxP/loxP*}::ROSA26^{mT/mG} mice), cells were cultured in 6-well plates at a density of 1 million cells/well. Two days after, cells were treated regular culture medium supplemented with 4-OH Tamoxifen (Afimoxifen; Sigma, USA) at a final concentration of 1 μ M for 5 consecutive days (daily change of medium). Given that cells carry a dual Cre-dependent fluorescent reporter construct, successful recombination was visualized at a BZ-9000 fluorescence microscope using 10x magnification objective (Keyence, Coporation Itasca, USA).

3.5 Human data

3.5.1 Correlating plasma leptin concentration with markers of microvascular function in humans

Human plasma samples were obtained from a previously conducted study (Joris et al., 2016), which was approved by the Medical Ethics Committee of Maastricht University Medical Center and registered at clinicaltrials.gov as NCT01675401. In the course of this study, 54 abdominally obese men (waist circumference: 102-110 cm) and were randomAll participants gave written, informed consent before entering the study.54 abdominally obese individuals were included with a waist circumference of 102– 110 cm (classified as abdominally obese).

At the day of visit (pre and post intervention), blood was sampled through an intravenous catheter into EDTA-coated vacutainer tubes (Becton, Dickinson and Company), which were cooled on ice and centrifuged at 1300 x g for 15 min at 4°C in order to obtain plasma. After centrifugation, plasma samples were immediately aliquoted and stored at -80°C until analysis. Plasma leptin levels were determined using a Leptin human ELISA Kit (Thermo Fisher Scientific Inc., Waltham, USA) according to the manufacturer's instructions.

3.5.2 Imaging of retinal microvasculature (*collaboration*)

Pre and post intervention, retinal vascular images of the study participants were obtained using a nonmydriatic retinal camera (Topcon TRC-NW-300; Topcon Co.). Study participants were seated, their head placed on a chinrest and the camera was focussed on the optic disc of the right eye. Images were digitized and subjected to analysis by calculating the mean arteriolar calibre, mean venular calibre, and the arteriolar-to-venule ratio using an appropriate software (Generalized Dual-Bootstrap Iterative Closest Point). Briefly, retinal images get automatically aligned by the software based on detected vascular centerlines by iteratively transforming the algorithm. A minimum of two arteriolar and two venular segments were measured and summarized by using Parr-Hubbard formulas. Segments were kept constant across pre-and post-assessment in every individual.

3.6 Statistics

Data analysis was conducted using GraphPad Prism (Version 5). Normally distributed data were analyzed by student's T-test or one-, two-way analysis of variance (ANOVA) with Bonferroni or Turkey *post-hoc* analyses to determine statically significant differences in the samples. Data were screened using the maximum normal residual Grubb's test to screen for singular, statistically significant outliers. P-values ≤ 0.05 were considered statistically significant. All data are presented as mean \pm standard error of the mean (SEM).

4 Results

4.1 Hypertension in obesity is driven by angiogenic signaling in hypothalamic astrocytes

4.1.1 HFHS feeding induces microangiopathy specifically in the hypothalamus prior to the development of systemic hypertension in mice

Feeding obesogenic diet to mice induces vascular dysfunction in various organ systems along the duration of exposure and is frequently used to model cardiovascular complication of human obesity. In order to define the exact temporal development of diet-induced vascular damage in the mouse, C57BL6J mice were exposed to a high-fat/high-sucrose (HFHS) diet either for short-or long-term and consequently analyzed for acquisition of vessel dysfunction in both the periphery as well as in the brain. Consistent with previous observations (Weisbrod et al., 2013), only chronic – but not short-term- feeding of a HFHS diet elevated systemic arterial blood pressure (**Figure 6A**). In contrast, however, neovascularization of the hypothalamus as another, recently uncovered consequence of high-calorie exposure (Yi et al., 2012) was found to occur more rapidly becoming significantly evident already upon only two weeks of HFHS feeding (**Figure 6A**). Furthermore, this diet-induced cerebrovascular remodeling appears highly region-specific. By combining fluorescent angiography, optical tissue clearing and 3D imaging of the whole mouse brain vasculature (Ertürk et al., 2012), this phenomenon was revealed to be restricted to only a few hypothalamic nuclei (**Figure 6B and C**). Notably, a substantial proportion of these more numerous hypothalamic vessels displayed signs of HFHS-induced impairment in both structure and function. Similar to what has been observed in various other tissues of obese, diabetic and hypertensive individuals (Tsilibary, 2003; Roggendorf et al., 1988), hypothalamic capillaries of HFHS-fed mice exhibited a marked thickening in their basement membrane as evidenced by increased deposition of the extracellular matrix proteins, collagen IV and laminin (**Figure 6D**). In addition, these microvessels frequently exhibited a discontinuous coverage by *Claudin-5*, an essential component of tight-junctions at the BBB, which was associated with higher extravasation of serum proteins such as albumin (vascular hyperpermeability), suggesting functional impairments in barrier properties (**Figure 6E**).

Results

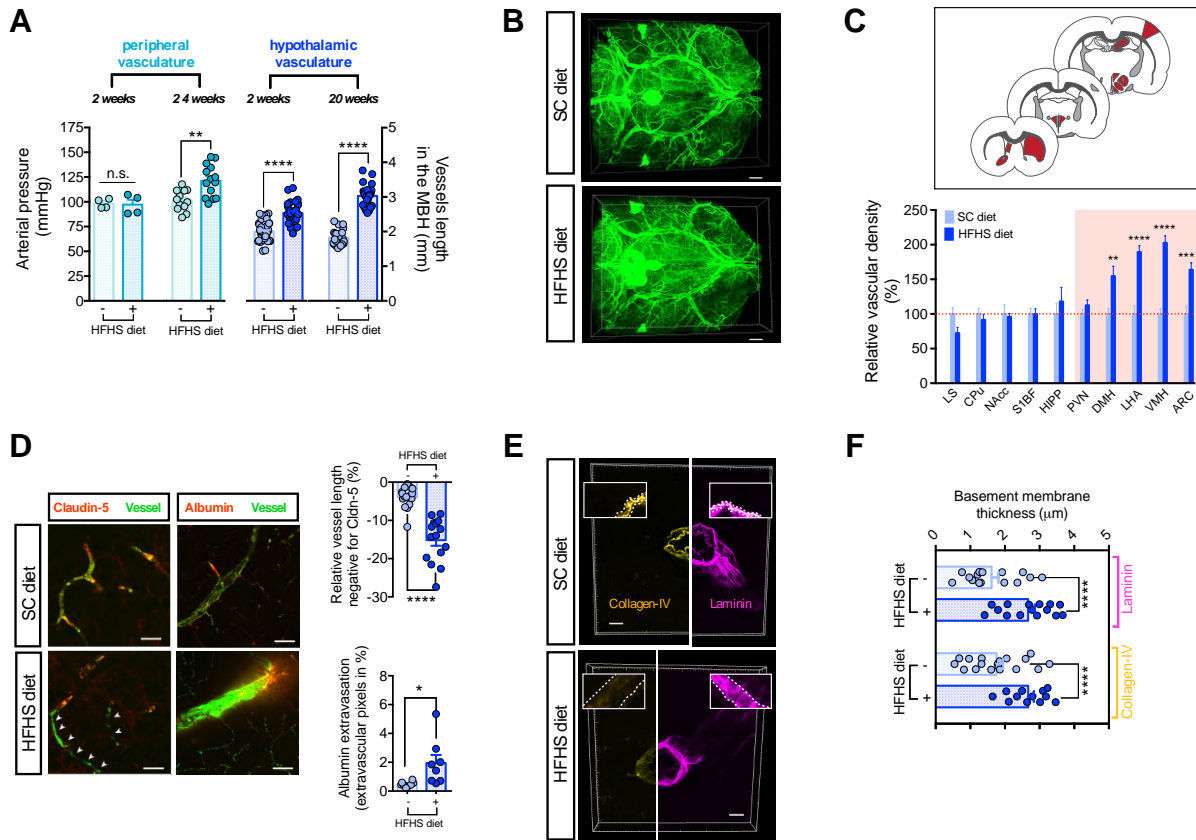


Figure 6: HFHS diet-feeding induces hypervascular microangiopathy specifically in the hypothalamus.

(A) Short-term HFHS diet exposure (two weeks) is insufficient to induce the development of systemic arterial hypertension in C57BL6J mice as compared to long-term HFHS feeding. In contrast, acute HFHS feeding is significantly increasing vascularity within the mediobasal hypothalamus already upon only two weeks of HFHS diet exposure. (B) Light-sheet microscopy images (ventral views) of the 3D whole-brain angioarchitecture in mice fed either SC or HFHS diet and subjected to perfusion-based fluorescent angiography; exposure to HFHS diet is associated with regionally-increased vascularity. (C) Quantitative assessment of vascular density throughout different brain regions revealed HFHS-induced hypervascularization to occur exclusively within hypothalamic areas while being absent from extrahypothalamic regions. (D) Confocal micrographs of hypothalamic microvessels (green) displaying decreased coverage by Cldn-5 (red; left panel) as well as increased extravasation of albumin (red; right panel) as a consequence of long-term HFHS exposure along with corresponding quantification. (E) High-resolution 3D-rendered confocal micrographs of cross-sectional hypothalamic microvessels (4-8 μm) depicting HFHS-induced thickening of the vascular basement membrane as evidenced by increased deposition collagen-IV (yellow) and laminin (magenta) and (F) corresponding quantification. SC diet: standard chow diet; HFHS diet: high-fat/high-sugar diet; LS: lateral septum; CPu: caudate putamen; NAcc: nucleus accumbens; S1BF: somatosensory cortex, barrel field; HIPP: hippocampus; PVN: paraventricular nucleus; DMH: dorsomedial hypothalamus; LHA: lateral hypothalamus; VMH: ventromedial hypothalamus; ARC: arcuate nucleus. Scale bar: 200 μm (C) and 10 μm in (E) and (G). P-values: **** $p < 0.001$; ** $p < 0.01$; * $p < 0.05$. One-way ANOVA or unpaired T-test.

Overall, these results reveal a particular vulnerability of distinct hypothalamic nuclei to develop hypervascular microangiopathy in response to short-term HFHS feeding substantially preceding any changes in systemic blood pressure

4.1.2 Hypervascular microangiopathy of the hypothalamus is reversible in male, but not in female mice

Several lines of evidence suggest that losing bodyweight can reverse some of the reactive changes occurring in the hypothalamus as a consequence of obesogenic diets (Berkseth et al., 2014). Thus, I wondered if diet-induced angiogenesis, which was observed in both sexes, exhibits a similar capacity to reverse upon cessation of caloric excess. Male, formerly obese mice were given SC diet for five weeks, which was found to be not only sufficient to make them lose their excess bodyweight (**Figure 7A**) but also - as revealed by *post-hoc* fluorescent angiography - to normalize the hypothalamic vessel profile to those of lean control mice (**Figure 7B**). Intriguingly however, the same diet reversal paradigm failed to trigger capillary regression in obese female mice suggesting an intriguing gender difference (**Figure 7B**). In addition, fluorescent angiography was applied in a cohort of aged mice (18 months) given that the capacity for vascular remodeling has been previously reported to decrease with age (Benderro and LaManna, 2011). While diet-induced angiogenesis was still evident, the relative extent of this vascularization response was found indeed to be significantly reduced in aged compared to young mice (**Figure 7B**). In conclusion, these results suggest that the diet-induced rearrangement of vascular networks within the hypothalamus is a highly dynamic process, which comprises both the formation of new as well as the regression of existing capillaries (Korn and Augustin, 2015).

Results

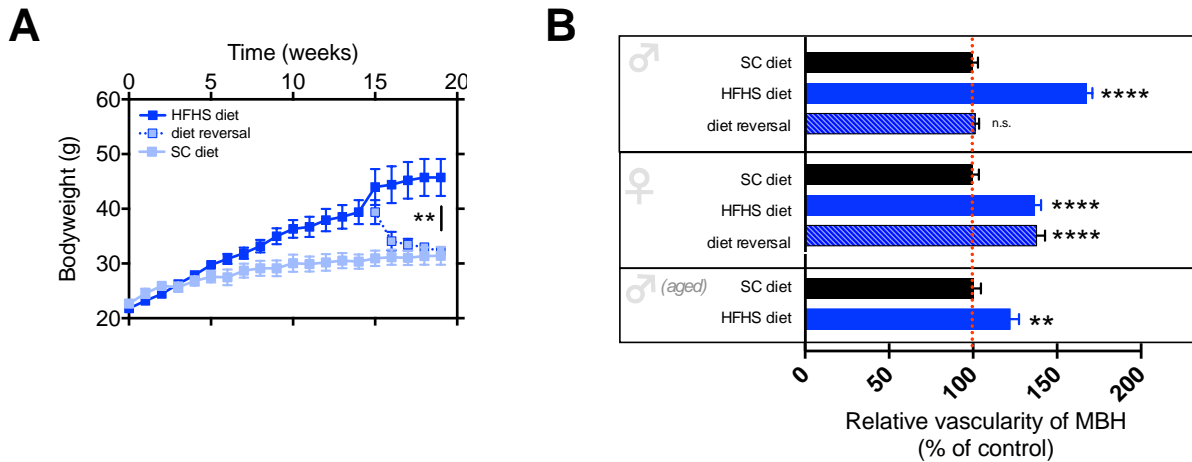


Figure 7: Diet-induced vascular changes are reversible by weight loss in male but not in female mice.

(A) Diet-induced obese male mice subjected to a diet switch back to SC diet for 5 weeks lost excess bodyweight. (B) Intriguingly, diet-reversed mice also showed complete normalization of their hypothalamic vessel profile as compared to mice continuously fed a SC diet. In contrast to male mice, this reversal was not observed in female mice following the same paradigm. Aged mice display a relatively reduced capacity for HFHS-induced hypervascularization. SC diet: standard chow diet; HFHS diet: high-fat/high-sugar diet. P-values: **** $p < 0.001$; ** $p < 0.01$; * $p < 0.05$. One-way ANOVA or unpaired T-test.

4.1.3 Hypothalamic microangiopathy occurs at the onset of bodyweight gain coinciding with increased circulating leptin levels

Obesogenic diets have been previously described to trigger profound cellular rearrangements affecting the cytoarchitecture of the hypothalamus, several of which occur at remarkable rapidity prior to any metabolic disturbances in the periphery (Horvath et al., 2010; Thaler et al., 2012). I thus sought to temporally pinpoint the exact initiation of the angiogenic response to HFHS feeding wondering if it occurs primary or secondary to bodyweight gain. No changes were yet found in hypothalamic vessel density upon 5 days HFHS diet feeding (Figure 8A), although this feeding paradigm was sufficient to impair peripheral glucose tolerance and insulin sensitivity in normal weight mice (Figure 8B). Likewise, no hypothalamic vascular changes were observed in a non-obese mouse model of STZ-induced type I diabetes (Figure 8C) despite a prolonged period of severe hyperglycemia (3weeks) (Figure 8D). Jointly, these findings argue against a causal role of impaired glucose metabolism in the process of hypothalamic vessel remodeling.

Results

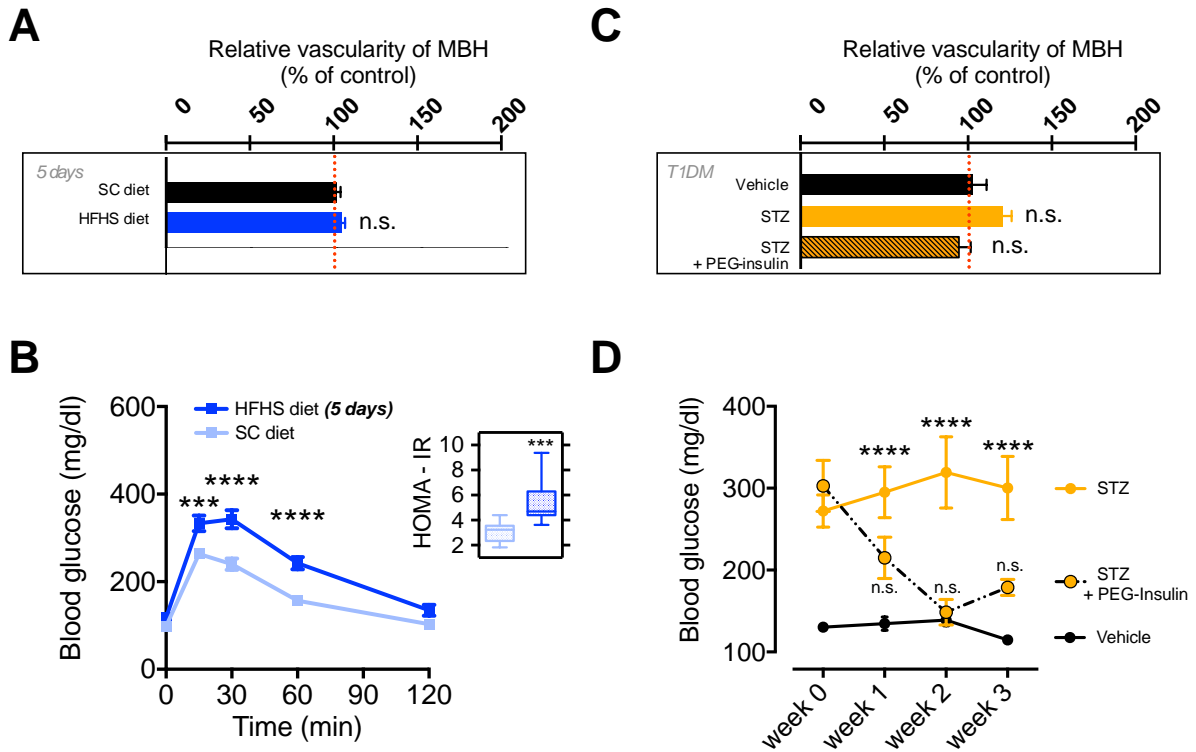


Figure 8: Impaired glucose metabolism does not induce vascular remodeling in the hypothalamus.

(A) Exposure to HFHS diet for 5 days fails to induce hypervascularization of the hypothalamus of C57Bl6/J mice. (B) Notably, this feeding paradigm is sufficient to readily impair glycemic control and insulin sensitivity of these mice as indicated by blood glucose traces upon a glucose tolerance test (2g/kg BW glucose *i.p.*) and HOMA-IR. (C) Likewise, non-obese mice subjected to STZ-induced diabetes do not exhibit alterations in their hypothalamic vessel density despite (D) chronic hyperglycemia over 3 weeks. SC diet: standard chow diet; HFHS diet: high-fat/high-sugar diet; MBH: mediobasal hypothalamus; T1DM: type 1 diabetes mellitus; STZ: streptozotocin; PEG-insulin: polyethylene glycol-attached, long-acting insulin. P-values: **** $p < 0.001$; ** $p < 0.01$; * $p < 0.05$. One-way ANOVA or unpaired T-test.

Instead, we revealed the onset of hypothalamic hypervascularization to occur when bodyweight started to significantly diverge under HFHS feeding (15 days exposure) (Figure 9A). Interestingly, this process was accompanied by the increased expression of pro-angiogenic genes in the hypothalamus but not in the cortex (Figure 9B) with vascular-endothelial growth factor A (VEGF) being among the most robustly HFHS-induced factors (Figure 9C). Notably, the moment of hypothalamic hypervascularization was not only concurrent with the moment of significant bodyweight gain, but additionally coincided with the moment of rising leptin levels on HFHS feeding (Figure 9D). In conclusion, hypothalamic vascularization is not modulated by elevated blood glucose levels but associates with increased bodyweight and serum leptin levels on a HFHS diet.

Results

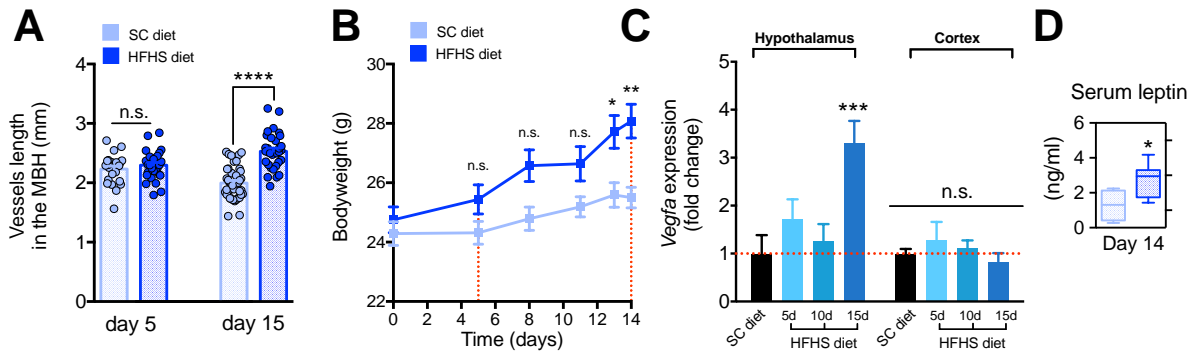


Figure 9: HFHS-induced hypervascularization of the hypothalamus coincides with significant bodyweight gain, hypothalamic expression of angiogenic genes and increased serum leptin.

(A) Hypervascularization of the hypothalamus occurs at the moment of significant bodyweight gain upon 15 days of HFHS feeding, however, not before (5 days). (B) Corresponding bodyweight trajectories of HFHS *versus* SC fed groups. (C) Increased vascularity is associated with gradually elevated expression of pro-angiogenic *Vegfa* mRNA in the hypothalamus, but not in the cortex, in response to different durations of HFHS exposure. (D) Serum leptin levels are significantly elevated upon 15 days of HFHS exposure coinciding with hypothalamic angiogenesis. SC diet: standard chow diet; HFHS diet: high-fat/high-sugar diet; MBH: mediobasal hypothalamus. P-values: **** $p < 0.001$; ** $p < 0.01$; * $p < 0.05$. One-way ANOVA or unpaired T-test.

4.1.4 Circulating leptin concentrations predict risk for CNS-microvascular abnormalities in obese humans and mice

Prompted by these findings in mice, further investigations were initiated in collaboration with the University of Maastricht (Peter Joris, Dr.) in order to disentangle the interrelations between adiposity, serum leptin and neurovasculopathy in human obesity. Over the past years, several properties of retinal blood vessels emerged as robust surrogate indicators of more generalized cerebrovascular damage while being readily accessible for non-invasive optical inspection (Wong et al., 2001; Witt et al., 2006). More recently, a randomized controlled trial demonstrated diet-based weight loss to benefit the function of retinal microvessels in abdominally obese men (Joris et al., 2016). Re-assessment of this previously obtained data provided intriguing evidence that neuro-microvascular improvement in the retina upon diet-intervention highly correlated with reductions in circulating leptin levels (Figure 10A). Notably, the individual extent of diet-induced leptin reduction was found to significantly correlate with improvements in both arteriolar caliber (AC; $r^2 = 0.443^{**}$) and arteriolar-to-venule ratio (AVR; $r^2 = 0.444^{**}$) in the human retina (Figure 10B and C). In addition to these morphometric parameters, certain circulating markers of microvascular

Results

endothelial function significantly correlated with individual leptin reduction, such as soluble endothelial (E)-selectin ($r^2=0.507^{**}$) and intercellular cell adhesion molecules (I-CAM; $r^2=0.292^*$). Interestingly, the improvements in CNS-microvascular parameters by weight loss intervention was not observed at macrovascular level in obese humans, suggesting that the period of intervention was not sufficient to restore macrovessel function (data not shown). Wondering if diet-induced weight loss intervention can reverse hypothalamic hypervascularization in mice, DIO mice were switched back to standard chow (SC) diet for five weeks to reduce excess bodyweight, fat mass and serum leptin levels. As revealed by *post-hoc* fluorescent angiography, diet reversal potently normalized the hypothalamic vessel profile to those of lean control mice permanently fed SC diet (**Figure 10D**). Intriguingly, the extent of hypothalamic vascularity was again highly correlated with both adiposity and circulating leptin across lean, DIO and diet-reversed, formerly DIO mice (**Figure 10E and F**). Overall, these results suggest that rearrangement of microvascular networks at CNS interfaces is a dynamic process in both mice and humans with the capacity to revert damage acquired over the course of dietary obesity. Lastly, changes in circulating leptin levels were found to be highly predictive of abnormalities in neuro-microvascular beds of both mice and humans.

Results

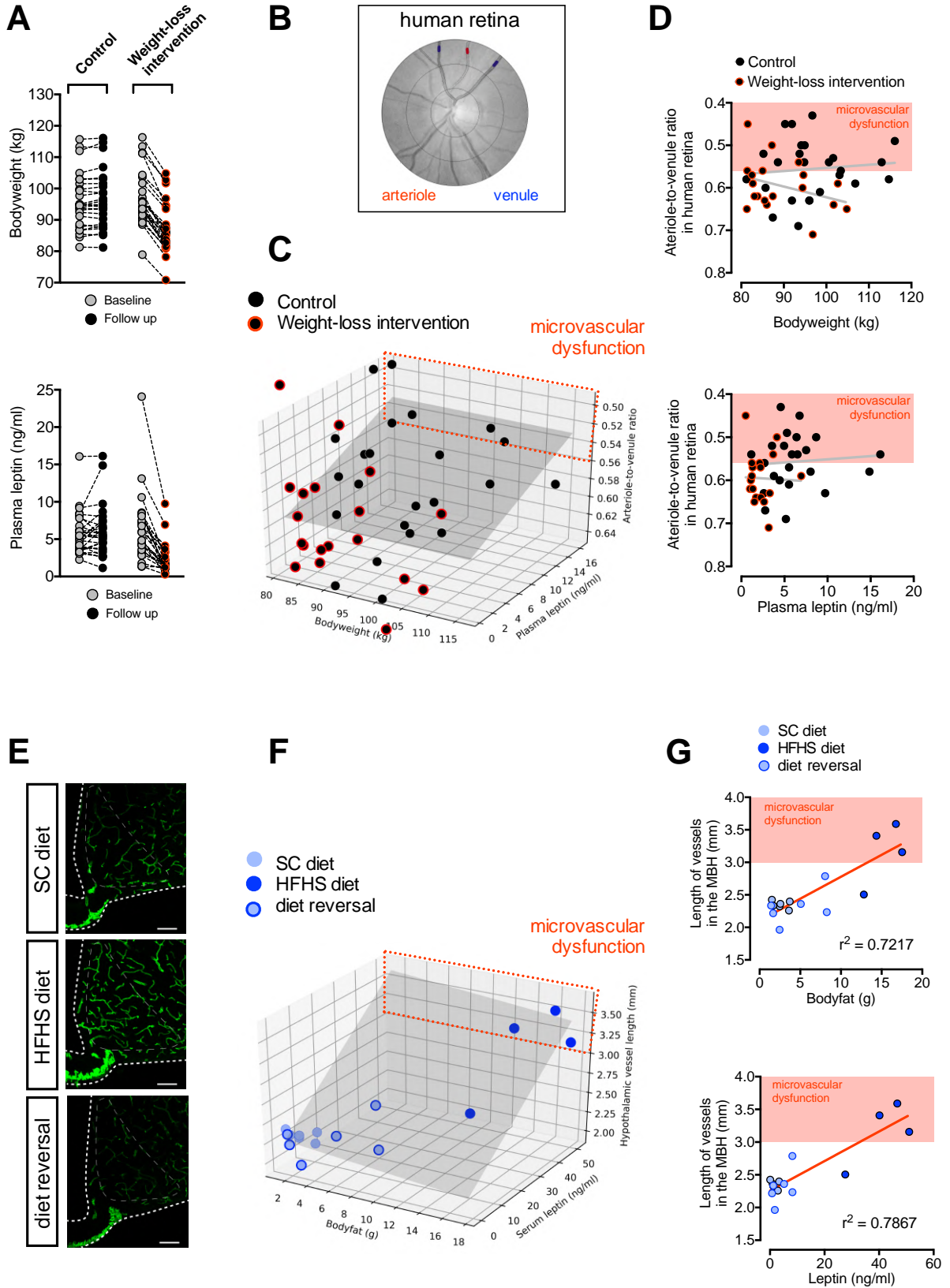


Figure 10: Circulating leptin levels predict neurovasculopathies in both human and mice.

Results

(A) Re-assessment of weight-loss-induced changes in microvascular and endocrine function of abdominally obese men obtained from a previously published randomized controlled trial (Joris et al., 2016). Diet intervention induced bodyweight loss and marked reduction in plasma leptin levels in abdominally obese men. (B) Illustrative retina scan of a study participant depicting arterioles (red) and venules (blue) whose respective calibers got employed as indicators for neurovascular function. (C) 3D scatter plot of multiple linear regressions displaying correlations for bodyweight, plasma leptin and arteriolar-to-venule ratio of individual subjects post-intervention. Individual linear regression correlating the arteriole-to-venule ratio with (D) bodyweight or (E) plasma leptin. (F) Confocal micrographs depicting the MBH vessel profile of SC-fed, HFHS-fed and diet reversed mice. (G) 3D scatter plot of multiple linear regressions displaying correlations for bodyfat, serum leptin and microvessel length in the MBH across individual mice. Individual linear regression correlating MBH vascularity with (H) bodyfat or (I) serum leptin. SC diet: standard chow diet; HFHS diet: high-fat/high-sugar diet; MBH: mediobasal hypothalamus. Scale bar: 100 μm . P-values: **** $p < 0.001$; ** $p < 0.01$; * $p < 0.05$. One-way ANOVA or unpaired T-test.

4.1.5 Leptin signaling in the brain rather than obesity *per se* acts as a driver in the development of hypothalamic neovascularization

Given the substantial cross-correlation between adiposity and leptin levels I aimed to functionally disentangle if hypothalamic microangiopathy could indeed be driven by HFHS-induced signals such as leptin or by adiposity *per se*. Thus, vascular profiles have been assessed from monogenetically obese leptin-deficient (Lep^{ob}), leptin receptor-deficient (Lep^{db}) and type 4 melanocortin receptor ($\text{MC}_4\text{R}^{-/-}$)-deficient mice all of which maintained on a SC diet. Despite the massive adiposity of these models, only $\text{MC}_4\text{R}^{-/-}$ mice showed increased hypothalamic vascularity compared to lean heterozygous littermate controls. In contrast, hypothalamic vessel density remained entirely unchanged in Lep^{ob} and Lep^{db} mice, both of which characterized by the single commonality of absent leptin signaling (**Figure 11A**). Intrigued by the different vascular profiles among genetically obese mouse models and the fact that $\text{MC}_4\text{R}^{-/-}$ mice are distinct in such that they retain intact leptin action, we further explored the involvement of leptin in promoting hypothalamic neovascularization. Thus, we tested this hypothesis by treating leptin-deficient Lep^{ob} mice with exogenous leptin (10 $\mu\text{g}/\text{mouse}/\text{day}$; *s.c.*). After 2 weeks of leptin replacement, Lep^{ob} mice displayed significant hypothalamic hypervascularization (**Figure 11A**). Consistently, leptin administration to lean C57BL6/J mice (3 mg/kg BW; *i.p.*) dramatically increased the pro-angiogenic VEGF signaling in the hypothalamus even exceeding the effect of HFHS diet (**Figure 11B and C**). Consistently, both HFHS feeding and an acute leptin administration (5 mg/kg BW; *i.p.*) result in the accumulation of HIF-1 α protein levels, the direct transcriptional regulator of VEGF, within the hypothalamus as determined by Western blot (**Figure 11D**). Notably, obese leptin-

Results

deficient Lep^{ob} mice tended to have overall reduced hypothalamic HIF-1 α protein levels. Likewise, hypothalamus-specific induction of HIF-1 α in response to leptin by using an *ex-vivo* readout in HIF-1/ODD-Luciferase mice (**Figure 11E**), altogether suggesting an interaction between leptin and HIF-1 α signaling in the hypothalamus. Overall these findings indicate that leptin signaling in the brain is a determining factor driving the upregulation of HIF-1 α /VEGF signaling in the hypothalamus in obese mice, which is associated with the initiation of hypothalamic hypervascularization, a recurrent phenomenon observed in DIO and $MC_4R^{-/-}$ mice but absent in Lep^{ob} and Lep^{db} mice.

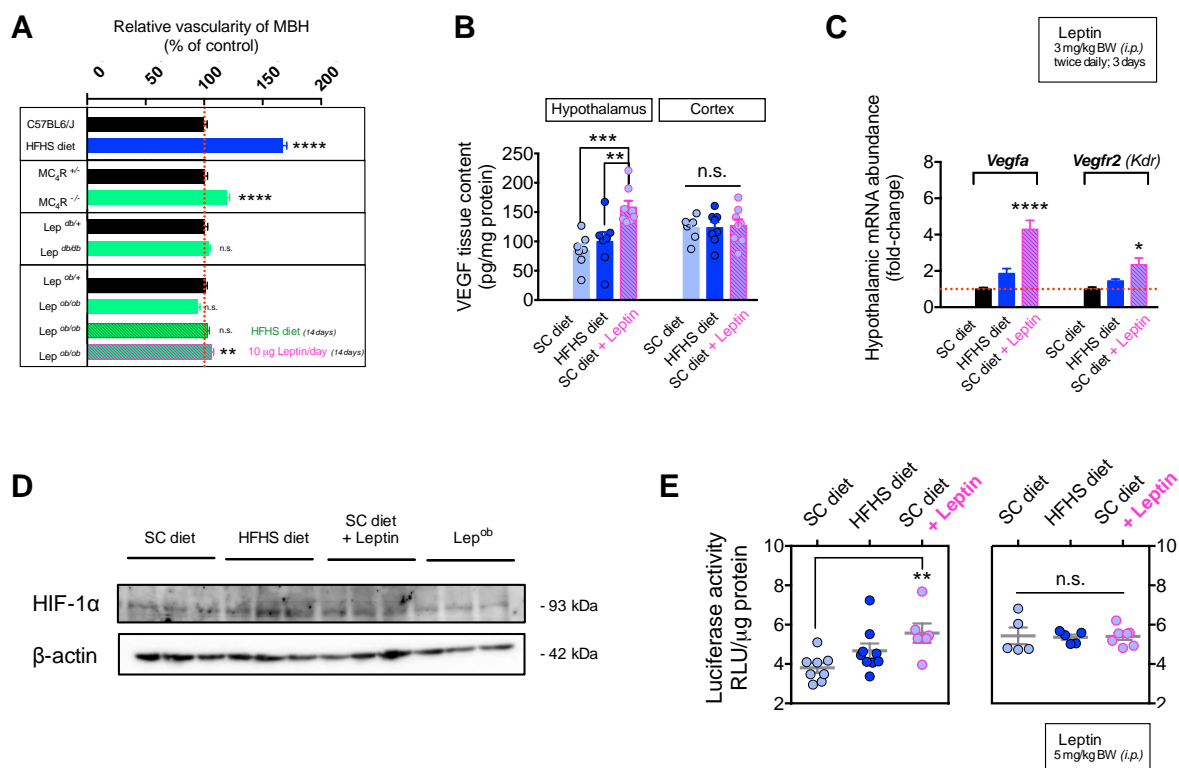


Figure 11: Leptin signaling induces pro-angiogenic signaling in the hypothalamus.

(A) Relative vascularity in the mediobasal hypothalamus (MBH) of diet-induced obese as well as genetically obese mice. While moderate but significant hypervascularization of the hypothalamus is present in MC_4R mutants, mice lacking leptin (Lep^{ob}) or leptin receptor (Lep^{db}) present normal vascular profiles despite massive obesity; chronic administration of exogenous leptin (10 μ g/mouse/day for 14 days, *s.c.*), but not feeding a HFHS diet, induced significant neovascularization in the hypothalamus of Lep^{ob} mice. (B) Repeated leptin administration to C57BL6/J mice (3mg/kg BW, twice daily for 3 days, *i.p.*) increased VEGF protein content of hypothalamic lysates as well as (C) the abundance of *Vegfa* and *Kdr/Vegfr2* mRNA relative to mice fed HFHS diet (15 days) or SC diet. (D) Western blot analysis of hypothalamic HIF-1 α protein content of mice exposed to SC diet, HFHS diet (5 days), acutely treated with leptin (5mg/kg BW, *i.p.*) as well as leptin-deficient Lep^{ob}

Results

mice. **(E)** Luciferase activity in hypothalamic lysates of HIF-1/ODD-Luciferase mice that were either fed SC diet, HFHS diet (5 days) or acutely treated with leptin (5mg/kg BW, *i.p.*). SC diet = standard chow diet; HFHS diet: high-fat/high-sugar diet; MC4R: melanocortin receptor 4; Lep^{db}: leptin-receptor deficient mouse mutant; Lep^{ob}: leptin-deficient mouse mutant; VEGF: vascular endothelial growth factor; *Vegfa*: mRNA transcript of vascular-endothelial growth factor; *Vegfr2/Kdr*: mRNA transcript of vascular endothelial growth factor receptor 2/kinase insert domain receptor; HIF-1 α : hypoxia-inducible factor 1 α . P-values: **** p<0.001; ** p<0.01; *p<0.05. One-way ANOVA or unpaired T-test.

4.1.6 Astrocytes regulate the production of VEGF within the hypothalamus via leptin receptor

In order to identify the cellular source of hypothalamic VEGF production upon either HFHS feeding or leptin treatment an array of double-immunohistochemical staining was conducted. In turn, VEGF immunoreactivity was revealed to exclusively co-localize with astrocytes positive for glial fibrillary acidic protein (GFAP⁺) (**Figure 12A**) while being absent from both neurons (NeuN⁺; **Figure 12B**) and microglia (Iba1⁺; **Figure 12C**). When comparing the hypothalamus from lean, SC diet-fed mice with obese, HFHS diet-fed mice a prominent increase in vascularity is observed, which is accompanied by increasingly abundant VEGF immunoreactivity localized to astroglial endfeet (**Figure 12D**).

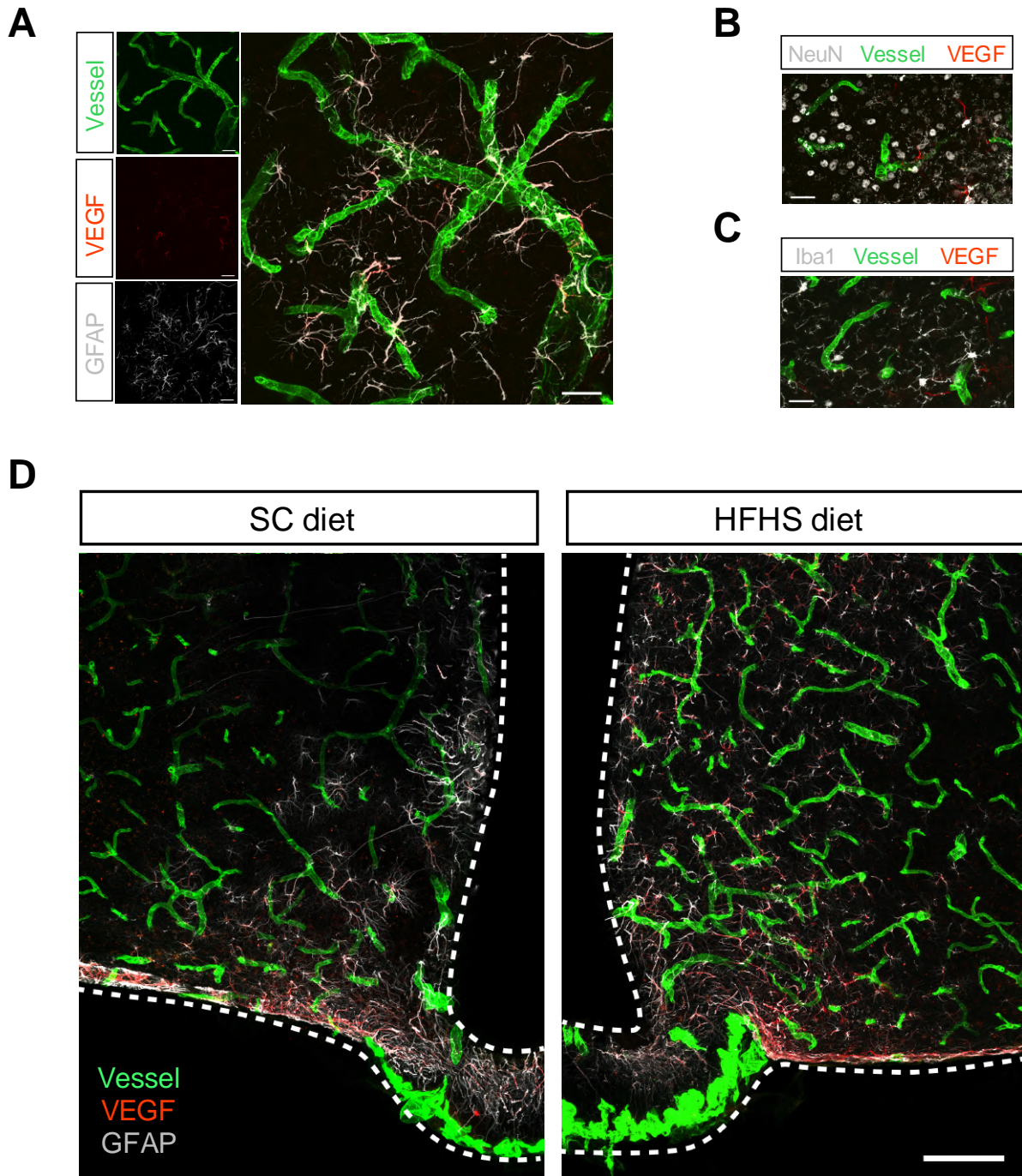


Figure 12: Hypothalamic astrocytes are the cellular source of HFHS-induced VEGF.

(A) Co-immunohistochemical staining reveals VEGF to primarily colocalize with GFAP-positive astrocytes, but neither with neurons (NeuN⁺; B) nor with microglia (Iba1⁺; C). (D) Confocal micrographs of mice fed HFHS diet for 20 weeks exhibit increased VEGF immunoreactivity and hypervascularization compared to SC fed mice. SC diet: standard chow diet; HFHS diet: high-fat/high-sugar diet; FITC: fluorescein isothiocyanate; VEGF: vascular endothelial growth factor; GFAP: glial-fibrillary acidic protein; NeuN: neuronal nuclei; Iba1: ionized calcium-binding adapter protein 1. Scale bar: 10 μ m (A,B & C) and 100 μ m (D).

Results

In order to gain genetic access to this particular subset of hypothalamic astrocytes that increase VEGF expression in response to both HFHS exposure or leptin administration, the recombination pattern of GFAP and GLutamate ASpartate Transporter (GLAST) inducible Cre-driver lines were assessed (GFAP.CreER^{T2} and GLAST.CreER^{T2}, respectively). Visualization of recombined astrocyte subpopulations was achieved for each of these astrocytic Cre-driver lines by crossing them with the Cre-dependent dual reporter mouse line ROSA26^{mT/mG} (**Figure 13A and B**). Interestingly, the induction of VEGF immunoreactivity by HFHS diet feeding was found to be substantially attributable to both GFAP.CreER^{T2}/mG⁺ astrocytes (55.6%; N⁰ =188 cells; 3 mice) and GLASTCreER^{T2}/mG⁺ astrocytes (65.9%; N⁰ =219 cells; 4 mice) (**Figure 13C**).

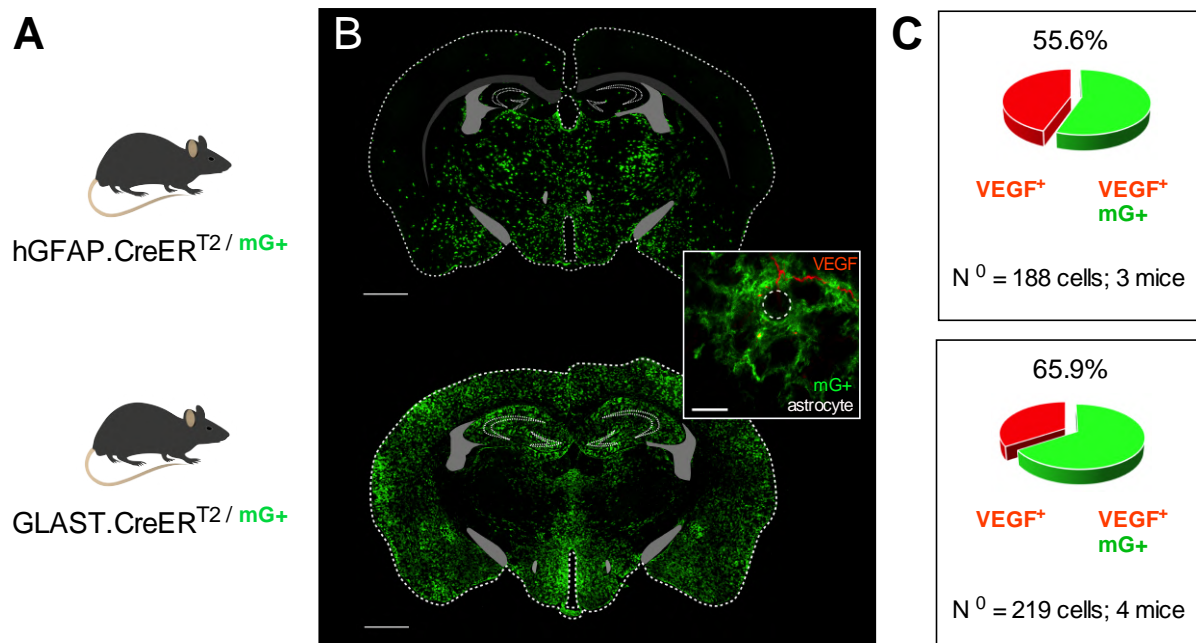


Figure 13: Evaluation of genetic mouse lines to target astroglial HIF-1 α /VEGF signaling.

(A) Two astrocyte-specific inducible Cre-driver lines were individually backcrossed to a Cre-dependent dual fluorescent reporter line in order to generate hGFAP.CreER^{T2/mG⁺} and GLAST.CreER^{T2/mG⁺}, respectively. (B) Confocal overview scans of respective fluorescent reporter mice demonstrate characteristic recombination patterns of astrocytes throughout the brain (green); insert depicting an individual hypothalamic astrocyte expressing VEGF (red) that was targeted by Cre-mediated recombination as evidenced by the induction of EGFP expression (mG⁺; green). (C) Pie chart analysis demonstrating the fraction of VEGF⁺ astrocytes in the hypothalamus targeted by Cre-mediated recombination in hGFAP.CreER^{T2/mG⁺} and GLAST.CreER^{T2/mG⁺}, respectively. Scale bar: 500 μ m and 10 μ m (insert).

Results

To assess if the production of VEGF in hypothalamic astrocytes might be mediated by the direct influence of leptin, the postnatal ablation of the long form of the leptin receptor (LepR) was induced in GFAP.CreER^{T2/+} positive cells (LepR^{ΔGFAP/+} mice) as previously described (Kim et al., 2014). Importantly, these LepR^{ΔGFAP/+} mice failed to increase astrocytic VEGF (Figure 14A and B) and showed a blunted pSTAT3 activation of astrocytes (Figure 14C) in response to repeated leptin administration (3mg/kg BW *i.p.*; 2x twice daily). In conclusion, these results suggest that astrocytes regulate VEGF production in the hypothalamus upon leptin injections *via* the activation of LepR signaling.

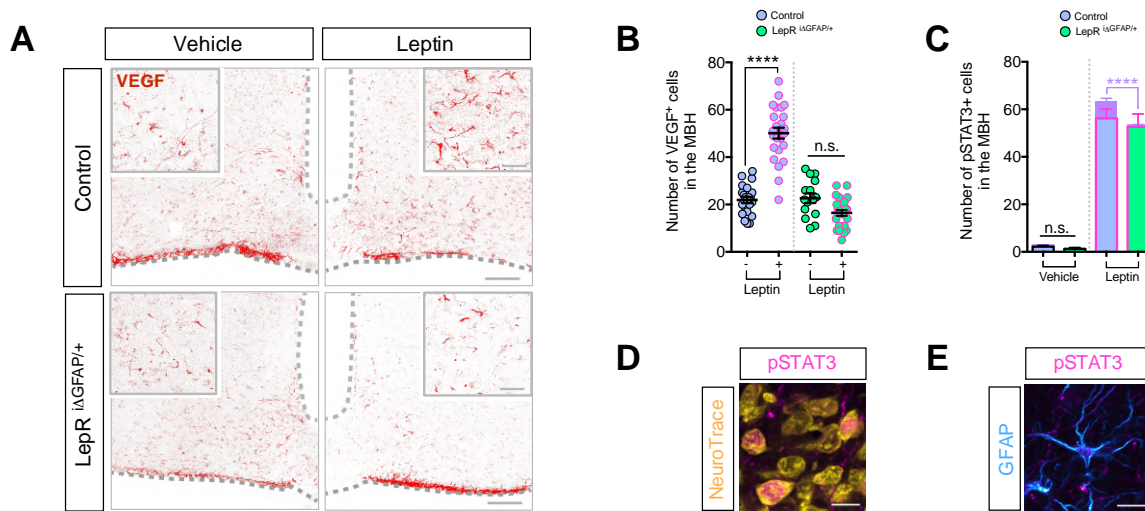


Figure 14: LepR signaling in hypothalamic astrocytes is required for VEGF induction upon leptin administration.

(A) Confocal micrographs depicting increased VEGF immunoreactivity in the MBH of mice that received repeated leptin injections (3mg/kg BW, twice daily for 3 days, *i.p.*) as compared to vehicle injected control animals; mice devoid of LepR specifically in astrocytes (LepR^{ΔGFAP/+} mice) do not show upregulated VEGF in response to leptin. (B) Corresponding quantification of VEGF immunopositive cells within the MBH. (C) Quantification of pSTAT3+ cells distinguishing neurons (NeuroTrace⁺) and astrocytes (GFAP⁺) showing a significant reduction in leptin-induced STAT3 phosphorylation in hypothalamic astrocytes of LepR^{ΔGFAP/+} mice. Illustrative high-magnification confocal scans of neuronal (NeuroTrace; yellow; D) or astroglial (GFAP; cyan; E) localized pSTAT3 (magenta). SC diet: standard chow diet; HFHS diet: high-fat/high-sugar diet; VEGF: vascular endothelial growth factor; GFAP: glial-fibrillary acidic protein; NeuN: neuronal nuclei; Iba1: ionized calcium-binding adapter protein 1. Scale bar: 100 μm (A) and 10 μm (D). P-values: **** p<0.001; ** p<0.01; *p<0.05. One-way ANOVA or unpaired T-test.

4.1.7 Astrocyte-specific loss of HIF-1 α abrogates HFHS-induced VEGF expression and hypervascularization in the hypothalamus

The preponderance of evidence prominently pointed towards leptin as a stimulator of HIF-1 α /VEGF signaling in hypothalamic astrocytes during HFHS feeding to in turn adjust local vessel density. In order to assess whether the dynamic remodeling of the hypothalamic vasculature by HFHS feeding is indeed depending on the expression of HIF-1 α by astrocytes, an array of genetic loss-of-function mouse models was generated. Therefore, HIF-1 α ^{loxP/loxP} mice were crossed with respective astrocytic Cre-driver lines giving rise to knockout HIF-1 α in GFAP or GLAST expressing astrocytes (HIF-1 α ^{i Δ GFAP/+} mice and HIF-1 α ^{i Δ GLAST/+} mice respectively).

For validating the successful postnatal ablation of HIF-1 α , HIF1 α ^{i Δ GFAP/+} mice were backcrossed with the Cre-dependent ROSA26^{mT/mG} reporter line. Upon induction of Cre-mediated recombination *via* tamoxifen administration in adulthood, mice were sacrificed, their brains collected and immediately subjected to magnetic-activated cell sorting and pre-enrichment of ACSA2⁺ astrocytes. Subsequently, fluorescence-assisted cell sorting (FACS) was employed to separate non-recombined (tdTomato⁺; red) from recombined (EGFP⁺; green) astrocytes in order to determine their expression of HIF-1 α (HIF-1 α downregulation in GFAP.CreER^{T2+} astrocytes: 79.8 ± 0.087 %; **Figure 15**).

Results

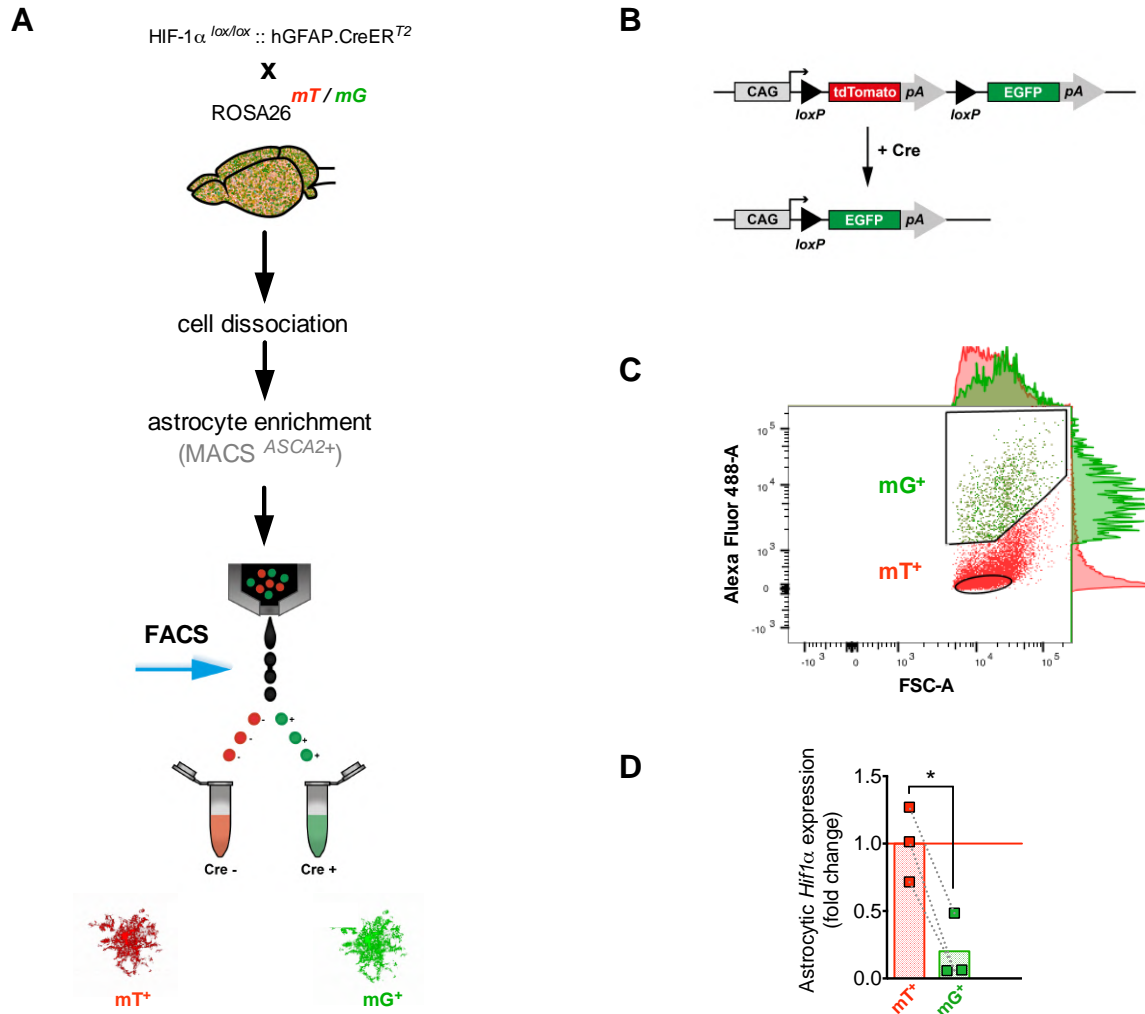


Figure 15 : Validation of the successful ablation of HIF-1 α exon 2 locus in astrocytes.

(A) Schematic diagram depicting the approach used to validate the genetic HIF-1 α ^{Δ GFAP/+} mouse model, which was therefore previously backcrossed to a dual fluorescent Cre-dependent reporter mouse line. Brains of tamoxifen-induced mice were dissociated and subjected to magnetic-assisted cell sorting using the marker ACSA2 in order to pre-enrich astrocytes. Non-recombined (red) and recombined (green) astrocytes were immediately separated using flow cytometry. (B) Schematic organization of the dual fluorescent Cre-dependent reporter allele. (C) Representative FACS plot with the x-axis representing forward scatter (FSC-A) and the y-axis representing Alexa Fluor 488 fluorescence; gating of mG⁺ (green) and mT⁺ (red) populations are indicated and the gating. (D) Gene expression analysis using exon 2 specific HIF-1 α probes showing marked reduction of transcripts in recombined (green) cells. MACS: magnetic-activated cell sorting; ACSA2: astrocyte-specific antigen 2; FACS: fluorescence-assisted cell sorting; mT: membrane-localized tdTomato; mG: membrane-localized EGFP; CAG: fusion promoter element consisting of cytomegalovirus early enhancer element, chicken β -actin promoter, intron 1 and exon 1, splice acceptor of β -globin gene; FCS-A: forward scatter; HIF-1 α : hypoxia-inducible factor 1 α . P-values: *p<0.05. Unpaired T-test.

Results

Interestingly, it was found that both HIF-1 α ^{i Δ GFAP/+} mice and HIF-1 α ^{i Δ GLAST/+} mice to be equally protected from inducing excessive VEGF expression in astrocytes upon HFHS feeding (**Figure 16A and 4B**). Interestingly, preventing excessive VEGF *in vivo* additionally abrogated the development of hypervascular angiopathy under HFHS feeding (**Figure 16C**). Lastly, the successful ablation of HIF-1 α was mimicked *in-vitro* using primary astrocyte cultures derived from HIF-1 α ^{i Δ GLAST/mG⁺} mice, which additionally allow the visualization of Cre-mediated recombination upon 4-OH-tamoxifen exposure by expression of membrane localized EGFP (**Figure 16D**). Besides the normalization of the hypothalamic vessel density, astroglial HIF-1 α deletion averted several hypothalamic microvessel-glia abnormalities as observed in HFHS fed mice such as basement membrane thickening based on increased laminin and collagen-IV (**Figure 17A**). In addition, astroglial HIF-1 α deletion rectified the reduced claudin-5 coverage of hypothalamic microvessels (**Figure 17B and C**) and microvascular hyperpermeability towards the serum protein albumin (**Figure 17D**). Lastly, mice lacking HIF-1 α in astrocytes were protected from HFHS-induced reactive microgliosis in the MBH, which is characterized by increased number of Iba⁺ microglial cell (**Figure 217E**).

Results

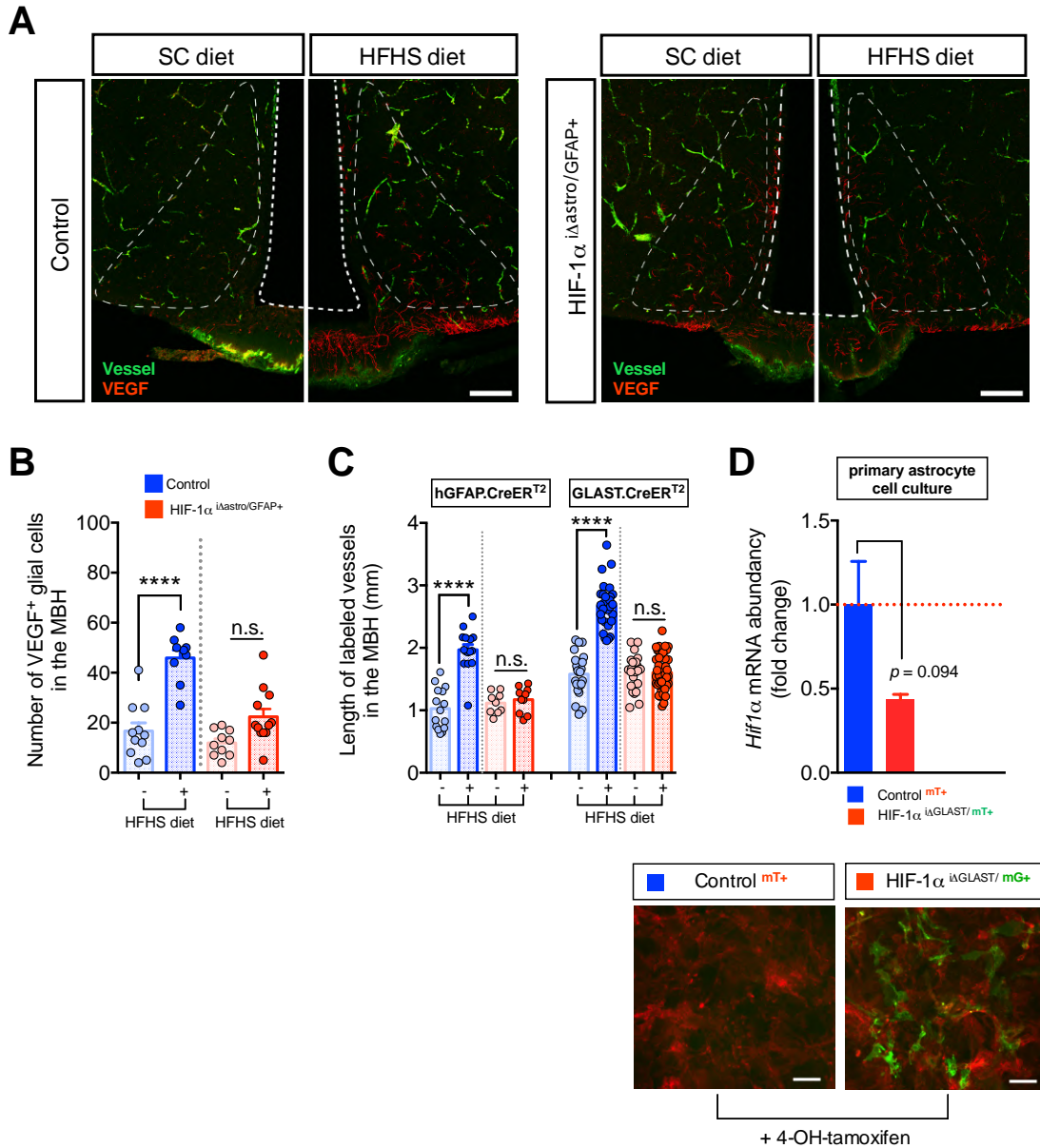


Figure 16: Astrocyte-specific loss of HIF-1 α abrogates VEGF upregulation and hypothalamic angiopathy in response to HFHS feeding.

(A) Representative confocal micrographs showing the vascular profile (green) and VEGF immunoreactivity (red) in the MBH of control mice and HIF-1 α Δ GFAP^{+/+} mice fed either SC or HFHS diet, respectively. (B) HIF-1 α Δ GFAP^{+/+} mice are protected from the HFHS-induced up-regulation of VEGF as well as from (C) developing hypothalamic angiopathy; ablating HIF-1 α from another astrocyte population (GLAST⁺) recapitulates this finding. (D) *In-vitro* validation using primary hypothalamic astrocytes cultured from Control ^{mT+} or HIF-1 α Δ GLAST/ mG⁺ mice. Exposure to 4-OH-tamoxifen induced a near-significant down-regulation of *Hif1a* mRNA; fluorescent micrographs of EGFP induction. SC diet: standard chow diet; HFHS diet: high-fat/high-sugar diet; HIF-1 α : hypoxia-inducible factor 1 α ; VEGF: vascular endothelial growth factor; GFAP: glial-fibrillary acidic protein; GLAST: glutamate aspartate transporter; MBH: mediobasal hypothalamus; Scale bar: 100 μ m. P-values: **** p<0.001; ** p<0.01; * p<0.05. One-way ANOVA or unpaired T-test.

Results

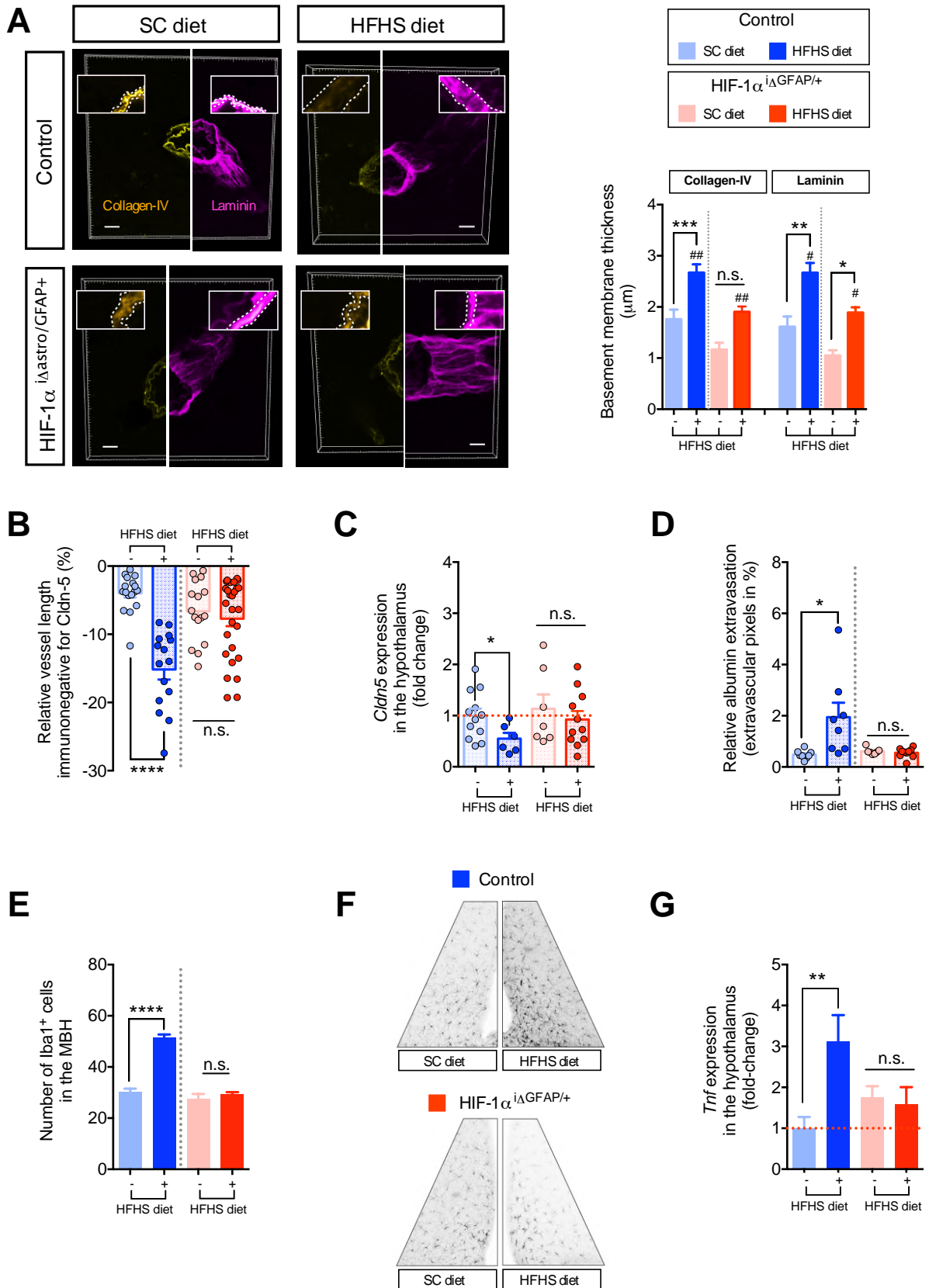


Figure 17: Loss of astroglial HIF-1a signaling prevents vascular impairment and reactive microgliosis under HFHS feeding.

Results

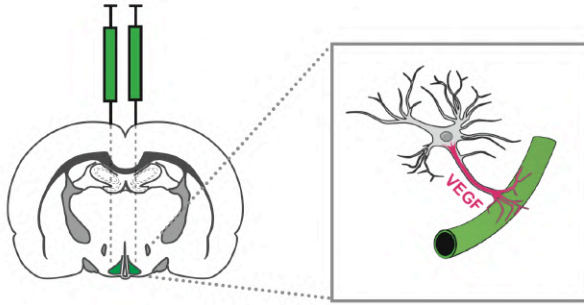
(A) 3D-rendered confocal micrographs depict HFHS-induced thickening of the vascular basement membrane as exemplified by collagen-IV (yellow) and laminin (magenta) and corresponding quantification. (B) Cldn-5 coverage of the hypothalamic vasculature as assessed by confocal microscopy of immunohistochemical visualization of endothelial tight-junctions. (C) Hypothalamic *Cldn5* expression is significantly reduced by HFHS feeding in control but not in HIF-1 α ^{i Δ GFAP/+} mice. (D) Quantification of albumin extravasation into the hypothalamic parenchyma as determined by confocal microscopy upon immunohistochemical detection. (E) Quantification of Iba1⁺ microglia in the MBH with representative confocal micrographs. SC diet: standard chow diet; HFHS diet: high-fat/high-sugar diet; HIF-1 α : hypoxia-inducible factor 1 α ; Cldn-5: Claudin-5; VEGF: vascular endothelial growth factor; GFAP: glial-fibrillary acidic protein; MBH: mediobasal hypothalamus. *Tnf*: tumor necrosis factor mRNA. Scale bar: 100 μ m. P-values: **** p<0.001; ** p<0.01; *p<0.05. One-way ANOVA or unpaired T-test.

4.1.8 Astrocyte-derived VEGF is necessary and sufficient for dynamic hypothalamic microvascular remodeling

In order to confirm that astrocyte-derived VEGF is the necessary and sufficient factor underlying the dynamic remodeling of the hypothalamic vasculature, I directly manipulated the expression of VEGF in astrocytes of the MBH by virus-mediated gene transfer (**Figure 18A**). In the first approach, local VEGF expression in MBH astrocytes was knocked-down using small hairpin (sh)RNA. Intriguingly, this interference readily abrogated the hypervascularization response to HFHS feeding in the MBH of shRNA(VEGF)^{v Δ GFAP/+} mice (**Figure 18B**) correlating with reduced VEGF⁺ cells (**Figure 18C**). Conversely, I next attempted to restore VEGF expression in astrocytes otherwise devoid of HIF-1 α and thus injected astrocyte-specific rAAV into HIF-1 α ^{v Δ GFAP/+} mice. Re-induction of astroglial VEGF expression in HIF-1 α ^{v Δ GFAP/+} mice proved sufficient for promoting marked hypervascularization even exceeding what is typically observed in HFHS-fed control mice (**Figure 18D**). Overall these findings indicate that MBH astroglial VEGF is necessary and sufficient for developing hypothalamic angiopathy in response to HFHS feeding.

Results

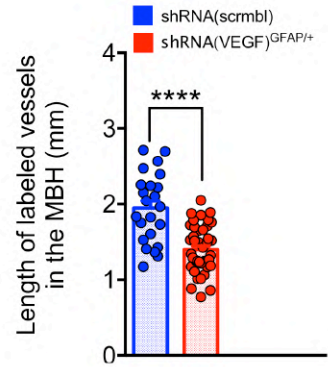
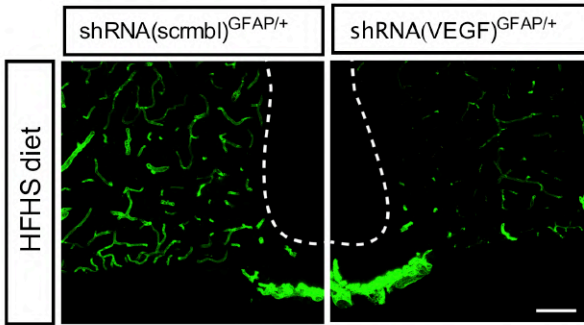
A



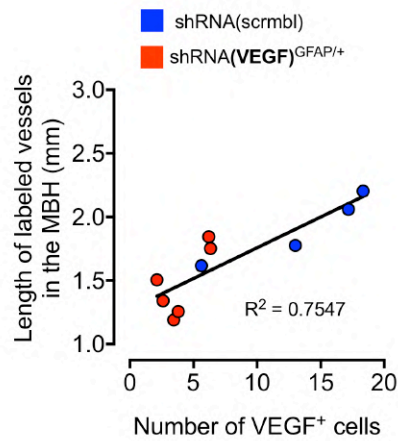
1.) VEGF knock-down

2.) VEGF rescue

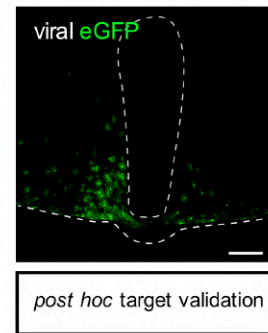
B



C



D



E

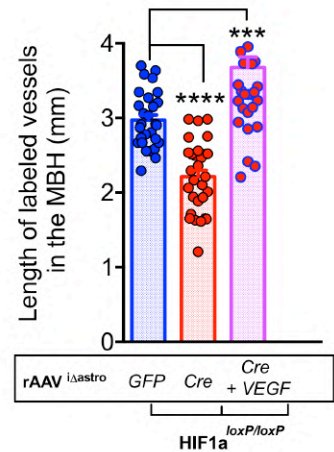
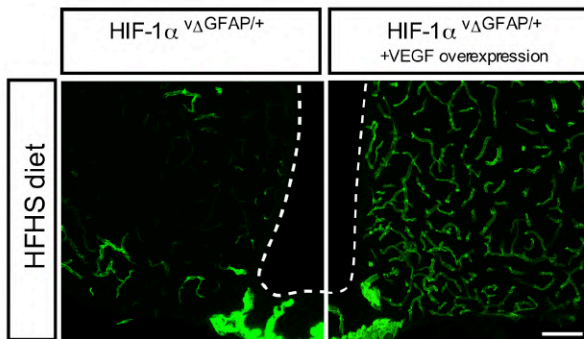


Figure 18 : Astroglial VEGF is necessary and sufficient to remodel the hypothalamic angioarchitecture upon HFHS feeding.

(A) Schematic diagram illustrating stereotaxic injections of rAAV into the MBH of mice in order to (1.) knock-down or (2.) rescue VEGF expression in hypothalamic astrocytes. (B) Confocal micrograph showing the vascular profile in the MBH of HFHS fed mice with astroglial knock-down of VEGF *versus* control including the corresponding quantification. (C) Linear regression plot correlating hypothalamic vessel length with number of VEGF⁺ cells in the hypothalamus. (D) Confocal image of the hypothalamus showing bilateral viral GFP expression upon stereotaxic injections. (E) Confocal micrograph showing the vascular profile in the MBH of HFHS fed mice overexpressing VEGF in astrocytes devoid HIF-1 α *versus* HIF-1 α ^{vΔGFAP/+} including the corresponding quantification. HFHS diet: high-fat/high-sugar diet; rAAV: recombinant Adeno-associated virus; shRNA: small hairpin RNA; scrmb1: scrambled control RNA; HIF-1 α : hypoxia-inducible factor 1 α ; VEGF: vascular endothelial growth factor; GFAP: glial-fibrillary acidic protein; MBH: mediobasal hypothalamus; Scale bar: 100 μ m. P-values: **** p<0.001; ** p<0.01; *p<0.05. One-way ANOVA or unpaired T-test.

4.1.9 Blocking VEGF expression in MBH astrocytes prevents arterial hypertension and sympathetic hyperactivity in diet-induced obesity.

Arterial hypertension is widely regarded as a significant contributor to microvascular remodeling (Folkow et al., 1958). However, as mentioned above, HFHS-induced astroglial VEGF induction and hypervascularization of the hypothalamus occur significantly prior to diet-induced arterial hypertension (**Figure 9A**). This unexpected temporal succession was prompting me to further explore if microvascular abnormalities in hypothalamic pre-autonomic areas impact central hypertensive regulation upon HFHS feeding. Strikingly, mice receiving virus-mediated blockade of astroglial VEGF expression were protected from developing arterial hypertension upon a HFHS diet despite being equally obese as control animals (**Figure 19A**). Therefore, such marked protection in obese shRNA(VEGF)^{vΔGFAP/+} mice was independent of changes in bodyweight (**Figure 19F**), serum leptin levels (**Figure 19G**) and basic endothelial function as measured by acetylcholine-induced vascular relaxation (**Figure 19H**). Instead, blockade of astroglial VEGF in DIO mice prevented the obesity-induced hyperactivation of sympathetic nerve activity (SNA) towards cardiovascular targets. By lowering blood pressure experimentally using intracarotid sodium nitroprusside (SNP), both experimental groups showed similar vasodilation (**Figure 19I**); however, obese shRNA(VEGF)^{vΔGFAP/+} mice displayed a blunted counterregulatory acceleration in heart rate *via* the sympathetically-mediated baroreflex as compared to HFHS littermates control mice (**Figure 19B**). In order to further assess sympathetic modulation of the cardiovascular system

Results

in this model, we probed $\beta_{1/2}$ -adrenoreceptor function by intracarotid infusion of its pharmacological agonist isoproterenol. While long-term feeding HFHS diet to control mice induced substantial resistance towards isoproterenol-mediated β_1 -stimulation of heart rate, obese $\text{shRNA(VEGF)}^{\Delta\text{GFAP}/+}$ mice retained sensitivity towards isoproterenol's chronotropic action (**Figure 19B**) despite showing the same grade of obesity. Even though no changes in circulating catecholamine were detected between groups (**Figure 19C**), $\text{shRNA(VEGF)}^{\Delta\text{GFAP}/+}$ mice fed a HFHS diet showed an intriguing increase in the expression of β_2 -adrenergic receptors in the heart (**Figure 19D**). Higher β_2 -adrenoreceptor density may underlie the restored contractile responsiveness of $\text{shRNA(VEGF)}^{\Delta\text{GFAP}/+}$ mice towards isoproterenol under HFHS feeding as well as the cardiovascular protection despite an obesogenic environment. Likewise, HFHS feeding failed to significantly increase heart weight in $\text{shRNA(VEGF)}^{\Delta\text{GFAP}/+}$ mice compared to respective SC fed controls as otherwise observed in shRNA(scrambl) control animals (**Figure 19E**). Overall these findings indicate that interfering with astroglial VEGF expression locally restricted to the MBH prevents the development of HFHS diet-induced arterial hypertension *via* the abrogation of hyperactive sympathetic outflow towards the cardiovascular system.

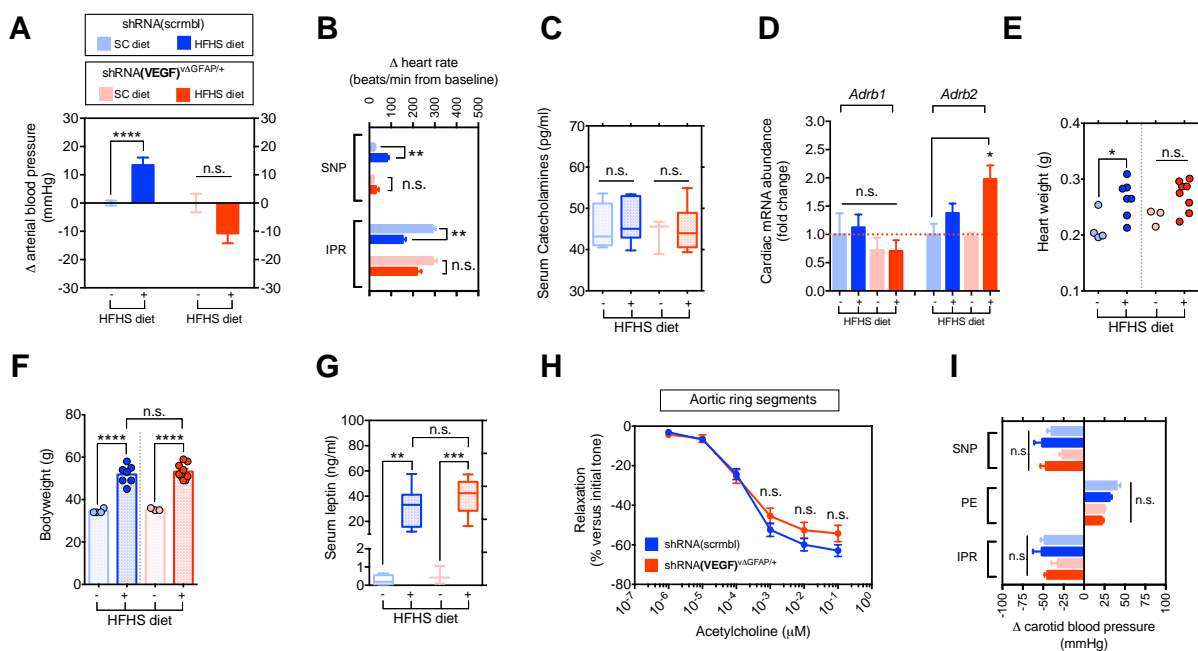


Figure 19: VEGF blockade in hypothalamic astrocytes protects from the development of HFHS-induced systemic hypertension.

Results

(A) Relative changes of arterial blood pressure in response to HFHS feeding in control *versus* shRNA(VEGF)^{vΔGFAP/+} mice. **(B)** Relative changes in heart rate are displayed upon *intracarotid* administration of vasoactive compounds SNP and IPR. Assessment of serum concentration of catecholamines **(C)** and the gene expression of β₁-and β₂ adrenoreceptor in the heart **(D)** as well as heart weight **(E)**. Bodyweights **(F)**, serum Leptin **(G)**, and acetylcholine-induced endothelial relaxation **(H)** show no differences between control and experimental groups on respective diets. Relative changes in blood pressure are displayed upon *intracarotid* administration of vasoactive compounds SNP, PE and IPR **(I)**. SC diet: standard chow diet; HFHS diet: high-fat/high-sugar diet; shRNA: small hairpin RNA; scrmb1: scrambled control RNA; *Adrb1*: β₁ adrenoreceptor mRNA; *Adrb2*: β₂ adrenoreceptor mRNA, VEGF: vascular endothelial growth factor; GFAP: glial-fibrillary acidic protein; SNP: sodium nitroprusside; IPR: isoproterenol; PE: phenylephrine.

5 Discussion

In the course of this thesis, I explored the involvement of astrocytes, an integral cell type at the body-brain interface, in the development of reactive changes found in the hypothalamus as a consequence of high-calorie diet. Importantly, astrocytes were found to contribute to an unprecedented extent in triggering perturbances in hypothalamic function upon HFHS feeding, which translated into systemic pathophysiological derangements such as the development of arterial hypertension.

5.1 Hypertension in obesity is driven by angiogenic signaling in hypothalamic astrocytes

Those perturbances were shown to comprise *inter alia* the development of hypervascular microangiopathy in the hypothalamus – a pathological remodeling of the local angioarchitecture that is characterized by increased vessel density and instability. This process was identified to crucially depend on glia-vascular interactions and specifically on the upregulation of pro-angiogenic HIF-1 α /VEGF signaling in hypothalamic astrocytes upon HFHS exposure. Strikingly, the signaling cue responsible for the induction of the HIF-1 α /VEGF cascade in astrocytes was identified to be the adipocyte-derived hormone leptin. Circulating in proportion to body fat stores, this hormone has been extensively studied for its role in the regulation of feeding behavior and energy expenditure. Here, however, obesity-associated hyperleptinemia was identified as the key signaling cue, which directly acts on hypothalamic leptin receptor-positive astrocytes in order to onset hypervascularization of the hypothalamus. Lastly, these regional changes in hypothalamic vascularity, which included pre-autonomic nuclei, were found to increase sympathetic outflow towards cardiovascular target and hence controlling systemic blood pressure. Up to date, this work is the first to address how microvascular remodeling in pre-autonomic hypothalamic nuclei impact hypertensive regulation in obesity and cardiovascular risk scores.

5.1.1 Astrocytic VEGF exerts unique effects at the cerebral endothelium as opposed to blood-borne, macrophage-derived VEGF

The mediobasal hypothalamus is well-documented to be subjected to a wide range of cytoarchitectural and metabolic disturbances as a consequence of short-term high-fat feeding. One of such derangements includes the transient impairment of brain glucose uptake in response to acute high-fat feeding. Interestingly, its rectification involves an adaptive increase in circulating VEGF, which was observed in both mice and humans as an instrumental counter-regulatory mechanism for reinstating proper glucose transport at the cerebral endothelium (Jais et al., 2016; Schüler et al., 2018). In the course of these studies, myeloid-derived perivascular CNS macrophages have been identified as the source of circulating VEGF. Consistent with these observations, hypothalamic astrocytes were here identified as another cellular source of VEGF induced by HFHS feeding. Of note, however, VEGF signaling at the cerebral endothelium operates in a highly polarized fashion with the side of ligand binding being a crucial determinant for its diverse downstream effects. For instance, it has been reported previously that blood-borne VEGF acts on endothelial cells from the luminal side exerting unequal response compared to tissue-produced or parenchymal VEGF, which acts on endothelial cells from the abluminal side (Hudson et al., 2014). Such differential VEGF signaling is predicated on a profound apicobasal polarizations in VEGFR-1 (luminal) and VEGFR-2 (abluminal) expression pattern. This mechanism may well explain why diet-induced VEGF promotes brain glucose uptake *via* GLUT-1 expression when acting from the circulation (Jais et al., 2016; Langlet et al., 2013), while it is highly angiogenic and permeability-enhancing when secreted by astrocytes acting from the parenchymal side. In conclusion, high-calorie diet exposure induces VEGF in various different cell types, including hypothalamic astrocytes as revealed in this thesis, which was further found to constitute the major cellular source of the VEGF fraction that acts on endothelial cells from the parenchymal side where it triggers hypervascularization and vessel instability.

5.1.2 Integration of tonic *versus* phasic metabolic information: differential roles of hypothalamic astrocytes and tanycytes?

In addition to astrocytes, tissue-borne VEGF is known to be also produced by adjacent tanycytes, which are specialized ependymal cells residing at the third ventricle. It has been shown that tanycytic VEGF levels are sensitive to acute changes of whole-body metabolic

status such as glucose-deprivation. Reduced systemic glucose availability, either induced by starvation or the injection of the non-metabolizable glucose analogue 2-deoxy-D-glucose (2-DG), significantly increase the release of tuncytic VEGF, which was found to act on a specialized type of blood vessel in the median eminence. As a consequence of increased VEGF in this brain structure, the local blood vessels increase their number of fenestrations, which are regulated openings between the endothelial cells, which in turn increase the accessibility of metabolic signals to the MBH in the context of fasting (Langlet et al., 2013). Notably, this tuncyte-mediated plasticity appears highly region-specific, phasic by nature and restricted to a small subset of fenestrated vessels. In contrast, results obtained in the course of this thesis suggest that neighboring astrocytes in the parenchyma are tuned instead to more tonic signals including hyperleptinemia, which reflect more long-term energy surplus.

5.1.3 Diet-induced hyperleptinemia contribute to microvascular dysfunction at body-brain interfaces

In the course of this work, leptin serum concentrations were found to be significantly elevated already upon two weeks of HFHS feeding coinciding with significant bodyweight gain and onset of hypothalamic hypervascularization. By a series of loss-and-gain of function experiments, diet-induced hyperleptinemia was here identified as the paramount factor responsible for the development of hypothalamic microangiopathy by inducing pro-angiogenic HIF-1 α /VEGF signaling in local astrocytes. In support of this finding, previous investigation found leptin to exert pro-angiogenic effects in the retina *via* increasing VEGF expression (Suganami et al., 2004; Cao et al., 2001). Here, it was shown that retinae derived from leptin-deficient Lep^{ob} mice exhibit significantly reduced VEGF expression, while conversely retinae from leptin-overproducing transgenic animals show excessive expression of VEGF. Consistently, clinical reports on human patients suffering from type 2 diabetes mellitus suggest that elevations in serum leptin levels, and even more so vitreal leptin levels, constitute independent predictors of diabetic retinopathy (Gariano et al., 2000; Afarid et al., 2018). In conjunction, these observations strongly support the findings reported in this thesis of hyperleptinemia mediating adverse effects on microvessel function, particularly at neurovascular beds.

5.1.4 Leptin and the post-translational regulation of HIF-1 α activity: a role of phosphorylation?

HIF-1 α constitutes an essential transcription factor that acts as a rheostat governing cellular homeostasis. Therefore, regulation of HIF-1 α activity is tuned by a broad range of stimuli integrating *e.g.* oxygen concentration, iron status, Krebs cycle intermediates as well as reactive oxygen species. The last two decades sketched out the prominent canonical HIF-1 α regulation centered at prolyl hydroxylation and consequent ubiquitination by the von-Hippel-Lindau protein under normoxic condition. More recently, an additional and previously unrecognized layer of post-translational HIF-1 α regulation stepped into the lime light: protein phosphorylation. In fact, however, the very first hint that phosphorylation might influence HIF-1 α activity stems from experiments conducted already more than 20 years ago. When calf intestinal alkaline phosphatase was given to hypoxic nuclear extracts, HIF-1 α DNA-binding was found to be profoundly perturbed (Wang et al., 1995). Meanwhile, several protein kinases have been identified either directly phosphorylating HIF- α subunits or modulating their activity indirectly by targeting HIF-regulating proteins (reviewed in Kietzmann et al., 2016). In light of the results obtained in the course of this work, we here postulate that phosphorylation events in hypothalamic astrocytes occur in response to activated LepR signaling to in turn increase HIF-1 α /VEGF signaling with adverse consequences for the local microvasculature. However, more detailed investigations are required in order to address the exact intracellular links between kinase activities and HIF induction in astrocytes.

5.1.5 Increased serum leptin bridges hypothalamic microangiopathy with the development of obesity-associated arterial hypertension

Beside microvascular damage, leptin has also been suggested to play a functional role in more systemic vascular function. For instance, it is pertinent to note that leptin-deficient mice and humans present with strikingly low blood pressure despite massive obesity (Mark et al., 1999; Ozata et al., 1999). Such an absence of hypertension in leptin-deficient obesity is considered the first hint that leptin signaling might be involved in the regulation of systemic hemodynamics. In support of this notion, leptin administration *via* various different routes potently increases heart rate and blood pressure in wildtype mice and rats (Dunbar et al., 1997; Shek et al., 1998) likely by interacting with adrenergic receptors (Carlyle et al., 2002).

Consistently, the acute intracerebroventricular infusion of a leptin antagonist into high fat-fed rabbits was shown to acutely reduce arterial hypertension (Lim et al., 2013). Most recently, an additional study furthered the compelling evidential base strongly suggesting that leptin constitutes the peripheral signal associating weight gain with the characteristic increase of systemic blood pressure on high-calorie diets (Simonds et al., 2014). In the course of this study it was demonstrated through multiple convergent approaches that increased leptin signaling in diet-induced obesity underlies the hyperactivation of the sympathetic nervous system. This study placed particular emphasis on how leptin directly affects pre-autonomic neurons in the dorsomedial hypothalamus putting forward the concept of ‘selective leptin resistance’. This concept suggests that diet-induced obesity abrogates leptin’s effect on reducing food intake while its central effect on increasing sympathetic tone, *e.g.* towards cardiovascular targets, remains still functional. Histological examinations further support this notion by demonstrating that several hypothalamic nuclei are differentially affected by diet-induced obesity; the dorsomedial hypothalamus, for instance, was found to largely retain leptin sensitivity as measured by pSTAT3 induction whereas the arcuate nucleus exhibited a marked reduction under high-calorie feeding in mice (Münzberg et al., 2004). By that, leptin might still exert a significant effect on hypertensive regulation in obesity, despite failing to reduce feeding and bodyweight.

5.1.6 Leptin-mediated remodeling of the hypothalamic microvasculature constitutes a prerequisite for obesity-associated arterial hypertension

Results obtained in this thesis now provide additional insights suggesting that hyperleptinemia triggers microvascular remodeling in pre-autonomic hypothalamic nuclei substantially prior to the development of arterial hypertension. By implication, microvascular remodeling thus develops independently from systemic hypertension, a notion contrasting the traditional assumption of increased blood pressure being a prerequisite for structural remodeling of microvascular beds. According to *The law of LaPlace*, it is reasoned that imposing increased capillary pressure would result in structural remodeling of retinal (Wong et al., 2016) and renal microvessels (Folkow et al., 1958). However, at least for the hypothalamic vasculature it is here demonstrated that microvascular remodeling may develop prior and independently of hypertension. In addition to this peculiar temporal succession it was furthermore demonstrated in the course of this thesis that such vessel remodeling in the pre-autonomic hypothalamus constitutes a necessary prerequisite for the development of

arterial hypertension under high-calorie diets. Further strengthening the importance of the glia-vascular interface for proper brain function, the collected results here suggest that localized perturbances of the brain microenvironment exerts various adverse effects, some of which even translating into systemic physiological derangements such as the chronic rise in blood pressure. Thus, diet-induced hyperleptinemia is speculated to impair the integrity of the local glia-vascular interface, what in turn induces adverse cellular responses including increased secretion of pro-inflammatory cytokines or promoting endoplasmic reticulum stress. As outlined previously (Khor and Cai, 2017 and references therein), these events have been repeatedly associated with sympathetically-driven hypertension. In conclusion, this part of the thesis at hand has identified regional interference with the leptin-induced upregulation of HIF-1a/VEGF signaling in hypothalamic astrocytes to constitute a tenable approach in order to prevent sympathetically-driven hypertension in obesity.

5.2 Conclusion and Outlook

Taken together, the work presented in this thesis unravels various novel roles of astrocytes in the control of metabolic homeostasis. In light of the ever-increasing prevalence of obesity and diabetes in the modern world, a better appreciation of the cellular and molecular underpinnings governing whole-body homeostasis is crucially warranted. By exploring vascular complications associated with obesity, this thesis first reveals the unprecedented involvement glia-vascular interplay in (a) remodeling the local hypothalamic vasculature and (b) driving the development of systemic hypertension *via* increased sympathetic outflow.

6 References

- Adams, R.H., Alitalo, K., 2007. Molecular regulation of angiogenesis and lymphangiogenesis. *Nat Rev Mol Cell Bio* 8, 464–478. <https://doi.org/10.1038/nrm2183>
- Adamsky, A., Kol, A., Kreisel, T., Doron, A., Ozeri-Engelhard, N., Melcer, T., Refaeli, R., Horn, H., Regev, L., Groysman, M., London, M., Goshen, I., 2018. Astrocytic Activation Generates De Novo Neuronal Potentiation and Memory Enhancement. *Cell* 174, 59-71.e14. <https://doi.org/10.1016/j.cell.2018.05.002>
- Aiello, L., Avery, R.L., Arrigg, P.G., Keyt, B.A., Jampel, H.D., Shah, S.T., Pasquale, L.R., Thieme, H., Iwamoto, M.A., Park, J.E., Nguyen, H.V., Aiello, L.M., Ferrara, N., King, G.L., 1994. Vascular endothelial growth factor in ocular fluid of patients with diabetic retinopathy and other retinal disorders.pdf. *N Engl J Med*. 331, 1480–1487.
- Appelhoff, R.J., Tian, Y.-M., Raval, R.R., Turley, H., Harris, A.L., Pugh, C.W., Ratcliffe, P.J., Gleadle, J.M., 2004. Differential Function of the Prolyl Hydroxylases PHD1, PHD2, and PHD3 in the Regulation of Hypoxia-inducible Factor. *J Biol Chem* 279, 38458–38465. <https://doi.org/10.1074/jbc.m406026200>
- Ashburner, M., Ball, C., Blake, J., Botstein, D., Butler, H., Cherry, J., Davis, A., Dolinski, K., Dwight, S., Eppig, J., Harris, M., Hill, D., Issel-Tarver, L., Kasarskis, A., Lewis, S., Matese, J., Richardson, J., Ringwald, M., Rubin, G., Sherlock, G., 2000. Gene ontology: tool for the unification of biology. The Gene Ontology Consortium. *Nature Genet* 25, 25–29.
- Batiuk, M.Y., de Vin, F., Duqué, S.I., Li, C., Saito, T., Saido, T., Fiers, M., Belgard, G.T., Holt, M.G., 2017. An immunoaffinity-based method for isolating ultrapure adult astrocytes based on ATP1B2 targeting by the ACSA-2 antibody. *J Biol Chem* 292, 8874–8891. <https://doi.org/10.1074/jbc.m116.765313>
- Benderro, G.F., LaManna, J.C., 2011. Hypoxia-induced angiogenesis is delayed in aging mouse brain. *Brain Res* 1389, 50–60. <https://doi.org/10.1016/j.brainres.2011.03.016>
- Berkseth, K.E., Guyenet, S.J., Melhorn, S.J., Lee, D., Thaler, J.P., Schur, E.A., and Schwartz, M.W., 2014. Hypothalamic Gliosis Associated With High-Fat Diet Feeding Is Reversible in Mice: A

References

- Combined Immunohistochemical and Magnetic Resonance Imaging Study. *Endocrinology* 155, 2858–2867.
- Bertout, J.A., Patel, S.A., Simon, C.M., 2008. The impact of O₂ availability on human cancer. *Nat Rev Cancer* 8, nrc2540. <https://doi.org/10.1038/nrc2540>
- Blinder, P., Tsai, P.S., Kaufhold, J.P., Knutsen, P.M., Suhl, H., Kleinfeld, D., 2013. The cortical angiome: an interconnected vascular network with noncolumnar patterns of blood flow. *Nat Neurosci* 16, 889–897. <https://doi.org/10.1038/nn.3426>
- Botusan, I., Sunkari, V., Savu, O., Catrina, A., Grünler, J., Lindberg, S., Pereira, T., Ylä-Herttuala, S., Poellinger, L., Brismar, K., Catrina, S.-B., 2008. Stabilization of HIF-1 α is critical to improve wound healing in diabetic mice. *Proc National Acad Sci* 105, 19426–19431. <https://doi.org/10.1073/pnas.0805230105>
- Bouyakdan, K., Martin, H., Liénard, F., Budry, L., Taib, B., Rodaros, D., Chrétien, C., Biron, É., Husson, Z., Cota, D., Pénicaud, L., Fulton, S., Fioramonti, X., Alquier, T., 2019. The gliotransmitter ACBP controls feeding and energy homeostasis via the melanocortin system. *J Clin Invest*. <https://doi.org/10.1172/jci123454>
- Bracken, C.P., Fedele, A.O., Linke, S., Balrak, W., Lisy, K., Whitelaw, M.L., Peet, D.J., 2006. Cell-specific Regulation of Hypoxia-inducible Factor (HIF)-1 α and HIF-2 α Stabilization and Transactivation in a Graded Oxygen Environment. *J Biol Chem* 281, 22575–22585. <https://doi.org/10.1074/jbc.m600288200>
- Brenner, M., Kisseberth, W., Su, Y., Besnard, F., Messing, A., 1994. GFAP promoter directs astrocyte-specific expression in transgenic mice. *J Neurosci* 14, 1030–1037. <https://doi.org/10.1523/jneurosci.14-03-01030.1994>
- Cao, L., Jiao, X., Zuzga, D.S., Liu, Y., Fong, D.M., Young, D., During, M.J., 2004. VEGF links hippocampal activity with neurogenesis, learning and memory. *Nat Genet* 36, ng1395. <https://doi.org/10.1038/ng1395>
- Carlyle, M., Jones, O.B., Kuo, J.J., Hall, J.E., 2002. Chronic cardiovascular and renal actions of leptin- role of adrenergic activity.pdf. *Hypertension* 39, 496–501.
- Coleman, D., 1973. Effects of parabiosis of obese with diabetes and normal mice. *Diabetologia* 9,

References

294–298. <https://doi.org/10.1007/bf01221857>

Considine, R.V., Sinha, M.K., Heiman, M.L., Kriauciunas, A., Stephens, T.W., Nyce, M.R., Ohannessian, J.P., Marco, C.C., McKee, L.J., Thomas, Bauer, L., Caro, J.F., 1996. Serum Immunoreactive-Leptin Concentrations in normal-weight and obese humans.pdf. *The New England Journal of Medicine* 334, 292–295.

Cui, Y., Yang, Y., Ni, Z., Dong, Y., Cai, G., Foncelle, A., Ma, S., Sang, K., Tang, S., Li, Y., Shen, Y., Berry, H., Wu, S., Hu, H., 2018. Astroglial Kir4.1 in the lateral habenula drives neuronal bursts in depression. *Nature* 554, 323. <https://doi.org/10.1038/nature25752>

Davis-Smyth, T., Chen, H., Park, J., Presta, L., Ferrara, N., 1996. The second immunoglobulin-like domain of the VEGF tyrosine kinase receptor Flt-1 determines ligand binding and may initiate a signal transduction cascade. *Embo J* 15, 4919–4927. <https://doi.org/10.1002/j.1460-2075.1996.tb00872.x>

Dayan, F., Roux, D., Brahimi-Horn, C.M., Pouyssegur, J., Mazure, N.M., 2006. The Oxygen Sensor Factor-Inhibiting Hypoxia-Inducible Factor-1 Controls Expression of Distinct Genes through the Bifunctional Transcriptional Character of Hypoxia-Inducible Factor-1 α . *Cancer Res* 66, 3688–3698. <https://doi.org/10.1158/0008-5472.can-05-4564>

de Groenendaal-van, M.D., den, A.M., Rijnders, S., Krebs-Brown, A., Kerbusch, V., Golor, G., Schaddelee, M., 2016. The Hypoxia-inducible Factor Prolyl-Hydroxylase Inhibitor Roxadustat (FG-4592) and Warfarin in Healthy Volunteers: A Pharmacokinetic and Pharmacodynamic Drug-Drug Interaction Study. *Clin Ther* 38, 918–928.

Dore-Duffy, P., Wang, X., Mehedi, A., Kreipke, C.W., Rafols, J.A., 2007. Differential expression of capillary VEGF isoforms following traumatic brain injury. *Neurological Research* 29, 395–403.

Dougher, M., Terman, B., n.d. Autophosphorylation of KDR in the kinase domain is required for maximal VEGF-stimulated kinase activity and receptor internalization. *Oncogene* 18, 1619–1627.

Dunbar, J.C., Hu, Y., Lu, H., 1997. Intracerebroventricular Leptin Increases Lumbar and Renal Sympathetic Nerve Activity and Blood Pressure in Normal Rats. *Diabetes* 46, 2040–2043. <https://doi.org/10.2337/diab.46.12.2040>

Ehinger, J.K., Piel, S., Ford, R., Karlsson, M., Sjövall, F., Frostner, E., Morota, S., Taylor, R.W.,

References

- Turnbull, D.M., Cornell, C., Moss, S.J., Metzsch, C., Hansson, M.J., Fliri, H., Elmér, E., 2016. Cell-permeable succinate prodrugs bypass mitochondrial complex I deficiency. *Nat Commun* 7, ncomms12317. <https://doi.org/10.1038/ncomms12317>
- Eng, L.F., Vanderhaeghen, J., Bignami, A., Gerstl, B., 1971. An acidic protein isolated from fibrous astrocytes.pdf. *Brain Research* 28, 351–354.
- Ertürk, A., Becker, K., Jährling, N., Mauch, C.P., Hojer, C.D., Egen, J.G., Hellal, F., Bradke, F., Sheng, M., Dodt, H.-U., 2012. Three-dimensional imaging of solvent-cleared organs using 3DISCO. *Nat Protoc* 7, 1983. <https://doi.org/10.1038/nprot.2012.119>
- Fago, A., Hundahl, C., Malte, H., Weber, R.E., 2004. Functional Properties of Neuroglobin and Cytoglobin. Insights into the Ancestral Physiological Roles of Globins. *Iubmb Life* 56, 689–696. <https://doi.org/10.1080/15216540500037299>
- Farmer, T.W., Abrahamsson, T., Chierzi, S., Lui, C., Zaelzer, C., Jones, E.V., Bally, B., Chen, G.G., Théroux, J.-F., Peng, J., Bourque, C.W., Charron, F., Ernst, C., Sjöström, J.P., Murai, K.K., 2016. Neurons diversify astrocytes in the adult brain through sonic hedgehog signaling. *Science* 351, 849–854. <https://doi.org/10.1126/science.aab3103>
- Ferrara, N., Gerber, H.-P., LeCouter, J., 2003. The biology of VEGF and its receptors. *Nat Med* 9, nm0603-669. <https://doi.org/10.1038/nm0603-669>
- Fischer, C., Jonckx, B., Mazzone, M., Zacchigna, S., Loges, S., Pattarini, L., Chorianopoulos, E., Liesenborghs, L., Koch, M., Mol, M., Autiero, M., Wyns, S., Plaisance, S., Moons, L., van Rooijen, N., Giacca, M., Stassen, J.-M., Dewerchin, M., Collen, D., Carmeliet, P., 2007. Anti-PlGF Inhibits Growth of VEGF(R)-Inhibitor-Resistant Tumors without Affecting Healthy Vessels. *Cell* 131, 463–475. <https://doi.org/10.1016/j.cell.2007.08.038>
- Folkow, B., Grimby, G., Thulesius, O., 1958. Adaptive structural changes of the vascular walls in hypertension and their relation to the control of the peripheral resistance. *Acta Physiol Scand.* 44, 255–272.
- Folsom, A., Prineas, R., Kaye, S., Munger, R., 2018. Incidence of hypertension and stroke in relation to body fat distribution and other risk factors in older women. *Stroke* 21, 701–706. <https://doi.org/10.1161/01.str.21.5.701>

References

- Franciosi, S., Gasperi, R., Dickstein, D.L., English, D.F., Rocher, A.B., Janssen, W., Christoffel, D., Sosa, M.A., Hof, P.R., Buxbaum, J.D., Elder, G.A., 2007. Pepsin pretreatment allows collagen IV immunostaining of blood vessels in adult mouse brain. *J Neurosci Meth* 163, 76–82.
<https://doi.org/10.1016/j.jneumeth.2007.02.020>
- Franklin, K., Paxinos, G., 2019. *Paxinos and Franklin's the Mouse Brain in Stereotaxic Coordinates, Compact*. Academic Press 1–246.
- Fuh, G., Li, B., Crowley, C., Cunningham, B., Wells, J., 1998. Requirements for binding and signaling of the kinase domain receptor for vascular endothelial growth factor. *J Biol Chem* 273, 11197–11204.
- Fujita, Y., Yamashita, T., 2019. The Effects of Leptin on Glial Cells in Neurological Diseases. *Front Neurosci-switz* 13, 828. <https://doi.org/10.3389/fnins.2019.00828>
- Golgi, C., 1903. *Opera Omnia*.
- Golgi, C., 1894. Untersuchungen über den feineren Bau des centralen und peripherischen Nervensystems.
- Greijer, A., van der Groep, P., Kemming, D., Shvarts, A., Semenza, G., Meijer, G., van de Wiel, M., Belien, J., van Diest, P., van der Wall, E., 2005. Up-regulation of gene expression by hypoxia is mediated predominantly by hypoxia-inducible factor 1 (HIF-1). *J Pathology* 206, 291–304.
<https://doi.org/10.1002/path.1778>
- Gros, G., Wittenberg, B.A., Jue, T., 2010. Myoglobin's old and new clothes: from molecular structure to function in living cells. *J Exp Biology* 213, 2713–2725. <https://doi.org/10.1242/jeb.043075>
- Guzy, R.D., Hoyos, B., Robin, E., Chen, H., Liu, L., Mansfield, K.D., Simon, C.M., Hammerling, U., Schumacker, P.T., 2005. Mitochondrial complex III is required for hypoxia-induced ROS production and cellular oxygen sensing. *Cell Metab* 1, 401–408. <https://doi.org/10.1016/j.cmet.2005.05.001>
- Haim, L., Rowitch, D.H., 2016. Functional diversity of astrocytes in neural circuit regulation. *Nat Rev Neurosci* 18, 31–41. <https://doi.org/10.1038/nrn.2016.159>
- Hall, C.N., Reynell, C., Gesslein, B., Hamilton, N.B., Mishra, A., Sutherland, B.A., O'Farrell, F.M., Buchan, A.M., Lauritzen, M., Attwell, D., 2014. Capillary pericytes regulate cerebral blood flow in

References

- health and disease. *Nature* 508, 55. <https://doi.org/10.1038/nature13165>
- Harper, S.J., Bates, D.O., 2008. VEGF-A splicing: the key to anti-angiogenic therapeutics? *Nat Rev Cancer* 8, 880–887. <https://doi.org/10.1038/nrc2505>
- Hayashi, T., Abe, K., Suzuki, H., Itoyama, Y., 1997. Rapid induction of vascular endothelial growth factor gene expression after transient middle cerebral artery occlusion in rats. *Stroke* 28, 2039–44.
- He, Z., Tessier-Lavigne, M., 1997. Neuropilin Is a Receptor for the Axonal Chemorepellent Semaphorin III. *Cell* 90, 739–751. [https://doi.org/10.1016/s0092-8674\(00\)80534-6](https://doi.org/10.1016/s0092-8674(00)80534-6)
- Hervey, G.R., 1959. The effects of lesions in the hypothalamus in parabiotic rats.pdf. *J.Physiol* 335–552.
- Hewitson, K.S., McNeill, L.A., Riordan, M.V., Tian, Y.-M., Bullock, A.N., Welford, R.W., Elkins, J.M., Oldham, N.J., Bhattacharya, S., Gleadle, J.M., Ratcliffe, P.J., Pugh, C.W., Schofield, C.J., 2002. Hypoxia-inducible Factor (HIF) Asparagine Hydroxylase Is Identical to Factor Inhibiting HIF (FIH) and Is Related to the Cupin Structural Family. *J Biol Chem* 277, 26351–26355. <https://doi.org/10.1074/jbc.c200273200>
- Hoppe, G., Yoon, S., Gopalan, B., Savage, A.R., Brown, R., Case, K., Vasanji, A., Chan, R.E., Silver, R.B., Sears, J.E., 2016. Comparative systems pharmacology of HIF stabilization in the prevention of retinopathy of prematurity. *Proc National Acad Sci* 113, E2516–E2525. <https://doi.org/10.1073/pnas.1523005113>
- Horvath, T.L., Diano, S., Tschöp, M., 2004. Brain Circuits Regulating Energy Homeostasis. *Neurosci* 10, 235–246. <https://doi.org/10.1177/1073858403262151>
- Hudlicka, O., Dodd, L., Renkin, E., and Gray, S., 1982. Early changes in fiber profile and capillary density in long-term stimulated muscles. *Am J Physiol* 243, 528–535.
- Hudson, N., Powner, M.B., Sarker, M.H., Burgoyne, T., Campbell, M., Ockrim, Z.K., Martinelli, R., Futter, C.E., Grant, M.B., Fraser, P.A., Shima, D.T., Greenwood, J., Turowski, P., 2014. Differential Apicobasal VEGF Signaling at Vascular Blood-Neural Barriers. *Dev Cell* 30, 541–552. <https://doi.org/10.1016/j.devcel.2014.06.027>
- Ide, A.G., Baker, N.H., Warren, S.L., 1939. Vascularization of the Brown Pearce rabbit epithelioma

References

transplant as seen in the transparent ear chamber. *Am J Roentgenol* 42, 891–899.

Ingalls, A.M., Dickie, M.M., Snell, G., 1950. Obese, a new mutation in the house mouse.pdf. *J. Hered* 41, 317–318.

Isaacs, J.S., Jung, Y., Mole, D.R., Lee, S., Torres-Cabala, C., Chung, Y.-L., Merino, M., Trepel, J., Zbar, B., Toro, J., Ratcliffe, P.J., Linehan, M.W., Neckers, L., 2005. HIF overexpression correlates with biallelic loss of fumarate hydratase in renal cancer: Novel role of fumarate in regulation of HIF stability. *Cancer Cell* 8, 143–153. <https://doi.org/10.1016/j.ccr.2005.06.017>

Ito, N., Wernstedt, C., Engstrom, U., and Claesson-Welsh, L., 1998. Identification of Vascular Endothelial Growth Factor Receptor-1 Tyrosine Phosphorylation Sites and Binding of SH2 Domain-containing Molecules.pdf. *Journal of Biological Chemistry* 273, 23410–23418.

Jain, R.K., 2003. Molecular regulation of vessel maturation. *Nat Med* 9, nm0603-685. <https://doi.org/10.1038/nm0603-685>

Jelkmann, W., 2007. Erythropoietin after a century of research: younger than ever. *Eur J Haematol* 78, 183–205. <https://doi.org/10.1111/j.1600-0609.2007.00818.x>

Jones, E.A., Yuan, L., Breant, C., Watts, R.J., Eichmann, A., 2008. Separating genetic and hemodynamic defects in neuropilin 1 knockout embryos. *Development* 135, 2479–2488. <https://doi.org/10.1242/dev.014902>

Joris, P.J., Plat, J., Kusters, Y., Houben, A., Stehouwer, C.D., Schalkwijk, C.G., Mensink, R.P., 2016. Diet-induced weight loss improves not only cardiometabolic risk markers but also markers of vascular function: a randomized controlled trial in abdominally obese men. *Am J Clin Nutrition* 105, 23–31. <https://doi.org/10.3945/ajcn.116.143552>

Joukov, V., Kaipainen, A., Jeltsch, M., Pajusola, K., Olofsson, B., Kumar, V., Eriksson, U., Alitalo, K., 1997. Vascular Endothelial Growth Factors VEGF-B and VEGF-C.pdf. *J Cell Physiol* 173, 211–215.

Józsa, L., Järvinen, M., Kvist, M., Lehto, M., Mikola, A., 1980. Capillary density of tenotomized skeletal muscles. I. Experimental study in the rat. *Eur J Appl Physiol Occup Physiol* 2, 175–181.

Kaelin, W.G., 2018. The von Hippel-Lindau tumor suppressor protein.pdf. *Annu. REv. Cancer Biol.*

References

- Kaelin, W.G., Ratcliffe, P.J., 2008. Oxygen Sensing by Metazoans: The Central Role of the HIF Hydroxylase Pathway. *Mol Cell* 30, 393–402. <https://doi.org/10.1016/j.molcel.2008.04.009>
- Kanehisa, M., Goto, S., 2000. KEGG: kyoto encyclopedia of genes and genomes. *Nucleic Acids Res* 28, 27–30.
- Kantzer, C.G., Boutin, C., Herzig, I.D., Wittwer, C., Reiß, S., Tiveron, M., Drewes, J., Rockel, T.D., Ohlig, S., Ninkovic, J., Cremer, H., Pennartz, S., Jungblut, M., Bosio, A., 2017. Anti-ACSA-2 defines a novel monoclonal antibody for prospective isolation of living neonatal and adult astrocytes. *Glia* 65, 990–1004. <https://doi.org/10.1002/glia.23140>
- Karuppagounder, S.S., Ratan, R.R., 2012. Hypoxia-Inducible Factor Prolyl Hydroxylase Inhibition: Robust New Target or Another Big Bust for Stroke Therapeutics? *J Cereb Blood Flow Metabolism* 32, 1347–1361. <https://doi.org/10.1038/jcbfm.2012.28>
- Kawasaki, T., Kitsukawa, T., Bekku, Y., Matsuda, Y., Sanbo, M., Yagi, T., Fujisawa, H., 1999. A requirement for neuropilin-1 in embryonic vessel formation. *Development* 126, 4895–902.
- Kayar, S.R., Hoppeler, H., Essen-Gustavsson, B., Schwerzmann, K., 1988. The similarity of mitochondrial distribution in equine skeletal muscles of differing oxidative capacity.pdf. *Journal of Experimental Biology* 137, 253–263.
- Kendall, R., Thomas, K., 1993. Inhibition of vascular endothelial cell growth factor activity by an endogenously encoded soluble receptor. *Proc National Acad Sci* 90, 10705–10709. <https://doi.org/10.1073/pnas.90.22.10705>
- Khor, S., Cai, D., 2017. Hypothalamic and inflammatory basis of hypertension. *Clin Sci* 131, 211–223. <https://doi.org/10.1042/cs20160001>
- Kietzmann, T., Mennerich, D., Dimova, E.Y., 2016. Hypoxia-Inducible Factors (HIFs) and Phosphorylation: Impact on Stability, Localization, and Transactivity. *Frontiers Cell Dev Biology* 4, 11. <https://doi.org/10.3389/fcell.2016.00011>
- Kirby, E.D., Kuwahara, A.A., Messer, R.L., Wyss-Coray, T., 2015. Adult hippocampal neural stem and progenitor cells regulate the neurogenic niche by secreting VEGF. *Proc National Acad Sci* 112, 4128–4133. <https://doi.org/10.1073/pnas.1422448112>

References

- Kitsukawa, T., Shimizu, M., Sanbo, M., Hirata, T., Taniguchi, M., Bekku, Y., Yagi, T., Fujisawa, H., 1997. Neuropilin–Semaphorin III:D-Mediated Chemorepulsive Signals Play a Crucial Role in Peripheral Nerve Projection in Mice. *pdf* 19, 9951005.
- Klimova, T., Chandel, N., 2008. Mitochondrial complex III regulates hypoxic activation of HIF. *Cell Death Differ* 15, 4402307. <https://doi.org/10.1038/sj.cdd.4402307>
- Knighton, D., Silver, I., Hunt, T., 1981. Regulation of wound-healing angiogenesis-effect of oxygen gradients and inspired oxygen concentration. *Surgery* 90, 262–270.
- Koh, M., Powis, G., 2012. Passing the baton: the HIF switch. *Trends Biochem Sci* 37, 364–372. <https://doi.org/10.1016/j.tibs.2012.06.004>
- Koivunen, P., Hirsilä, M., Remes, A.M., Hassinen, I.E., Kivirikko, K.I., Myllyharju, J., 2007. Inhibition of Hypoxia-inducible Factor (HIF) Hydroxylases by Citric Acid Cycle Intermediates POSSIBLE LINKS BETWEEN CELL METABOLISM AND STABILIZATION OF HIF. *J Biol Chem* 282, 4524–4532. <https://doi.org/10.1074/jbc.m610415200>
- Korn, C., Augustin, H.G., 2015. Mechanisms of Vessel Pruning and Regression. *Dev Cell* 34, 5–17. <https://doi.org/10.1016/j.devcel.2015.06.004>
- Krogh, A., 1919a. The supply of oxygen to the tissues and the regulation of the capillary circulation. *J Physiology* 52, 457–474. <https://doi.org/10.1113/jphysiol.1919.sp001844>
- Krogh, A., 1919b. The number and distribution of capillaries in muscles with calculations of the oxygen pressure head necessary for supplying the tissue. *J Physiology* 52, 409–415. <https://doi.org/10.1113/jphysiol.1919.sp001839>
- Lando, D., Peet, D.J., Gorman, J.J., Whelan, D.A., Whitelaw, M.L., Bruick, R.K., 2002. FIH-1 is an asparaginyl hydroxylase enzyme that regulates the transcriptional activity of hypoxia-inducible factor. *Gene Dev* 16, 1466–1471. <https://doi.org/10.1101/gad.991402>
- Lange, C., Storkebaum, E., de Almodóvar, C., Dewerchin, M., Carmeliet, P., 2016. Vascular endothelial growth factor: a neurovascular target in neurological diseases. *Nat Rev Neurol* 12, 439–454. <https://doi.org/10.1038/nrneurol.2016.88>

References

- Langlet, F., Levin, B.E., Luquet, S., Mazzone, M., Messina, A., Dunn-Meynell, A.A., Balland, E., Lacombe, A., Mazur, D., Carmeliet, P., Bouret, S.G., Prevot, V., Dehouck, B., 2013. Tanycytic VEGF-A Boosts Blood-Hypothalamus Barrier Plasticity and Access of Metabolic Signals to the Arcuate Nucleus in Response to Fasting. *Cell Metab* 17, 607–617.
<https://doi.org/10.1016/j.cmet.2013.03.004>
- Lavie, C.J., Milani, R.V., Ventura, H.O., 2009. Obesity and Cardiovascular Disease Risk Factor, Paradox, and Impact of Weight Loss. *J Am Coll Cardiol* 53, 1925–1932.
<https://doi.org/10.1016/j.jacc.2008.12.068>
- Lim, K., Burke, S.L., Head, G.A., 2013. Obesity-Related Hypertension and the Role of Insulin and Leptin in High-Fat-Fed Rabbits.pdf. *Hypertension* 61, 628–634.
- Lindahl, P., Johansson, B.R., Levéen, P., Betsholtz, C., 1997. Pericyte Loss and Microaneurysm Formation in PDGF-B-Deficient Mice. *Science* 277, 242–245.
<https://doi.org/10.1126/science.277.5323.242>
- MacKenzie, E.D., Selak, M.A., Tennant, D.A., Payne, L.J., Crosby, S., Frederiksen, C.M., Watson, D.G., Gottlieb, E., 2007. Cell-Permeating α -Ketoglutarate Derivatives Alleviate Pseudohypoxia in Succinate Dehydrogenase-Deficient Cells ∇ . *Mol Cell Biol* 27, 3282–3289.
<https://doi.org/10.1128/mcb.01927-06>
- Mahon, P.C., Hirota, K., Semenza, G.L., 2001. FIH-1: a novel protein that interacts with HIF-1 α and VHL to mediate repression of HIF-1 transcriptional activity. *Gene Dev* 15, 2675–2686.
<https://doi.org/10.1101/gad.924501>
- Mark, A.L., Shaffer, R.A., Correia, M., Morgan, D.A., Sigmund, C.D., Haynes, W.G., 1999. Contrasting blood pressure effects of obesity in leptin- deficient ob:ob mice and agouti yellow obese mice.pdf. *Journal of Hypertension* 17.
- Matthews, D., Hosker, J., Rudenski, A., Naylor, Treacher, D., Turner, R., 1985. Homeostasis model assessment: insulin resistance and beta-cell function from fasting plasma glucose and insulin concentrations in man. *Diabetologia* 28, 412–419.
- McMinn, J., Liu, Liu, H., Dragatsis, I., Dietrich, P., Ludwig, T., Boozer, C., Jr., C.S., 2005. Neuronal deletion of *Lepr* elicits diabetes in mice without affecting cold tolerance or fertility. *Am J Physiol Endocrinol Metab* 289.

References

- Mole, D.R., Blancher, C., Copley, R.R., Pollard, P.J., Gleadle, J.M., Ragoussis, J., Ratcliffe, P.J., 2009. Genome-wide Association of Hypoxia-inducible Factor (HIF)-1 α and HIF-2 α DNA Binding with Expression Profiling of Hypoxia-inducible Transcripts*. *J Biological Chem* 284, 16767–16775. <https://doi.org/10.1074/jbc.m901790200>
- Mori, T., Tanaka, K., Buffo, A., Wurst, W., Kühn, R., Götz, M., 2006. Inducible gene deletion in astroglia and radial glia--a valuable tool for functional and lineage analysis. *Glia* 54, 21–34.
- Münzberg, H., Flier, J.S., Bjørnbæk, C., 2004. Region-Specific Leptin Resistance within the Hypothalamus of Diet-Induced Obese Mice. *Endocrinology* 145, 4880–4889. <https://doi.org/10.1210/en.2004-0726>
- Myers, M.G., Cowley, M.A., Münzberg, H., 2008. Mechanisms of Leptin Action and Leptin Resistance. *Annu Rev Physiol* 70, 537–556. <https://doi.org/10.1146/annurev.physiol.70.113006.100707>
- Nortley, R., Korte, N., Izqueredo, P., Hirunpattarasilp, C., Mishra, A., Jaunmuktane, Z., Kyrargyri, V., Pfeiffer, T., Khennouf, L., Madra, C., Gong, H., Angela Richard-Loendt, Huang, W., Saito, T., Saido, T.C., Brandner, S., Sethi, H., Attwell, D., 2019. Amyloid b oligomers constrict human capillaries in Alzheimer's disease via signaling to pericytes.pdf. *Science* 250.
- Oberheim, N., Takano, T., Han, X., He, W., Lin, J.H., Wang, F., Xu, Q., Wyatt, J.D., Pilcher, W., Ojemann, J.G., Ransom, B.R., Goldman, S.A., Nedergaard, M., 2009. Uniquely Hominid Features of Adult Human Astrocytes. *J Neurosci* 29, 3276–3287. <https://doi.org/10.1523/jneurosci.4707-08.2009>
- Oberheim, N., Wang, X., Goldman, S., Nedergaard, M., 2006. Astrocytic complexity distinguishes the human brain. *Trends Neurosci* 29, 547–553. <https://doi.org/10.1016/j.tins.2006.08.004>
- Octeau, C.J., Chai, H., Jiang, R., Bonanno, S.L., Martin, K.C., Khakh, B.S., 2018. An Optical Neuron-Astrocyte Proximity Assay at Synaptic Distance Scales. *Neuron* 98, 49-66.e9. <https://doi.org/10.1016/j.neuron.2018.03.003>
- Ogura, S., Kurata, K., Hattori, Y., Takase, H., Ishiguro-Oonuma, T., Hwang, Y., Ahn, S., Park, I., Ikeda, W., Kusuhara, S., Fukushima, Y., Nara, H., Sakai, H., Fujiwara, T., Matsushita, J., Ema, M., Hirashima, M., Minami, T., Shibuya, M., Takakura, N., Kim, P., Miyata, T., Ogura, Y., Uemura, A., 2017. Sustained inflammation after pericyte depletion induces irreversible blood-retina barrier

References

breakdown. *Jci Insight* 2, e90905. <https://doi.org/10.1172/jci.insight.90905>

Olsson, A.-K., Dimberg, A., Kreuger, J., Claesson-Welsh, L., 2006. VEGF receptor signalling ? in control of vascular function. *Nat Rev Mol Cell Bio* 7, nrm1911. <https://doi.org/10.1038/nrm1911>

P1, C., Moons, L., Luttun, A., Vincenti, V., Compornolle, V., De, M.M., Wu, Y., Bono, F., Devy, L., Beck, H., Scholz, D., Acker, T., DiPalma, T., Dewerchin, M., Noel, A., Stalmans, I., Barra, A., Blacher, S., VandenDriessche, T., Ponten, A., Eriksson, U., Plate, K., Foidart, J., Schaper, W., Charnock-Jones, D., Hicklin, D., Herbert, J., Collen, D., Persico, M., 2001. Synergism between vascular endothelial growth factor and placental growth factor contributes to angiogenesis and plasma extravasation in pathological conditions.pdf. *Nat. Med.* 7, 575–583.

Papouin, T., Dunphy, J.M., Tolman, M., Dineley, K.T., Haydon, P.G., 2017. Septal Cholinergic Neuromodulation Tunes the Astrocyte-Dependent Gating of Hippocampal NMDA Receptors to Wakefulness. *Neuron* 94, 840-854.e7. <https://doi.org/10.1016/j.neuron.2017.04.021>

Park, J.E., Helen, H.Chen, Winer, J., HouckS, K.A., and Ferrara, N., 1994. Placenta Growth Factor.pdf. *The Journal of Biological Chemistry* 269, 25646–25654.

Petzold, G.C., Murthy, V.N., 2011. Role of Astrocytes in Neurovascular Coupling. *Neuron* 71, 782–797. <https://doi.org/10.1016/j.neuron.2011.08.009>

Poirier, P., Giles, T.D., Bray, G.A., Hong, Y., Stern, J.S., Pi-Sunyer, X.F., Eckel, R.H., 2006. Obesity and Cardiovascular Disease: Pathophysiology, Evaluation, and Effect of Weight Loss. *Circulation* 113, 898–918. <https://doi.org/10.1161/circulationaha.106.171016>

Pollard, P.J., Brière, J.J., Alam, N.A., Barwell, J., Barclay, E., Wortham, N.C., Hunt, T., Mitchell, M., Olpin, S., Moat, S.J., Hargreaves, I.P., Heales, S.J., Chung, Y.L., Griffiths, J.R., Dalglish, A., McGrath, J.A., Gleeson, M.J., Hodgson, S.V., Poulson, R., Rustin, P., Tomlinson, I.P.M., 2005. Accumulation of Krebs cycle intermediates and over-expression of HIF1 α in tumours which result from germline FH and SDH mutations. *Hum Mol Genet* 14, 2231–2239. <https://doi.org/10.1093/hmg/ddi227>

Rask-Madsen, C., King, G.L., 2013. Vascular Complications of Diabetes: Mechanisms of Injury and Protective Factors. *Cell Metab* 17, 20–33. <https://doi.org/10.1016/j.cmet.2012.11.012>

Ruch, C., Skiniotis, G., Steinmetz, M.O., Walz, T., Ballmer-Hofer, K., 2007. Structure of a VEGF–

References

- VEGF receptor complex determined by electron microscopy. *Nat Struct Mol Biol* 14, 249–250.
<https://doi.org/10.1038/nsmb1202>
- Ruhrberg, C., Bautch, V.L., 2013. Neurovascular development and links to disease. *Cell Mol Life Sci* 70, 1675–1684. <https://doi.org/10.1007/s00018-013-1277-5>
- Ruiz de Almodovar, C., Fabre, P.J., Knevels, E., Coulon, C., Segura, I., Haddick, P., Aerts, L., Delattin, N., Strasser, G., Oh, W.-J., Lange, C., Vinckier, S., Haigh, J., Fouquet, C., Gu, C., Alitalo, K., Castellani, V., Tessier-Lavigne, M., Chedotal, A., Charron, F., Carmeliet, P., 2011. VEGF Mediates Commissural Axon Chemoattraction through Its Receptor Flk1. *Neuron* 70, 966–978.
<https://doi.org/10.1016/j.neuron.2011.04.014>
- Ryan, H., Poloni, M., McNulty, W., Elson, D., Gassmann, M., Arbeit, J., Johnson, R., 2015. Hypoxia-inducible factor-1alpha is a positive factor in solid tumor growth. *Cancer Res* 60, 4010–4015.
- Safran, M., Kim, W.Y., O’Connell, F., Flippin, L., Günzler, V., Horner, J.W., DePinho, R.A., Kaelin, W.G., 2006. Mouse model for noninvasive imaging of HIF prolyl hydroxylase activity: Assessment of an oral agent that stimulates erythropoietin production. *P Natl Acad Sci Usa* 103, 105–110.
<https://doi.org/10.1073/pnas.0509459103>
- Schödel, J., Oikonomopoulos, S., Ragoussis, J., Pugh, C.W., Ratcliffe, P.J., Mole, D.R., 2011. High-resolution genome-wide mapping of HIF-binding sites by ChIP-seq. *Blood* 117, e207–e217.
<https://doi.org/10.1182/blood-2010-10-314427>
- Schwarz, Q., Gu, C., Fujisawa, H., Sabelko, K., Gertsenstein, M., Nagy, A., Taniguchi, M., Kolodkin, A.L., Ginty, D.D., Shima, D.T., Ruhrberg, C., 2004. Vascular endothelial growth factor controls neuronal migration and cooperates with Sema3A to pattern distinct compartments of the facial nerve. *Gene Dev* 18, 2822–2834. <https://doi.org/10.1101/gad.322904>
- Selak, M.A., Armour, S.M., MacKenzie, E.D., Boulahbel, H., Watson, D.G., Mansfield, K.D., Pan, Y., Simon, M.C., Thompson, C.B., Gottlieb, E., 2005. Succinate links TCA cycle dysfunction to oncogenesis by inhibiting HIF- α prolyl hydroxylase. *Cancer Cell* 7, 77–85.
<https://doi.org/10.1016/j.ccr.2004.11.022>
- Semenza, G., Wang, G., 1992. A nuclear factor induced by hypoxia via de novo protein synthesis binds to the human erythropoietin gene enhancer at a site required for transcriptional activation. *Mol Cell Biol* 12, 5447–5454. <https://doi.org/10.1128/mcb.12.12.5447>

References

Senger, D., de Van, W.L., Brown, L., Nagy, J., Yeo, K., Yeo, T., Berse, B., Jackman, R., Dvorak, A., Dvorak, H., 1993. Vascular permeability factor (VPF, VEGF) in tumor biology. *Cancer Metastasis Rev* 12, 303–324.

Senger, D.R., Galli, S.J., A.orak, Perruzzi, C.A., Harvey, S.V., Dvorak, H.F., n.d. Tumor cells secrete a vascular permeability factor that promotes accumulation of ascites fluid. *Science* 219, 983–985.

Shek, E.W., Brands, M.W., Hall, J.E., 1998. Chronic leptin infusion increases arterial pressure.pdf. *Hypertension* 31, 409–414.

Shibuya, M., 2013. VEGFR and Type-V RTK Activation and Signaling. *Csh Perspect Biol* 5, a009092. <https://doi.org/10.1101/cshperspect.a009092>

Soker, S., Takashima, S., Miao, H., Neufeld, G., Klagsbrun, M., 1998. Neuropilin-1 Is Expressed by Endothelial and Tumor Cells as an Isoform-Specific Receptor for Vascular Endothelial Growth Factor.pdf. *Cell* 92, 735–745.

Sun, M., Honey, C., Berk, C., Wong, N., Tsui, J., 2003. Regulation of aquaporin-4 in a traumatic brain injury model in rats. *J Neurosurg.* 98, 565–569.

Suto, K., Yamazaki, Y., Morita, T., Mizuno, H., 2005. Crystal Structures of Novel Vascular Endothelial Growth Factors (VEGF) from Snake Venoms INSIGHT INTO SELECTIVE VEGF BINDING TO KINASE INSERT DOMAIN-CONTAINING RECEPTOR BUT NOT TO fms-LIKE TYROSINE KINASE-1. *J Biol Chem* 280, 2126–2131. <https://doi.org/10.1074/jbc.m411395200>

Swanson, H.I., Chan, W.K., Bradfield, C.A., 1995. DNA binding specificities and pairing rules of the Ah receptor, ARNT and SIM proteins.pdf. *The Journal of Biological Chemistry.*

Takashima, S., Kitakaze, M., Asakura, M., Asanuma, H., Sanada, S., Tashiro, F., Niwa, H., Miyazaki, J., Hirota, S., Kitamura, Y., Kitsukawa, T., Fujisawa, H., Klagsbrun, M., Hori, M., 2002. Targeting of both mouse neuropilin-1 and neuropilin-2 genes severely impairs developmental yolk sac and embryonic angiogenesis. *Proc National Acad Sci* 99, 3657–3662. <https://doi.org/10.1073/pnas.022017899>

Tammela, T., Alitalo, K., 2010. Lymphangiogenesis: Molecular Mechanisms and Future Promise. *Cell* 140, 460–476. <https://doi.org/10.1016/j.cell.2010.01.045>

References

- Terman, B.I., Dougher-Vermazen, M., Carrion, M.E., Dimitrov, D., Armellino, D.C., Gospodarowicz, D., Böhlen, P., 1992. Identification of the KDR tyrosine kinase as a receptor for vascular endothelial cell growth factor. *Biochem Biophys Res Commun* 187, 1579–1586. [https://doi.org/10.1016/0006-291x\(92\)90483-2](https://doi.org/10.1016/0006-291x(92)90483-2)
- Thomlinson, R., Gray, L., 1955. The Histological Structure of Some Human Lung Cancers and the Possible Implications for Radiotherapy. *Brit J Cancer* 9, bjc195555. <https://doi.org/10.1038/bjc.1955.55>
- Todorov, M., Paetzold, J.C., Schoppe, O., Tetteh, G., Efremov, V., Voelgyi, K., Duering, M., Dichgans, M., Piraud, M., Menze, B., Erturk, A., 2019. Automated analysis of whole brain vasculature using machine learning. *Biorxiv* 613257. <https://doi.org/10.1101/613257>
- van den Berg, E., Kloppenborg, R.P., Kessels, R., Kappelle, J.L., Biessels, G., 2009. Type 2 diabetes mellitus, hypertension, dyslipidemia and obesity: A systematic comparison of their impact on cognition. *Biochimica Et Biophysica Acta Bba - Mol Basis Dis* 1792, 470–481. <https://doi.org/10.1016/j.bbadis.2008.09.004>
- Virchow, R., n.d. *Gesammelten Abhandlungen zur wissenschaftlichen Medicin.pdf*. Verlag von Meidinger Sohn & Comp. Frankfurt A.M. .
- Wang, G.L., Jiang, B.-H., Rue, E.A., Semenza, G.L., 1995. Hypoxia-inducible factor 1 is a basic-helix-loop-helix-PAS heterodimer regulated by cellular O₂.pdf.
- Wang, G.L., Semenza, G.L., 1993. Characterization of hypoxia-inducible factor 1 and regulation of DNA binding activity by hypoxia..pdf. *The Journal of Biological Chemistry*.
- Wang, J., Tu, J., Cao, B., Mu, L., Yang, X., Cong, M., Ramkrishnan, A.S., Chan, R., Wang, L., Li, Y., 2017. Astrocytic l-Lactate Signaling Facilitates Amygdala-Anterior Cingulate Cortex Synchrony and Decision Making in Rats. *Cell Reports* 21, 2407–2418. <https://doi.org/10.1016/j.celrep.2017.11.012>
- Wang, W.Y., Dong, J.H., Liu, X., Wang, Y., Ying, G.X., Ni, Z.M., Zhou, C.F., 2005. Vascular endothelial growth factor and its receptor Flk-1 are expressed in the hippocampus following entorhinal deafferentation. *Neuroscience* 134, 1167–1178. <https://doi.org/10.1016/j.neuroscience.2005.04.064>

References

- Weisbrod, R., Shiang, T., Al, S.L., Fry, J., Bajpai, S., Reinhart-King, C., Lob, H., Santhanam, L., Mitchell, G., Cohen, R., Seta, F., 2013. Arterial Stiffening Precedes Systolic Hypertension in Diet-Induced Obesity.pdf. *Hypertension* 62, 1105–1110.
- Wenger, R.H., Stiehl, D.P., Camenisch, G., 2005. Integration of Oxygen Signaling at the Consensus HRE. *Sci Stke* 2005, re12–re12. <https://doi.org/10.1126/stke.3062005re12>
- Wiesmann, C., Fuh, G., Christinger, H.W., Eigenbrot, C., Wells, J.A., de Vos, A.M., 1997. Crystal Structure at 1.7 Å Resolution of VEGF in Complex with Domain 2 of the Flt-1 Receptor. *Cell* 91, 695–704. [https://doi.org/10.1016/s0092-8674\(00\)80456-0](https://doi.org/10.1016/s0092-8674(00)80456-0)
- Winkler, E.A., Sengillo, J.D., Sullivan, J.S., Henkel, J.S., Appel, S.H., Zlokovic, B.V., 2013. Blood–spinal cord barrier breakdown and pericyte reductions in amyotrophic lateral sclerosis. *Acta Neuropathol* 125, 111–120. <https://doi.org/10.1007/s00401-012-1039-8>
- Wolfe, B.E., Jimerson, D.C., Orlova, C., Mantzoros, C.S., 2004. Effect of dieting on plasma leptin, soluble leptin receptor, adiponectin and resistin levels in healthy volunteers. *Clin Endocrinol* 61, 332–338. <https://doi.org/10.1111/j.1365-2265.2004.02101.x>
- Wong, T.Y., Cheung, C., Larsen, M., Sharma, S., Simó, R., 2016. Diabetic retinopathy. *Nat Rev Dis Primers* 2, nrdp201612. <https://doi.org/10.1038/nrdp.2016.12>
- Wu, D., Potluri, N., Lu, J., Kim, Y., Rastinejad, F., 2015. Structural integration in hypoxia-inducible factors. *Nature* 524, 303. <https://doi.org/10.1038/nature14883>
- Xia, X., Kung, A.L., 2009. Preferential binding of HIF-1 to transcriptionally active loci determines cell-type specific response to hypoxia. *Genome Biol* 10, R113. <https://doi.org/10.1186/gb-2009-10-10-r113>
- Xiong, B., Li, A., Lou, Y., Chen, S., Long, B., Peng, J., Yang, Z., Xu, T., Yang, X., Li, X., Jiang, T., Luo, Q., Gong, H., 2017. Precise Cerebral Vascular Atlas in Stereotaxic Coordinates of Whole Mouse Brain. *Front Neuroanat* 11, 128. <https://doi.org/10.3389/fnana.2017.00128>
- y Cajal, S., 1955. *Studie on the Cerebral Cortex (Limbic Structures)*.
- Yao, Y., Chen, Z.-L., Norris, E.H., Strickland, S., 2014. Astrocytic laminin regulates pericyte differentiation and maintains blood brain barrier integrity. *Nat Commun* 5, 3413.

References

<https://doi.org/10.1038/ncomms4413>

Yi, C.-X., Gericke, M., Krüger, M., Alkemade, A., Kabra, D.G., Hanske, S., Filosa, J., Pfluger, P., Bingham, N., Woods, S.C., Herman, J., Kalsbeek, A., Baumann, M., Lang, R., Stern, J.E., Bechmann, I., Tschöp, M.H., 2012. High calorie diet triggers hypothalamic angiopathy. *Mol Metab* 1, 95–100. <https://doi.org/10.1016/j.molmet.2012.08.004>

Zeltser, L.M., Seeley, R.J., Tschöp, M.H., 2012. Synaptic plasticity in neuronal circuits regulating energy balance. *Nat Neurosci* 15, 1336. <https://doi.org/10.1038/nn.3219>

VIII. Appendix

Table 4: Reagents and chemicals

Name	Provider	Product code
4-OH-tamoxifen (<i>Afimoxifen</i>)	Sigma-Aldrich Chemie GmbH, Taufkirchen, Germany	H-7904
Adult brain dissociation kit	Milteny BioTec, USA	Milteny BioTec, USA
Agarose	Biozym Scientific GmbH, Hessisch Oldendorf, Germany	840004
Anti-Anti (100x)	Gibco/Thermo Fisher Scientific Inc., Waltham, USA	115240-062
Benzyl alcohol	Sigma-Aldrich Chemie GmbH, Taufkirchen, Germany	24122-1L
Benzyl benzoate	Sigma-Aldrich Chemie GmbH, Taufkirchen, Germany	B6630-250ML
Betaine (5 M), PCR reagent	Sigma-Aldrich Chemie GmbH, Taufkirchen, Germany	B0300
Bright-Glo™ Luciferase Assay System	Promega	E2610
Carbonyl cyanide-p- trifluoromethoxyphenylhydrazone (FCCP)	Sigma-Aldrich Chemie GmbH, Taufkirchen, Germany	C2920
CHCl ₃	C2432-500ML	Sigma-Aldrich Chemie GmbH
chemiluminescent HRP substrate	Immobilion Western, Millipore	/
Clodrosome® (clodronate liposomes)	Encapsulated Nano Sciences, USA	/
Cobalt (II) chloride hexahydrate	Sigma-Aldrich Chemie GmbH, Taufkirchen, Germany	C8661-25G
D-(+)-glucose	Carl Roth GmbH+CoKG, Karlsruhe, Germany	HN06.4
D-(+)Saccharose (sucrose)	Carl Roth GmbH+CoKG, Karlsruhe, Germany	4621.1
Dichloromethane	Sigma-Aldrich Chemie GmbH, Taufkirchen, Germany	270997-100ML
DMEM XF Assay medium	Seahorse Bioscience/Agilent, Waldbronn, Germany	102365-100
DMSO	Carl Roth GmbH+CoKG,	A994.2

Appendix

	Karlsruhe, Germany	
DNA/RNA-Farbstoff, peqGREEN	VWR International GmbH, Darmstadt, Germany	732-2960
Ethanol	Th. Geyer GmbH+CoKG, Renningen, Germany	1.00983.2500
Fetal bovine serum (FBS)	Gibco/Thermo Fisher Scientific Inc., Waltham, USA	10270-106
Gelatin from porcine skin (SUMI)	VWR International GmbH, Darmstadt, Germany	SAFSG1890
Glo Lysis Buffer	Promega	E2661
Guanidine hydrochloride	Sigma-Aldrich Chemie GmbH, Taufkirchen, Germany	G4505-500G
Halt™ protease and phosphatase inhibitors (100x)	Thermo Fisher Scientific Inc., Waltham, USA	78446
HBSS (Hank's balanced salt solution)	Gibco/Thermo Fisher Scientific Inc., Waltham, USA	14175-053
HEPES	Gibco/ Thermo Fisher Scientific Inc.,Waltham, USA	15630080
Injectable saline (0.9% NaCl)	B.Braun, Melsungen, Germany	162618091
L-carnitin HCl	Santa Cruz Biotechnology	Sc-204782
MEM	Gibco/Thermo Fisher Scientific Inc., Waltham, USA	31095-029
MTBE	Sigma-Aldrich Chemie GmbH, Taufkirchen, Germany	1634-04-4
NuPAGE® LDS sample buffer (4x)	Novex/Life Technologies, USA	NP008
Paraformaldehyde	Carl Roth GmbH+CoKG, Karlsruhe, Germany	0335.2
PBS (1X), liquid; pH:7.4	Gibco/Thermo Fisher Scientific Inc., Waltham, USA	10010056
Pepsin	DAKO/Agilent	S3002
Pierce BCA protein assay	Thermo Fisher Scientific Inc., Waltham, USA	23228
Primers	Thermo Fisher Scientific Inc., Waltham, USA	/
QuickDetect™ catecholamine (mouse) ELISA Kit	Enzo Lifesciences,	E4462
Radioimmunoprecipitation assay	Sigma-Aldrich Chemie GmbH,	R0278-500ML

Appendix

(RIPA) buffer	Taufkirchen, Germany	
Recombinant mouse leptin	R&D systems	498-OB
Skim milk powder	Sigma-Aldrich Chemie GmbH, Taufkirchen, Germany	70166-500g
Sodium dodecanoate	Sigma-Aldrich Chemie GmbH, Taufkirchen, Germany	L9755-5G
Tamoxifen	T5648-1g	Sigma-Aldrich Chemie GmbH
TaqMan Gene Expression Assay	Thermo Fisher Scientific Inc., Waltham, USA	/
TaqMan Universal Master Mix II, no UNG	Thermo Fisher Scientific Inc., Waltham, USA	4440040
Tetrahydrofuran	Sigma-Aldrich Chemie GmbH, Taufkirchen, Germany	186562-1L
Thioglycolic acid	Sigma-Aldrich Chemie GmbH, Taufkirchen, Germany	T3758-500ML
TRIS PUFFERAN®	Carl Roth GmbH+CoKG, Karlsruhe, Germany	4855.5
Triton X-100	Roche Diagnostics GmbH, Mannheim, Germany	11858620
Trypsin/EDTA solution	Biochrome GmbH	L 2143
Tween-20	Sigma-Aldrich Chemie GmbH, Taufkirchen, Germany	9005-64-5

Table 5: Antibodies and fluorescent dyes

Target	Host	Conjugate	Dilution	Product code	Provider
--------	------	-----------	----------	--------------	----------

Primary antibodies

ACSA-2	rat	/	10 µl / 10 ⁷ cells	130-097-678	Milteny, BioTec, USA
Albumin	sheep	/	1/500	Ab8940	Abcam, USA
Claudin-5	mouse	/	1/500	352500	Life techn., USA
Collagen IV	goat	/	1/500	AB769	Chemicon/Merck, Germany
GFAP	goat	/	1/1000	Z0334	Dako, USA
GFP	chicken	/	1/500	Ab13970	Abcam, USA

Appendix

HIF-1 α	rabbit	/	1/1000	Ab82832	Abcam, USA
Iba1	goat	/	1/1000	234003	Synaptic Systems, USA
Laminin	rabbit	/	1/500	ZO097	Dako, USA
NeuN	mouse	/	1/300	2950736	Merck, Germany
pSTAT3 (Tyr705) (D3A7)	rabbit	/	1/1000	#9145S	Cell Signaling Technology, USA
VEGF (A-20)	rabbit	/	1/500	Sc-152 <i>(discontinued)</i>	Santa Cruz, USA
β -actin (AC-15) (HRP)	mouse	Horseradish peroxidase	1/1000	Ab49900	Abcam, USA

Secondary antibodies

chicken IgG	goat	Alexa Fluor 488	1/1000	A11039	Invitrogen, USA
goat IgG	donkey	Alexa Fluor 647	1/1000	A21447	Invitrogen, USA
mouse IgG	goat	Alexa Fluor 405	1/1000	A31553	Invitrogen, USA
rabbit IgG	donkey	Alexa Fluor 568	1/1000	A10042	Invitrogen, USA
rabbit IgG	donkey	Alexa Fluor 647	1/1000	A31573	Invitrogen, USA
sheep IgG	donkey	Alexa Fluor 647	1/1000	A21448	Invitrogen, USA

Fluorescent dyes

Lectin-FITC conjugate	Triticum vulgaris	FITC	25 μ g/ml	L4895	Thermo Fisher Scientific, USA
WGA-Alexa Fluor 647 TM	Triticum vulgaris	Alexa Fluor 647	25 μ g/ml	W32466	Thermo Fisher Scientific, USA
NeuroTrace TM 435/455	/	435/455	1/500	N21479	Thermo Fisher Scientific, USA
NeuroTrace TM 500/525	/	500/525	1/500	N21480	Thermo Fisher Scientific, USA

Appendix

Genotyping protocols

In order to analyze the genotypes of HIF-1 α ^{loxP/loxP} mice, HIF-1 α ^{loxP/loxP} mice positive or negative mice were assessed using the HIF-1 α ^{loxP/loxP} PCR protocol (**Table 5**) applying HIF-1 α ^{loxP/loxP} specific PCR conditions (**Table 6**).

Table 5: Genotyping PCR for HIF-1 α ^{loxP/loxP} mice

Substance	Concentration	Volume (μ l)
MilliQ H ₂ O		4.35
Promega buffer	5 x	2.5
MgCl ₂	25 mM	1
dNTP	10 mM	0.25
HIF-1 α (fwd. primer 13109)	20 μ M	0.25
HIF-1 α (rev. primer 13110)	20 μ M	0.25
Betaine	5 M	2.5
Promega Go-Taq flexi	5 U/ μ l	0.15

HIF-1 α primer 13109 5'–GGTGCTGGTGTCCAAAATGT–3' forward

HIF-1 α primer 13110 5'–GGGCAGTACTGGAAAGATGG–3' reverse

Table 6: Genotyping PCR for HIF-1 α ^{loxP/loxP} mice

Temperature [°C]	Time	cycles
94	2 min	1
94	20 s	10
65	15 s	10 (-1.5°C per cycle)
68	10	10
94	15	25
50	15	25
72	10	25
72	2	1
4	∞	

The control band appear at 295 bp and the mutant band at 324 bp. PCR products were loaded on a 2% agarose gel ran in TAE buffer (2 M Tris, 1 M glacial acetic acid, 0.5 M EDTA) to be separated by molecular weight.

Appendix

In order to evaluate the genotypes of LepR^{loxP/loxP} mice, LepR^{loxP/loxP} mice positive or negative mice were assessed using the HIF-1 α ^{loxP/loxP} PCR protocol (**Table 7**) applying LepR^{loxP/loxP} specific PCR conditions (**Table 8**).

Table 7: Genotyping PCR for LepR^{loxP/loxP} mice

Substance	Concentration	Volume (μ l)
MilliQ H ₂ O		3.6
Promega buffer	5 x	2.5
MgCl ₂	25 mM	1.5
dNTP	10 mM	0.25
Lep (fwd primer 65A)	20 μ M	0.25
Lep (rev. primer 105)	20 μ M	0.25
LepR (fwd primer 106)	20 μ M	0.25
Betaine	5 M	2.5
Promega Go-Taq flexi	5 U/ μ l	0.15

LepR primer 65A 5' – AGAATGAAAAAGTTGTTTTGGGA -3' forward

LepR primer 105 5' – ACAGGCTTGAGAACATGAACAC -3' reverse

LepR primer 106 5' - GTCTGATTTGATAGATGGTCTT -3' forward

Table 8: Genotyping PCR for LepR^{loxP/loxP} mice

Step	Temperature [°C]	Time	cycles
Initial denaturation	95	2 min	1
Denaturation	94	20 s	40
Annealing	54	30	
Elongation	72	45	
Final Elongation	72	5 min	1
Hold	4	∞	

The control band appear at 200 bp and the mutant band at 250 bp. PCR products were loaded on a 2% agarose gel ran in TAE buffer (2 M Tris, 1 M glacial acetic acid, 0.5 M EDTA) to be separated by molecular weight.

Appendix

In order to evaluate the genotypes of GLAST.CreER^{T2} mice, GLAST.CreER^{T2} mice positive or negative mice were assessed using the GLAST.CreER^{T2} PCR protocol (**Table 9**) applying GLAST.CreER^{T2} specific PCR conditions (**Table 10**).

Table 9: Genotyping PCR for GLAST.CreER^{T2} mice

Substance	Concentration	Volume (µl)
MilliQ H ₂ O		4.375
KAPA2G Fast Mix		6.25
GLAST.CreERT2 (primer F8)	20 µM	0.625
GLAST.CreERT2 (primer R3)	120 µM	0.625
CER1	20 µM	0.625

GLAST.CreERT2 primer F8 5' – GAGGCACTTGGCTAGGCTCTGAGG -3' forward

GLAST.CreERT2 primer R3 5' – GAGGAGATCCTGACCGATCAGTGGG -3' reverse

CER1 primer 5' - GGTGTACGGTCAGTAAATTGGACAT -3' (*CreER^{T2}-specific*)

Table 10: Genotyping PCR for GLAST.CreER^{T2} mice

Step	Temperature [°C]	Time	cycles
Initial denaturation	95	3 min	1
Denaturation	95	15 s	40
Annealing	60	40	
Elongation	72	15	
Final Elongation	72	1 min	1
Hold	10	∞	

The control band appear at 700 bp and the mutant band at 400 bp. PCR products were loaded on a 2% agarose gel ran in TAE buffer (2 M Tris, 1 M glacial acetic acid, 0.5 M EDTA) to be separated by molecular weight.

Appendix

In order to analyze the genotypes of hGFAP.CreER^{T2} mice, hGFAP.CreER^{T2} mice positive or negative mice were assessed using the hGFAP.CreER^{T2} PCR protocol (**Table 11**) applying hGFAP.CreER^{T2} specific PCR conditions (**Table 12**).

Table 11: Genotyping PCR for hGFAP.CreER^{T2} mice

Substance	Concentration	Volume (µl)
Promega buffer	5 x	2.5
MgCl ₂	25 mM	1
dNTP	10 mM	0.25
Cre (primer 1084)	20 µM	0.25
Cre (primer 1084)	20 µM	0.25
Cre (primer 42)	20 µM	0.25
Cre (primer 43)	20 µM	0.25
Betaine	5 M	2.5
Promega Go-Taq flexi	5 U/µl	0.15

Cre primer 1084 5' –GCGGTCTGGCAGTAAAACTATC -3'

Cre primer 1085 5' – GTGAAACAGCATTGCTGTCACCTT -3'

Cre primer 42 5' - CTAGGCCACAGAATTGAAAGATCT -3'

Cre primer 43 5' - GTAGGTGGAAATTCTAGCATCATCATC -3'

Table 12: Genotyping PCR for hGFAP.CreER^{T2} mice

Step	Temperature [°C]	Time	cycles
Initial denaturation	95	3 min	1
Denaturation	95	15 s	40
Annealing	60	40	
Elongation	72	15	
Final Elongation	72	1 min	1
Hold	10	∞	

The control band appear at 324 bp and the mutant band at 100 bp. PCR products were loaded on a 2% agarose gel ran in TAE buffer (2 M Tris, 1 M glacial acetic acid, 0.5 M EDTA) to be separated by molecular weight.

Appendix

Table 13: TaqMan probes

Gene name	Acronym	Identifier
<i>Vascular-endothelial growth factor</i>	<i>Vegfa</i>	<i>Mm00437306-m1</i>
<i>Kinase insert domain receptor</i>	<i>Kdr (Vegfr2)</i>	<i>Mm01222421-m1</i>
<i>β_1-adrenoreceptor</i>	<i>Adrb1</i>	<i>Mm00431701-m1</i>
<i>β_2-adrenoreceptor</i>	<i>Adrb2</i>	<i>Mm02524224-m1</i>
<i>Claudin-5</i>	<i>Cldn-5</i>	<i>Mm00727012-s1</i>
<i>Hypoxia-inducible factor 1α</i>	<i>Hif1α</i>	<i>Mm01283757-m1</i>
<i>Hypoxanthine guanine phosphoribosyl transferase</i>	<i>Hprt</i>	<i>Mm01545399m1</i>
<i>Mitochondrial ribosomal protein L32</i>	<i>Mrpl32</i>	<i>Mm00777741_sH</i>

Table 14: Viral vectors

Name	Serotype	Promoter	Linker and Enhancer	Titer (gc/ml)	Provider
rAAV.GFAPp.GFP.VEGF	2/5	Gfa2 (2.2kb)	2A linker WPRE	10 ¹³	Vectorbiolabs, Malvern, USA
rAAV.GFAPp.GFP.VEGF.shRNAmir	2/5	Gfa2 (2.2kb)	2A linker WPRE	10 ¹³	Vectorbiolabs, Malvern, USA
rAAV.GFAPp.eGFP	2/5	Gfa2 (2.2kb)	WPRE	10 ¹³	Vectorbiolabs, Malvern, USA
rAAV.GFAPp.iCre	2/5	Gfa2 (2.2kb)	WPRE	10 ¹³	Vectorbiolabs, Malvern, USA

Table 15: Software

Name	Provider	Version
GraphPad PRISM	GraphPad Software, Inc. La Jolla, USA	6
SPSS	IBM, USA	
ImageJ / FIJI	ImageJ	3.7.3
Python	Conda Forge	
IMARIS	Oxford Instruments	
Microsoft® Office for Mac	Microsoft	

Table 16: Instruments

Item	Name	Provider
Body Composition Analyzer for Live Small Animals (Mice), Organs and Biopsies	EchoMRI 3-in-1	EchoMRI, Houston, USA
Cell dissociation	Gentle MACS Octo Dissociator	Milteny, BioTec, USA
Confocal Microscope	Leica TCS SP5	Leica Mikrosysteme Vertrieb GmbH, Wetzlar, Germany
Cryostat	Leica CM3050 S Research Cryostat	Leica Mikrosysteme Vertrieb GmbH, Wetzlar, Germany
Extracellular Flux Analyzer	Seahorse XF24 Analyser	Agilent, Waldbronn, Germany
Fluorescence Microscope	BZ-9000 fluorescence microscope	Keyence Corporation, Itasca, USA
Light-sheet fluorescence microscope	Ultramicroscope II	LaVision BioTec
Microplate Reader	HTS Microplate Reader – PHERAstar F	MBG LABTECH GmbH, Ortenberg, Germany
qPCR cyclers	QuantStudio	Thermo Fisher Scientific Inc., Waltham, USA

IX. Curriculum vitae

